

Silicon-oxygen bond formation for the novel synthesis of siloxane molecules and structures

By

© 2021

Dakota Even

B.S., Iowa State University

Submitted to the graduate degree program in Department of Chemical and Petroleum Engineering and the Graduate Faculty of the University of Kansas in partial fulfillment of the requirements for the degree of Master of Science.

Chair: Cory Berkland

Mark Shiflett

Sabrina Torres

Date Defended: 22nd of April, 2021

The thesis committee for Dakota Even certifies that this is the approved version of the following thesis:

Silicon-oxygen bond formation for the novel synthesis of siloxane molecules and structures

Chair: Cory Berkland

Date Approved: 22nd of April, 2021

Abstract

The extended bond length and bond angle of the Si-O linkage yields molecules with properties far different than their carbon analogues—alcohols and ethers. Particularly, Si-O bonds exhibit depressed basicity despite the higher electropositivity of silicon to carbon, giving Si-O bonds good chemical inertness and leading to applications in organic synthesis and industrially significant siloxane polymers. In this study, Si-O bond formation is investigated from Si-H precursors along with siloxane polymers to fabricate novel siloxane molecules and structures.

Chapter 1 focuses on silicon-oxygen bond formation by base catalyzed dehydrogenation between silanes and hydroxyl groups. The dehydrogenation of diphenylsilane, a highly reactive silane species with two reactive hydrogens, was the silane of interest. Various catalyst types were explored for facilitating the reaction including three hydroxides, six amines, and an N-heterocyclic carbene-copper alkoxide complex (CuIPr-NHC). Reactions were monitored via FTIR to observe stepwise consumption of both Si-H bonds in diphenylsilane in the presence of water and various alcohols. Hydroxide catalysts with sodium, potassium, and tetramethylammonium (TMA) cations showed strong dependence of cation identity on reaction rate and observable rate order but did not lead to accumulation of a once-oxidized silane. Amine catalysts exhibited varying levels selectivity to the once oxidized silane, leading to accumulation of diphenylsilanol and hydride terminated oligomers with relative reaction rates seemingly dependent on the size of alkyl substituents. Uniquely, CuIPr-NHC showed very limited reactivity to the second dehydrogenation step. Leveraging this, the production of diphenyl(monoalkoxy)silanes has been demonstrated with primary and secondary alcohols with CuIPr-NHC and alkoxide base activators.

Chapter 2 focuses on the continuous production of PDMS microspheres using microfluidics and premix emulsification. Generally, traditional microfluidics are used for this process with unparalleled control over microsphere size and distribution at the tradeoff of low throughput (100s of $\mu\text{L/hr}$). Using an

easily replicated membrane system, premix emulsification is demonstrated to be a viable alternative with reasonable control over microsphere size and polydispersity. Four different membranes were chosen to demonstrate system capabilities, with median microspheres diameters ranging from 5 to 45 μm .

Chapter 3 leverages the topics of Chapter 1 and Chapter 2. Base catalyzed dehydrogenation is applied as a method for interfacial polymerization to stabilize W/O/W double emulsions and to produce PDMS microfoam structures. Dehydrogenation of poly(dimethyl, methylhydro siloxane) with polyethylene glycol effectively forms amphiphilic co-polymer networks that function as surfactants at water-PDMS interfaces. The interfacial reaction is applied as a means of encapsulating water cores inside of PDMS microspheres. This method was found to be an improvement over the use of non-reactive silicone emulsifiers for forming double emulsion microspheres during high shear emulsification processes, however droplet breakup for microspheres under 50 μm becomes difficult. The interfacial reaction also produced high amounts of hydrogen gas, which can be captured within nascent microspheres yielding a high internal phase with tunable mechanical properties.

Table of Contents

Chapter 1: Catalytic studies on base catalyzed dehydrogenation of diphenylsilane	1
1.1 Introduction	1
1.2 Literature review.....	2
1.2.1 Review of existing catalysts	2
1.2.2 Stability and deprotection in silylethers.....	7
1.2.3 Restrictions and limitations to silane protection of alcohols	8
1.2.4 Dehydrogenation of dihydrosilanes and potential applications	9
1.3 Materials and methods.....	12
1.3.1 Materials	12
1.3.2 Procedure for ionic base catalyzed dehydrogenation	13
1.3.3 Procedure for amine catalyzed dehydrogenation	14
1.3.4 Procedure for CuIPr-NHC catalyzed dehydrogenation	15
1.3.2 Reaction monitoring, data treatment, and product confirmation.....	16
1.4 Results and discussion	18
1.4.1 Steric inhibitions in Ph_2SiH_2 dehydrogenation	18
1.4.2 Catalytic activity of hydroxides	20
1.4.3 Catalytic activity of amines	32
1.4.4 Monoalkoxylated diphenylsilane synthesis by CuIPr-NHC.....	36
1.5 Conclusions.....	41
Supplementary Information	44
References	51
Chapter 2: Tunable PDMS microspheres by continuous flow emulsification.....	55
2.1 Introduction	55
2.2 Literature review.....	56
2.2.1 Linear polysiloxane chemistry	56
2.2.2 Applications of PDMS and PDMS microspheres	59
2.2.2 Emulsion stabilization	61
2.2.3 Methods of emulsification and microsphere synthesis	63
2.3 Materials and Methods.....	68
2.4 Design of continuous flow system.....	69
2.5 Results and discussion.....	71
2.6 Conclusions.....	77

References	78
Chapter 3: Double emulsion PDMS microspheres by interfacial reactive stabilization	82
3.1 Introduction	82
3.2 Literature Review	83
3.3 Materials and Methods.....	84
3.4 Results and discussion	85
3.5 Conclusions	92
3.6 Future directions.....	93
References	94

List of Figures

Figure 1.1: Synthesis routes for Ph8D4.....	11
Figure 1.2: Example deconvolution using Python's LMFIT package.	17
Figure 1.3: IR spectra of Ph_2SiH_2 dehydrogenation with alcohols by KOtBu.....	19
Figure 1.4: Dehydrogenation profile of Ph_2SiH_2 with IPA and KOtBu catalyst.	20
Figure 1.5: Ph_2SiH_2 forming Ph8D4 in the presence of water.	21
Figure 1.6: Ph8D4 crystals as collected product.	21
Figure 1.7: Rate constants versus catalyst concentration of Ph_2SiH_2 dehydrogenation.....	22
Figure 1.8: Arrhenius plot for the dehydrogenation of Ph_2SiH_2 with water.	24
Figure 1.9: Parity plot of Ph_2SiH_2 consumption with NaOH catalyst at 50°C.....	32
Figure 1.10: Dehydrogenation profile of Ph_2SiH_2 by diisopropylethylamine.	34
Figure 1.11: Dehydrogenation profile of Ph_2SiH_2 by Et_3N THF and 4:1 THF/DMSO.	35
Figure 1.12: Dehydrogenation profile of Ph_2SiH_2 by CuIPr-NHC and KOH catalyst with water.....	37
Figure 1.13: Deconvolved peak heights dehydrogenation by CuIPr-NHC and alcohols.....	38
Figure 1.14: Dehydrogenation profile by CuIPr-NHC and KOtBu with IPA.....	40
Figure 1.15: Proposed activation for CuIPr-NHC.....	41
Figure S1: FTIR calibration by phenyl group concentration.....	44
Figure S2: Si-H bond Voigt peak fitting.....	44
Figure S3: FITR calibration for Si-H bond monitoring.....	45
Figure S4: FTIR correction curve for temperature.....	46
Figure S5: NaOH dehydrogenation with and without excess water.....	46
Figure S6: Dehydrogenation profiles for amine catalyzed reactions.....	47
Figure S7: 1H NMR spectra for Ph_2SiH_2	48
Figure S8: 1H NMR spectra for isopropoxydiphenylsilane	49
Figure S9: 1H NMR spectra for ethoxydiphenylsilane.....	50
Figure 2.1: Condensation/hydrolysis between silanol groups in a polysiloxane system.	57
Figure 2.2: Ring opening polymerization of D4.....	58
Figure 2.3: Large-scale emulsification methods.....	64
Figure 2.4: Microfluidic methods for uniform droplet generation.....	65
Figure 2.5: Membrane emulsification methods.....	66
Figure 2.6: Particle size distributions using a double-syringe premix emulsification method	67
Figure 2.7: Continuous flow system for microsphere production.....	70
Figure 2.8: Emulsification column.....	71
Figure 2.9: Pressure loss profile for Whatman Grade 3 cellulose membrane.....	72
Figure 2.10: PDMS microsphere sizes by 20 μ m track etched membrane.....	73
Figure 2.11: PDMS microsphere sizes by various membranes.....	74
Figure 2.12: PDMS microsphere sizes by double syringe method.....	75
Figure 3.1: Schematic summary of interfacial polymerization.....	83
Figure 3.2: Fluorescein tagged double emulsion PDMS microspheres.....	86
Figure 3.3: Inverted double emulsions.....	88
Figure 3.4: Double emulsion microspheres produced by double syringe method.....	90

Figure 3.5: Isolated Sylgard 184 PDMS microsphere with porous structure.....91
 Figure 3.6: PDMS microspheres made using silanol dehydrogenation by metal salt cured.....92

List of Tables

Table 1.1: Reactions of base-silane systems.....9
 Table 1.2: Materials list.....13
 Table 1.3: Amine catalysts reviewed in this study.....15
 Table 1.4: Summary of system reactive species26
 Table 1.5: Observed rate constants of amine catalysts34

Table 3.1: Materials used for porous PDMS microsphere fabrication85
 Table 3.2: Hydrogen bonding abilities of solvents86

Chapter 1: Catalytic studies on base catalyzed dehydrogenation of diphenylsilane

1.1 Introduction

Multistep organic synthesis of complex molecules may rely on functional group protection or modification, with temporary linkages that can be readily reverted to the original functionality or new linkages to introduce new functionality. Hydroxyl group conversion to Si-O bonds is an important subdomain used for alcohol protection, oligomer coupling, and polysiloxane modification that has been dominated by chlorosilanes for more than half a century [1]. For alcohol protection using chlorosilanes, continued improvements have emerged in stereoselectivity and selective deprotection [2]. Chlorosilanes have also been used as a surface treatment method for decades, providing easy and effective means of adding functionality, protectivity, and hydrophobicity to a variety of materials [3-8]. In polysiloxane chemistry, chlorosilanes react with silanols and have been used to consume reactive hydroxyl terminal groups and control desired functionality [9-11] and also act as parent molecules for siloxane, dictated through the Rochow process [12]. The major inhibition to chlorosilane applications is the production of stoichiometric amounts of hydrochloric acid. Ultimately, this requires a scavenger agent, which complicates purification to remove the residual chloride salts and hinders process yield and purity. As an attractive alternative to chlorosilanes, the Si-H bond in silanes can be readily activated under facile conditions in the presence of many catalysts for the same purpose but with the strong advantage of hydrogen gas as the only byproduct. The coupling of silanes to free hydroxyl groups through dehydrogenation has been well known for decades [13] but it took several more decades before wide-breadth studies of silane dehydrogenation gained traction as a viable alternative to chlorosilanes [14, 15].

Despite the attractive benefit of silanes, replacement of chlorosilanes with silanes remains atypical. In addition, previous literature has identified reactions inhibited by steric effect, solvent selection, and base identity, but little direct kinetic comparison on these effects has been published. In

this study, the dehydrogenation of diphenylsilane (Ph_2SiH_2), a dihydrosilane with two reactive hydrogens, is explored with a variety of catalysts and hydroxyl group donors. FTIR analysis is used for *in situ* reaction monitoring of the dehydrogenation reaction. The two reactive sites of Ph_2SiH_2 allow for minimal silane use for alcohol protection while the two electronegative sp^2 carbons bound to the silicon center make it a highly reactive species in facile conditions with minimal catalyst presence. Further, the dual active site capabilities of Ph_2SiH_2 open its viability as a coupling agent for hydroxyl terminated polymers and oligomers that have previously been positions held by chlorosilanes [9].

Dehydrogenation of the silane with water has also been a reported synthesis route for the cyclic tetramer, octaphenylcyclotetrasiloxane (Ph_8D_4). In this study, dehydrogenation with water will be used as a model reaction to ensure consistent base anion identity throughout all reactions. Three hydroxyl catalysts, six amine catalysts, and an N-heterocyclic carbene-copper alkoxide complex (CuIPr-NHC) were used in the reaction, with *in situ* FTIR monitoring. This approach provided a direct comparison of cation and amine identity versus reactivity patterns, hydrogen selectivity, temperature responsiveness, and reaction rates which have not been previously investigated.

1.2 Literature review

1.2.1 Review of existing catalysts

Many complexes using transition metal catalysts to activate the Si-H bond have been developed over time. Gold nanoparticles on Al_2O_3 has been shown to work with dominant selectivity for primary alcohols [16]. Among a slew of inorganic catalysts that showed some level of activity, screening by Sridhar *et al.* found $InBr_3$ to be effective in the dehydrogenation reaction between menthol and triethylsilane with high selectivity to the alcohol functionality over a variety of unsaturated bonds [17]. The efficacy of the reaction was also strongly affected by solvent choice, with toluene showing significantly improved reactivity over tetrahydrofuran and acetonitrile, while dichloromethane, 1,2-dichloroethane, and diethyl

ether did not promote the reaction. Introduction of benzophenone as a radical scavenger also inhibited the reaction indicating a radical-dependent mechanism. Kim *et al.* provided examples of ruthenium catalysts show good activity with a variety of silanes and alcohols [18]. Ventura-Espinosa *et al.* demonstrated high activity of complexes based on both ruthenium and iridium with fast kinetics at room temperature [19, 20]. It has even been proposed that these compounds be used for on-demand hydrogen generation from silane coupling with methanol.

Albright and Gawley reported a more unique method for Si-O bond formation by investigating the activity of Chloro[1,3-bis(2,6-diisopropylphenyl)imidazol-2-ylidene]copper(I) N-heterocyclic carbene (CuIPr-NHC) with sodium tertbutoxide (NaOtBu) as a co-catalyst. After treating CuIPr-NHC with the base, the complex was found to be highly active for the hydrosilylation of ketones. In the absence of ketone, dehydrogenation of Ph_2SiH_2 to Ph_8D_4 was also seen [21, 22]. Unlike the previously mentioned catalysts, the Albright and Gawley suggested Si-O bond formation using O_2 , rather than an exposed alcohol, leading to a novel synthesis route. The reaction was rapid and facile, with full conversion of the silane in one hour at room temperature and pressure, which is a reactivity among the highest of the catalysts listed. The original claim was that silanols were produced by Si-O bond formation which underwent condensation or dehydrogenation to create Si-O-Si oligomers, since vigorous bubbling (hydrogen release) was still reported in their reaction system. Similar NHC catalysts have been used with silanes for a variety of reactions, such as Santoro *et al.*'s use of similar copper-alkoxide NHC complexes for the methylation of amines using CO_2 [23]. The proposed mechanism for such a system relies on hydrogen donation from a silane to the NHC complex, promoting silyl ether formation with formate. Welle *et al.* used this family of complexed to optimize the reductive adol reaction of double bonds and aldehydes using a multiple different alkoxy and phenylated silanes [24].

Despite the use of NHC copper-alkoxide systems in these other silane applications, several key factors stand out from Albright's report that require further scrutiny. The primary concern is that four

times more NaOtBu was used than CuIPr-NHC, meaning base catalyzed dehydrogenation alone could have dominated the reaction system if water was not carefully excluded. The report made no mention of rigorous water removal, and Albright's workup described that the reaction flask was exposed directly to the atmosphere and thus atmospheric humidity could act to provide water as the oxygen source rather than O_2 . In addition, little discussion of mechanism and no in-depth experimentation to review the claims were made other than the identification of the final product and some qualitative observations. It is then impossible to deconvolve the effects of CuIPr-NHC, NaOtBu, water, and O_2 .

Alkoxide-catalyzed coupling of silanes provides an alternate method for silane protection of alcohols that avoids expensive or hard-to-remove inorganic compounds by replacing them with common base alternatives. Weickgenannt and Oestreich developed a reactivity guide considering the protection of alcohols using potassium tertbutoxide, although low cost and stable hydroxides have also been shown to activate a wide variety of silanes [27]. Weickgenannt and Oestreich converted six alcohols to silyl-ethers using methyldiphenylsilane, $MePh_2SiH$, at room temperature over five hours. In each case, 100% conversion was observed with high yield of the isolated modified alcohol [15]. Weickgenannt and Oestreich also demonstrated the reactivity pattern of in silanes based on substituent group contributions. With ionic bases as catalysts, it is generally accepted that the silicon center undergoes nucleophilic attack [13, 15, 25], resulting in strong electron withdrawing groups (EWGs) increasing the reactivity of the silane significantly. The most reactive organosilanes recorded in literature are those with sp^2 carbons (mostly phenyl groups) bonded to the silicon; the degree of aromatic substitution is also important with reactivity order being $Ph_3SiH \approx Ph_2SiH > Me_2PhSiH$. As substituent volumes increase, steric impacts begin to significantly limit reactivity; large alkyl groups, such as t-butyl have been found to reduce reactivity significantly.

Charge density is well known strongly influence reactivity in systems with poor solvation stability of ions. This is reflected in silane chemistry where smaller cations react significantly slower, as

demonstrated by Grajewska and Oestreich who showed in one study that coupling of Ph_2SiH_2 with 3-phenyl-1,3-butane diol was successful using alkali carbonates with the reaction proceeded over 24 times faster with Cs_2CO_3 than with K_2CO_3 [14]. The atomic radii of Cs and K are 1.33Å and 1.69Å respectively resulting in significantly lower charge density in the Cs atom, a considerable aspect of tuning reactivity with ionic species [26].

Other basic species may also be used if they produce a corresponding hydroxide or alkoxide in the reaction system. Amines have been shown to be reasonable for the dehydrogenation reaction by Deka who identified triethylenetetramine as a means for the dehydrogenation of phenylated silanes in acetonitrile and water [28]. More recently Voronova completed NMR, FTIR, and UV-vis analysis on the dehydrogenation of phenyl silanes with 1,1,1,3,3,3-hexafluoro-2-propanol (HFIP) using triethylamine, Et_3N [29]. With the use of amines, kinetic analysis by Voronova found strong dependence of the observable rate constant and the ratio of silane:alcohol:amine in the system. For example, rate constant showed a well-defined maximum with relation to the amount excess alcohol added when amine and silane concentration were constant. Higher than 3 equivalents of HFIP in the system resulted in lower reaction rate, possibly due to coordination of the alkoxy base and excess alcohol, which prevented coordination of the base at the silicon center [29]. It is believed that the amine itself is not catalytic but deprotonates available alcohols and acts as the counter cation to the alkoxide base to promote the dehydrogenation. Voronova noted Et_3N concentration strongly increased the reaction rate but only up to the concentration of the reactive alcohol, likely due to protonation of the amine to make the true catalyst. With this, depletion of source alcohol for coupling can become a limiting factor in conversion. *In situ* IR monitoring found strong depletion of protonated amine over the course of the reaction, which supposedly indicated the reversion of alkoxide-protonated amine pair to alcohol and amine. The alcohol then is consumed by coupling with the silane.

Whether the active cation is an amine or alkali metal, base catalyzed dehydrogenation is generally considered to undergo a two-step process. Step one is silane activation by nucleophilic attack on the silicon atom to form a pentacoordinate intermediate, which then undergoes a dehydrogenation step with an available hydroxyl groups [25, 29].



A is the appropriate counterion in the above scheme. As a charged intermediate is required, the identity of the cation and anion (with ionic catalysts), solvation effects, and substituent group effects all have been shown to significantly alter reactivity. With the first step being rate limited, a pseudo-steady state assumption may be applied to the charged intermediate so that its concentration is constant and generally low when silane concentration far exceeds catalyst concentration.

Solvation effects play roles both as a means of stabilizing the charged silane intermediate species as well as interacting with the target hydroxyl carrying species. For example, Weickgenannt and Oestreich showed that the dehydrogenation of *Et*₃*SiH* with alcohols was not measurable in straight THF, however addition of DMF to THF in a 1:4 ratio facilitated the reaction nicely [15]. Similarly, pure DMF was able to activate *tBuMe*₂*SiH* dehydrogenation. Potassium tert-butoxide was used as the catalyst in both cases. The addition of DMSO, which acts as a supporting Lewis base, is believed to promote the Lewis acidity of the system silane, thus facilitating a more rapid reaction. These solvation effects are also apparent in amines as Voronova noted dehydrogenation rates of *Ph*₂*SiH*₂ with *HFIP* was 5.4 and 3.1 time slower in THF than in toluene and n-hexane respectively using *Et*₃*N* [29]. THF is believed to reduce the reactivity due to polar coordination of the solvent with either the reactive alcohol or the formed alkoxide as previously mentioned.

1.2.2 Stability and deprotection in silyl ethers

Deprotection of silyl ethers for hydroxyl protection is a broad topic with multiple guides and reviews available, which describe, in detail, the variety of silyl ether cleavage by acid, base, and fluorinated compounds [2, 30-33]. Because selection of deprotection conditions depends heavily on the system at hand, a brief overview of general trends is provided in this section.

Observation of the hydrolysis for methoxy silanes was first presented in the 1950's as a mechanism for the first ever synthesis of dimethylsilanediol [34], as other synthesis routes were inhibited by the rapid condensation of silanol groups. It was later confirmed that the hydrolysis of alkoxy silanes is catalyzed in both acidic and basic conditions [35] and that alkoxy silanes are stable and unreactive with water in non-glass containers with ultralow concentrations of ions [36].

Hydrolysis rates of silyl ethers and alkoxy silanes were observed to be heavily dependent on steric effects [37, 38]. For example, the hydrolysis rate of methoxy groups was 6-10 times faster than ethoxy silanes [36]. Increases in the size of substituents on the silicon atom or hydroxyl carrying carbon generally led to reduced cleavage rates. Modification of substituent electronegativity was another major factor for selective deprotection. In a basic environment, electron withdrawing groups promoted the rate of hydrolysis but the opposite was true under acidic conditions [30, 32]. Additionally, increased organic substitution, rather than alkoxy substitution, also improved reactivity. The reactivity rate was also affected strongly by electronic influences of other components present in the silane, shown when methacryloyloxyalkyl functionalized with a methyl spacer showed a significant increase in reactivity over a propyl spacer [38].

Solvent choice not only impact formation rates of silyl ethers but also on their rate of cleavage [37, 39], however these effects varied depending on whether hydrolysis occurred in acidic or basic conditions. Direct comparison of the hydrolysis of methyltriethoxyorthosilicate showed that reaction

rates increased in an order of MeOH > EtOH > dioxane > DMF. Finally, once hydrolyzed, the produced silanol groups were subject to polycondensation to form gel networks or other polymeric structures, which were more prominent under basic conditions.

1.2.3 Restrictions and limitations to silane protection of alcohols

Base catalyzed dehydrogenation of silane for the protection of alcohols must compete with unwanted side reactions which present limitations to yield in complex molecules. Revunova and Nikonov reviewed the mechanistic aspects base catalyzed reduction using silanes regarding unsaturated carbon-oxygen and carbon-nitrogen functional groups. Ketones, aldehydes, esters, aldimines, and amides all showed varying levels of reactivity towards a wide variety of silanes [40] with phenylated silanes as widely available methyl-hydro containing polysiloxane species used as hydrogen sources. At higher temperatures (80-165°C), Et_3SiH was used to reduce aryl-ethers to alcohols in the presence of tertbutoxide catalysts [41]. Silane addition was also observed on the aromatic ring in multiple positions, a trend that decreased with increasing temperature and decreasing silane and catalyst concentration. It is important to note that Revunova and Nikonov's study showed high conversion with no reported addition, not multiple species with aromatic rings. Coupling of silanes with amines has also been reported, catalyzed by a variety of alkaline-earth metal complexes [42, 43] and inorganic salts like copper(I) chloride [44] to form silazanes and other species. Deka speculated that silazane formation may cause the apparent lack of catalytic ability of several amines for the dehydrogenation of Ph_2SiH_2 , however no experimental data was published to support this claim. Specifically noted are the lack of activity in diethylamine and diisopropylamine. To the best of our knowledge, no major reviews revolving around selectivity of silyl ether formation and saturation of C-O and C-N pi bonds are available. Thus, alcohol protection via silane dehydrogenation may still be a viable option depending on structure and selectivity. Table 1.1 provides a summary of published functional groups that react with silanes in basic conditions.

Table 1.1: Base catalyzed reactions of hydrosilanes ($H - SiR_3$) with various functional groups. ^a Speculated by source, confirmation data not available. ^b Tertiary amides only; primary and secondary amides showed no reaction. ^c AR represents an aryl group

ID			Source
1		[13, 15, 28, 29]	
2		[28] ^a	
3		[40]	
4		[40] ^b	
5		[40]	
6		[41] ^c	

Despite the high activity of the base-silane system, row 6 in Table 1.1 requires significantly harsher conditions than the others. Selective reduction of unsaturated C-O bonds tends towards aldehydes over ketones, and ketones can be fully selected for over aldehydes. Alkenes, alkynes, epoxy, cyclopropyl, and halo groups all appear to be unfavored targets in silane-base systems [40], leaving broad room for application.

1.2.4 Dehydrogenation of dihydrosilanes and potential applications

Dihydrosilanes are species with two reactive hydrogen groups, which extend the utility of the dehydrogenation reaction outside of traditional alcohol protection. Many times, dihydrosilanes find use

as a reducing agent and as a radical transfer agent in a variety of systems [45] [46, 47]. With the emerging concept of silane protection of alcohols, dihydrosilanes have an obvious benefit of minimizing molar amounts of raw silane added to a system. Grajewska and Oestreich showed that the coupling of diphenylsilane in the presence of Cs_2CO_3 was capable of dual protection of diols, so long as they were not 1,2 diols. In the instance of 1,2 diols, two silanes reacted to form a 7 or more membered ring. More sterically hindered silanes, such as di-tert-butylsilane, showed no reactivity. It was also noted that diphenyl protected groups underwent hydrolysis over extended exposure on silica gel, signaling a facile removal process. Depending on the application and synthesis steps, the ease of hydrolysis may be encouraging to recover protected silanes, or an inhibition if the system promotes hydrolysis before it is desirable. Single protection of alcohols on multiple sites has also been demonstrated with HFIP [29] and benzyl alcohol[27], both of which were coupled with Ph_2SiH_2 in high yields. In the case of the former, where sampling throughout the experiment was robust, little to no accumulation of the once-oxidized silane, $Ph_2SiH - OR$, was observed. This low accumulation suggests steric inhibition may not be a significant inhibitor for silyl ether formation of Ph_2SiORH that is seen in sterically clustered species, like diphenyl tert-butylsilane, that prevent efficient linkages at hydroxyl sites.

Ph_2SiH_2 also showed rapid, facile synthesis of the cyclic siloxane, octaphenylcyclotetrasiloxane, Ph_8D_4 [28]. Traditionally, Ph_8D_4 is synthesized in a similar manner to other cyclic siloxanes: chlorosilanes are converted to silanols which undergo condensation, promoted by a catalyst. Removal of system water ensures the condensation reaction moves forward with relative ease and high yields. Likewise, silanes are synthesized from their chlorosilane analogs with treatment of $LiAlH_4$ or $NaBH_4$ as a hydrogen source [48]. Silanes offer an alternate method for Ph_8D_4 synthesis by conversion of silanes to silanols through dehydrogenation with water. Silanols then can undergo condensation or convert directly to the cyclic in the presence of stoichiometric amounts of water and silane.

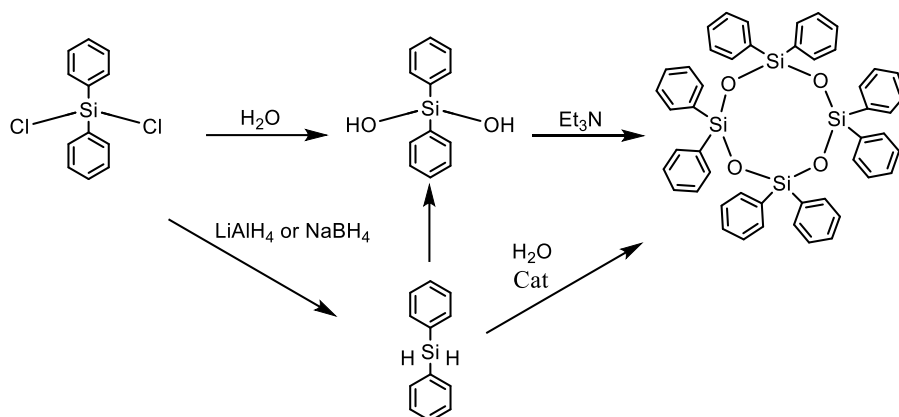


Figure 1.1: Synthesis routes for Ph_8D_4 .

Dehydrogenation of monohydrosilanes using triethylenetetramine in acetonitrile and water led to predominant formation of silyl ethers over silanols, suggesting strong selectivity of silanols over water during dehydrogenation [28], which may promote cyclic siloxane formation even in excess water environments. The dual active sites of dihydrosilanes can also be used as a coupling agent between diols, resulting in an organic siloxane co-polymer, as demonstrated with Ph_2SiH_2 and diols with lengths up to 1,10-decanol[28]. The sensitivity of the Si-O-C bond to hydrolysis may make these polymers attractive, since many siloxanes are considered biologically benign [49]. Similarly, a coupling effect of Ph_2SiH_2 may be attractive to PDMS systems with unwanted hydroxyl groups. Discussed in further detail in the next chapter, hydroxyl groups can be undesirable in the polymerization of PDMS. If not appropriately removed, these silanols will undergo condensation over time and increase the molecular weight and physical properties (*i.e.*, viscosity) of the polymers. In response, α, ω – *bissilanolates* can be employed. These straight chain oligomers are synthesized in small batches by ring opening polymerization of cyclic siloxanes with high concentrations of base catalyst, identical to the main polymerization mechanism. To get dual functionality and remove silanols, the reaction system must be designed to expel water and force condensation. Reviewed methods introduce a water azeotropic agent, such as cyclohexane, with a Dean-Stark trap with the optional addition of a purging gas (dry N_2) [50-53]. The condensation route is relatively

slow, and processing requires up to 24 hours for total removal of silanol. Since base catalysts used in the polymerization also activate dehydrogenation, terminal silanol groups can be actively and rapidly removed. This proposed process would possibly insert additional functionality to the polymer backbone. In the case of using phenylated silanes as coupling agents, phenyl groups are excellent suppressors of glass transition temperatures, and have been employed for ultra-low temperature environments [52].

1.3 Materials and methods

1.3.1 Materials

PhSiH₂ dehydrogenation was reviewed using a variety of alcohols, solvents, and catalysts. Table 1.2 below details materials purchased for all experiments. Unless otherwise noted, materials were used as received.

Table 1.2: Materials list

Material	Abbreviation	Purity	Source
Hydrochloric acid	HCl	1N, certified	Honeywell
Sodium hydroxide	NaOH	1N; certified	Fisher
Potassium hydroxide	KOH	>86.0%	Sigma
Tetramethylammonium hydroxide	TMAH	>97.0%	Sigma
Sodium tert-butoxide	NaOtBu	>97.0%	Sigma
Potassium tert-butoxide	KOtBu	>97.0%	TCI
Ammonium hydroxide solution	--	--	Sigma
Triethylamine	<i>Et</i> ₃ <i>N</i>	>97.0%	Fisher
N,N,N',N'-tetramethylethylenediamine	TMEDA	~99%	Sigma
Isopropylamine	IPrA	>99.0%	TCI
Diisopropylethylamine	DIPrEA	>99.0%	TCI
N,N-diisopropylethylenediamine	DIPrEDA	>97.0%	TCI
Diphenylsilane	<i>Ph</i> ₂ <i>SiH</i> ₂	>97.0%	Sigma
Octaphenylcyclotetrasiloxane	<i>Ph</i> ₈ <i>D</i> ₄	>98.0%	TCI
Tertbutanol	tBuOH	Certified grade	Fisher
Isopropyl alcohol	IPA	99%	Swan
Ethanol	EtOH	200 proof	Fisher
Tetrahydrofuran, inhibitor free	THF	>99.9%	Fisher
Dimethyl sulfone	DMSO	HPLC grade	Sigma
N,N'-bis(2,6-diisopropylphenyl)imidazole -2-ylidene n-heterocyclic carbene	CuIPr-NHC	--	Sigma

1.3.2 Procedure for ionic base catalyzed dehydrogenation

Catalyst solutions of sodium, potassium and tetramethyl ammonium hydroxides were prepared as aqueous stock solutions. Sodium hydroxide solution was diluted from 1N certified stock solution. Potassium hydroxide and TMAH solutions were prepared from solid crystal. Potassium hydroxide pellets were rinsed with 18 MΩ water to remove surface impurities (carbonates) before being dissolved in 18 MΩ. Freshly procured tetramethylammonium hydroxide (TMAH) pentahydrate crystal was dissolved directly into 18 MΩ water to form a stock solution. The stock solutions were titrated in triplicate using an

Orion pH probe against 1N certified HCl solution and diluted as necessary for use. KOtBu used as a catalyst was added to appropriate flasks by dry weight measurements.

Reaction flasks were flame dried, equipped with stir bar, stops, dry components, and charged with dry nitrogen before addition of dry THF stored over molecular sieves. The flask was submerged in a heated water bath ranging from 20-60°C and allowed to reach temperature before addition of silane and catalyst solutions. Aside from a hypodermic needle used for venting H_2 , the reaction flask remained fully sealed. Liquid components (catalyst solution, silane, water, or other solvents) were injected into the reaction flask via micropipette under nitrogen as needed.

Dehydrogenation of Ph_2SiH_2 was done using ethanol, isopropanol, and tertbutanol as representative 1°, 2°, and 3° alcohols at 43°C. tBuOH and EtOH systems were catalyzed by KOtBu concentration at 10.1 mM while IPA systems were catalyzed by KOtBu at 5.8mM. Ph_2SiH_2 (150 mM) was pipetted into the system with the alkoxide; the Si-H peak signal was allowed to stabilize before addition of the target alcohol to ensure no residual water existed in the system. All alcohols were stored over molecular sieves.

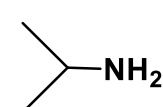
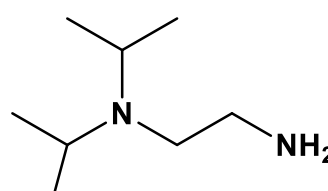
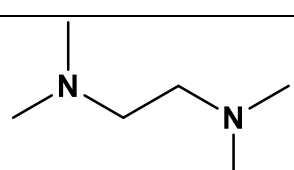
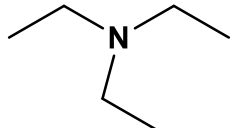
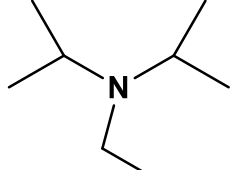
Hydroxide catalyzed systems were loaded with catalyst 1.73 mM for each of the three hydroxides, and additional data was collected at catalyst concentrations of 0.89 mM for TMAH and 0.74 mM for KOH. Ph_2SiH_2 was added in equimolar amount to the water loading level. At these dilute loadings, volume changes by the oligomerization of Ph_2SiH_2 , temperature changes due to the exothermicity of the reaction, and phase separation between water and silane phases were negligible.

1.3.3 Procedure for amine catalyzed dehydrogenation

Six amines with varying levels of alkyl substitution were investigated, as shown in Table 1.3. Experimental setup and material handling followed the same process as hydroxide and alkoxide catalyzed systems described above. Catalyst, Ph_2SiH_2 , and water were added to THF in concentrations

of 80 mM, 250 mM, and 620 mM respectively. Excess water was added to the system to ensure moderate levels of active hydroxide catalyst to facilitate the reaction. System temperature was maintained at 43°C by a heated bath for each experiment.

Table 1.3: Amine catalysts reviewed in this study.

ID	Structure
1	NH_3
2	
3	
4	
5	
6	

1.3.4 Procedure for CuIPr-NHC catalyzed dehydrogenation

Experimental setup and material handling followed the same process as hydroxide and alkoxide catalyzed systems previously described. Solutions of CuIPr-NHC catalyst with base activator were prepared in and mixed for a minimum of 15 minutes prior to addition to the reaction system; all catalyst solutions were used same-day as their preparation. Flame dried reaction flasks charged with dry nitrogen headspace were used in all catalyst solution preparations. Dehydrogenation reactions of Ph_2SiH_2 was done with water and several alcohols as hydroxyl sources.

Experiments where water provided hydroxyl sources used aqueous KOH, rather than an alkoxide, as the base activator. This was done to prevent the alkoxide species decaying into unwanted alcohols but did not inhibit observed reactivity of CuIPr-NHC. The overall concentration of CuIPr-NHC in

the system was 1.85 mM with KOH added at 0.79 mM. Excess CuIPr-NHC was done to ensure the base was fully complexed and that effects of complex were observed rather than dehydrogenation by KOH alone. It should be noted that CuIPr-NHC alone was found to have no effect on Ph_2SiH_2 in the absence of a base activator and excess CuIPr-NHC was not expected to impact results.

Stock solution of CuIPr-NHC (15 mM) was prepared in THF with KOtBu (10 mM) and as the base activator for dehydrogenative coupling with alcohols. KOtBu was chosen to replace KOH as the base species to reduce potential for water contamination. Reaction flasks were flame dried and purged with dry nitrogen, then loaded with dry THF and catalyst solution (1.4 mM by KOtBu concentration) and heated to 40°C. Ph_2SiH_2 was added and the Si-H bond peak at 844 cm^{-1} was monitored for stability prior to addition of alcohols, which indicated no residual water was present in the system. EtOH, IPA, and tBuOH were again used as representative alcohols.

1.3.2 Reaction monitoring, data treatment, and product confirmation

Reaction temperature and concentrations were monitored real-time by a Mettler Toledo ReactIR702L FTIR equipped with DiComp probe tip from 750 to 3000 cm^{-1} . Concentration of the Si-H bond is monitored at 844 cm^{-1} and 2140 cm^{-1} . Absorbance corresponding to the Si-O linkages is primarily monitored by twin peaks between $1100\text{--}1160\text{ cm}^{-1}$. These peaks have little interference from other components and low dependence on siloxane structure (linear or cyclic). To ensure proper concentration of Ph_2SiH_2 loading, net concentration is monitored by the peak at 1428 cm^{-1} , corresponding to the phenyl moiety. This peak is unaffected by the oxidation of the silicon atom and does not experience interference with other peaks.

Calibration data for Ph_2SiH_2 and Ph_8D_4 of absorbance versus concentration of each peak are available in the Appendix. A temperature correction curve was developed with a sweep of 20°C-60°C, also

available in the Appendix. Absorbance data is corrected for temperature and converted to concentration prior to fitting to appropriate kinetic models.

Where applicable, concentrations were determined using peak heights by the two-point baseline method. In instances of significant peak overlap, deconvolution was used to provide best estimate of absorbances. Deconvolution was done using Python's LMFIT package by applying least squares estimation of spectral data to compound models. Figure 1.2 below demonstrates a deconvolution fit of experimental FTIR data using a three peak compound model and linear baseline.

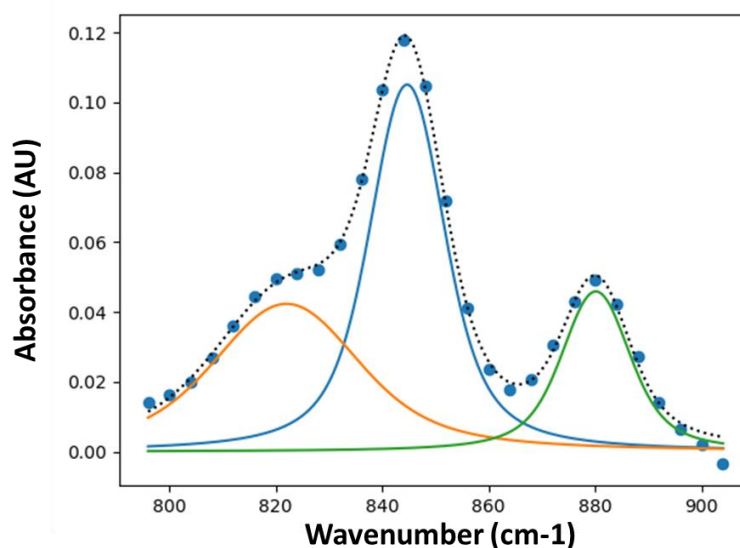


Figure 1.2: Example deconvolution for a three peak spectral window using Python's LMFIT package.

These compound models contain a peak for each component in the spectral window and a linear model to offset drift in the spectra baseline. Voigt models were used to fit the underlying absorbance peaks. Voigt peaks are a convolution of a Gaussian and Cauchy-Lorentz distribution defined by the following equations where $erfc$ is the error function, A is the peak amplitude, μ is the peak center, σ as the characteristic width. The parameter γ was constrained to the value of σ for all model fits.

$$f(x; A, \mu, \sigma, \gamma) = A \frac{Re[w(z)]}{\sigma\sqrt{2\pi}} \quad 3$$

$$z = \frac{x - \mu + i\gamma}{\sigma\sqrt{2}} \quad 4$$

$$w(z) = e^{-z^2} \operatorname{erfc}(-iz) \quad 5$$

Least squares fitting of needed peaks requires fitting of the values $A, \mu, \sigma,$ and γ . At constant environmental conditions (*i.e.* temperature and solvent), the latter three parameters are expected to be constant throughout an experiment with little change to bonding environment, except for slight variations from instrument noise. Parameter selection for $\mu, \sigma,$ and γ was done by fitting a compound model to the average of all spectra in the time domain. These values were then applied to each measurement in the time domain with baseline and peak height variables freely fitted.

Base catalysts were neutralized using 1M HCl prior to product purification. Products were separated from solvents by a Rotovap system. Solid crystalline products were collected, rinsed twice with acetone, and identified by determination of triclinic crystalline structure. Liquid products, such as alkoxyated silanes, probed by ^1H NMR in CDCl_3 using an Avance AVIII 500 MHz spectrometer.

1.4 Results and discussion

1.4.1 Steric inhibitions in Ph_2SiH_2 dehydrogenation

To understand limitations with regards to Ph_2SiH_2 dehydrogenation, silyether formation was done with primary, secondary, and tertiary alcohols. The reaction between Ph_2SiH_2 and tBuOH with KOtBu was complete in less than one minute with a new peak apparent at 824 cm^{-1} indicating formation of diphenyltertbutoxysilane. The peak at 824 cm^{-1} was stable and did not undergo further decay even with excess alcohol added. For unknown reasons, the peak at 844 cm^{-1} showed a decrease in peak height to only 30% of its original value. To check reactivity of the newly formed silane, anhydrous ethanol was added to the system, leading to full consumption of both peaks at 844 and 824 cm^{-1} over several minutes.

This indicates activity of the silane's to primary alcohols even with the tertbutoxy functionality. ^1H NMR Singlet peak corresponding to the t-butoxy hydrogens was lower than expected. Instead, the ratio of phenyl hydrogen matched the signal mostly ratios expected for diethoxydiphenylsilane. The first dehydrogenation step towards tBuOH is readily done, but addition of the primary alcohol may have led to a substitution of the tertbutoxy group to the ethoxy group.

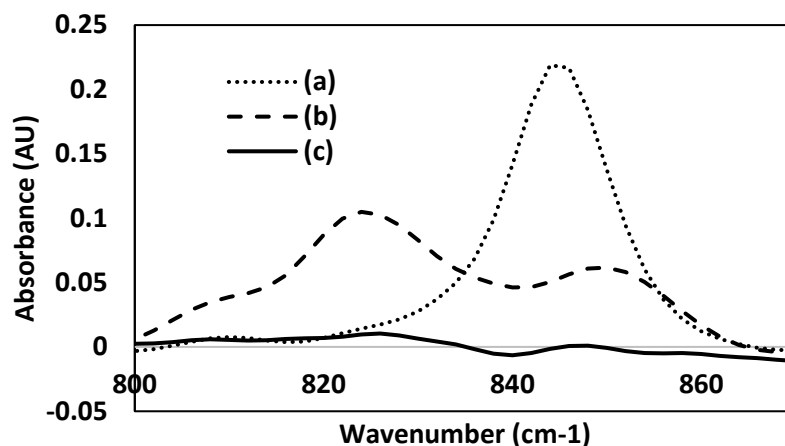


Figure 1.3: IR spectra of the Si-H bond during KOTu catalyzed dehydrogenation of Ph_2SiH_2 (a) prior to alcohol addition (b) after addition of excess tBuOH with two peaks corresponding to diphenyl tertbutoxy silane (c) after further addition of anhydrous EtOH.

With dehydrogenation apparently limited to only one hydrogen site when working with tertiary alcohol protection with large catalysts, it is necessary to determine if this effect is also significant in secondary alcohols. Reaction of Ph_2SiH_2 with anhydrous IPA showed rapid decay of the Si-H peak at 844 cm^{-1} and subsequent growth of a peak at 824 cm^{-1} that indicated diphenylisopropoxysilane accumulation in moderate amounts. Unlike the reaction with tBuOH, the once-alkoxylated silane was able to readily undergo the second dehydrogenation step and fully decay with time. Using the deconvolved peak heights, shown in Figure 1.4, rate constants for the first and second dehydrogenation step were estimated by assuming a first-order reaction in silane and zero-order reaction in alcohol.

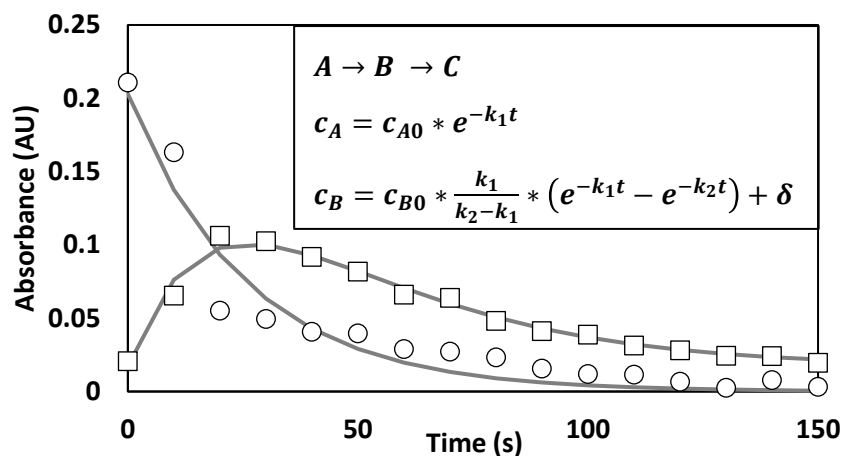


Figure 1.4: Si-H bond measurements via FTIR for the stepwise dehydrogenation of Ph_2SiH_2 with IPA with $KOtBu$ catalyst (\circ) Ph_2SiH_2 signal at 844 cm^{-1} (\square) isopropoxy diphenyl silane signal at 824 cm^{-1} . Solid lines indicate fitted models. Scaling factors were applied to model fits to account for measurement delay. δ accounts for a non-zero asymptotic value observed in the spectra post-alcohol addition.

The assumption of first-order models proves to be a good estimate for the system. A rate constant ratio of $\frac{k_2}{k_1} = 0.95$ is estimated, indicating near similar selectivity between the original silane and the once-oxidized silane. This represents a drastic improvement over addition to tertiary alcohols where only one hydrogen site is accepting of bond formation.

1.4.2 Catalytic activity of hydroxides

Reaction rate in silane couplings with alcohols and other hydroxyls has been shown to be strongly dependent on the cation identity of the ionic catalyst used but no direct studies of kinetics and observable rate constants comparing different cations have been presented [14]. It should be noted that while solvent selection will have significant impact on the reaction rates, it is still beneficial to compare the relative kinetics of each cation and whether certain cations lead to different rate models or selectivity to the two reactive hydrogen sites. Understanding the cation effects does not apply only to the examples highlighted in this study but extends into many other applications of silane dehydrogenation. Effects of cation identity

in sodium, potassium, and tetramethyl ammonium hydroxides are explored using FTIR monitoring for the dehydrogenation of Ph_2SiH_2 water to produce Ph_8D_4 , and important additive to polysiloxane systems.

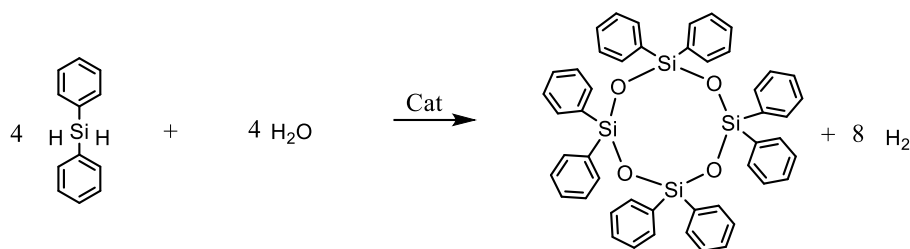


Figure 1.5: Ph_2SiH_2 forming Ph_8D_4 in the presence of water.

Dehydrogenation of Ph_2SiH_2 occurred smoothly for each catalyst with no peak interference for monitoring Si-H bond decay at the 844 cm^{-1} peak. For each hydroxide, once-oxidized silanes ($RO - Ph_2SiH$), created no meaningful signal and were not readily detectable from signal background. This contrasts with the KOtBu-alcohol systems previously discussed and indicated that the once-oxidized silane will much more readily undergo dehydrogenation compared to the original. This is an observation that also agrees with other work using phenylsilanes [29]. Addition of hydroxide salts to the THF system initially formed a slightly turbid solution, which indicated the precipitation of the salt from solution. However, the system cleared in only a few seconds likely indicating binding to the silane described in Eq 1.

Once the reaction had reached completion, the collected crystal product was separated from solvent and analyzed by XRD with triclinic structure ($a = 10.7188\text{ \AA}$; $b = 10.7707\text{ \AA}$; $c = 19.1412\text{ \AA}$; $\alpha = 83.760^\circ$; $\beta = 83.067^\circ$; $\gamma = 76.140^\circ$) matching structures of Ph_8D_4 available in literature[21, 54]. IR spectra was also matched to a reference sample of Ph_8D_4 .

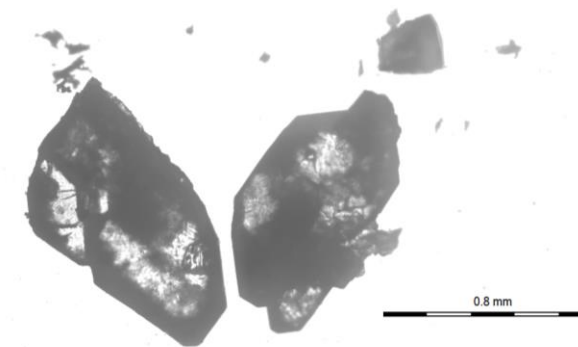


Figure 1.6: Brightfield microscope image of Ph_8D_4 crystals as collected product.

Response to catalyst loading level was varied to confirm the linear response that is expected from literature. TMAH catalyst was added to the system at five different dilution levels with at least two trials per dilution level; total system hydroxide concentration was maintained below 1 mM. As expected according to the first-order rate-limiting step of Eq1, variation with catalyst concentration was linear and first-order response was seen, even though excess water was not added to the system. It was also noted a non-zero intercept was determined by the linear regression, which may indicate some interference from the THF used.

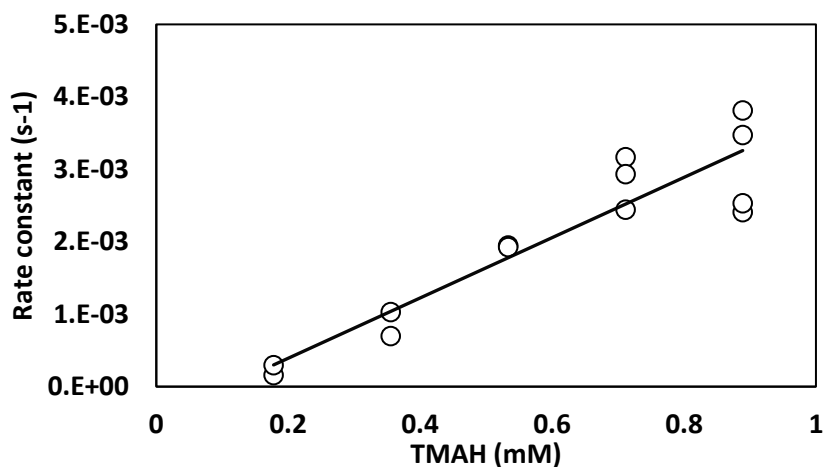


Figure 1.7: Observed rate constants for a first-order model in the dehydrogenation between Ph_2SiH_2 and water catalyzed by TMAH.

TMAH and KOH catalyzed systems maintained a first-order response to silane concentration and zero order response to water concentration when silane and water were in equivalent molar amounts, even as reaction extent approached completion. In select experiments, a check for residual water was done at the end of data collection by dosing the reaction system with excess Ph_2SiH_2 after the original reaction had gone to completion and monitoring for any additional Si-H peak decay; no major decay was observed in each instance. For each trial where KOH and TMAH were used as the catalyst, effective rate constants were fit using least square estimation by conversion of the first-order model to linear form. Temperature response was similar among both hydroxide types, suggesting there may be minimal

observable mechanistic change based on the cation identity. Because of this, rate constants estimated for the four sets of data were combined for Arrhenius modeling to estimate a single shared value for the activation energy of the reaction. This was accomplished by dividing each rate constant by its preexponential factor and completing linear regression based on the linear form of the Arrhenius model.

$$\ln\left(\frac{k}{A}\right) = -E_a/RT \quad 3$$

With k and A being the observed rate constant and preexponential factors respectively. E_a/R is the activation energy scaled by the gas constant and T is the temperature in Kelvin. For comparison, values of the preexponential factor were divided by catalyst concentration and reported with units of $\frac{L}{mol*s^{-1}}$. TMAH was much faster than KOH with a preexponential factor 16.9 times higher than KOH's.

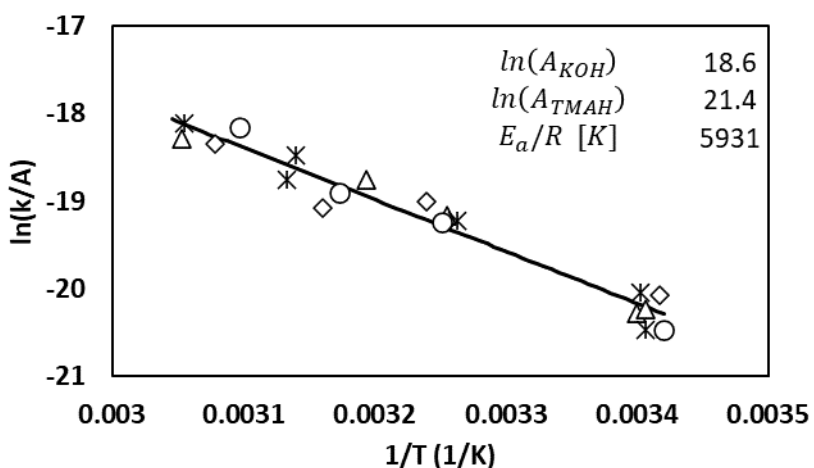


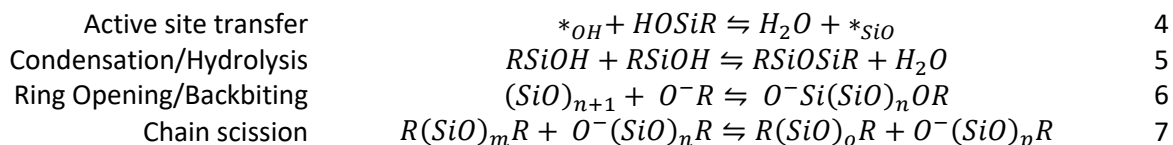
Figure 1.8: Arrhenius plot (N=19) for the dehydrogenation of Ph_2SiH_2 catalyzed by (\diamond) TMAH at 1.73mM and (*) TMAH at 0.88mM (\circ) KOH, 1.73mM (Δ) KOH, 0.74mM. Preexponential parameters shown are scaled by the molar loading concentration [L/mol*s]. E_a/R %RSE of 5.3%.

NaOH did not display clean first-order kinetics. Instead, when water and silane were present in equimolar amounts, the response was nearly second-order near 20°C and first-order at temperatures

above 50°C. First-order response in silane was also seen at all temperatures when 10x excess water was used in the system. A comparison between an observed reaction profile at 20°C with excess water and stoichiometric equivalent water is shown in Figure S5 and only pseudo-first-order responses to silane have been previously been described in literature. If the reaction step between the pentacoordinated silicon and a hydroxyl group (Eq 2) is not sufficiently fast compared to the rate of formation of the pentacoordinated silicon (Eq 1), an observed deviation from first-order response is expected because of failure in the quasi-state state approximation. Response to temperature was observed by addition of 10x excess water for the dehydrogenation to silane reaction, with observable rate constants based on a first-order model. The reaction showed a clear linear response as indicated by Eq 3, which suggests a single limiting reaction dominates the temperature response at these conditions. Likely, an order-of-magnitude increase in the concentration of available hydroxyl groups increased the reaction rate of the hydrogen evolution reaction (Eq 2) sufficiently past the rate of pentacoordination (Eq 1) so that the later becomes the rate limiting step. As further evidence for this, Arrhenius treatment of the data performs very well ($r^2 = 0.9956$) when the activation energy is fixed to the value determined with the other two hydroxides. This treatment estimates an $\ln(A_{NaOH})$ value of 18.69, or nearly identical to the value determined using KOH. This is a rather surprising result given that decreased cation charge density typically results in an increase in reaction rate, generally suggesting the potassium cation would lead to higher reaction rates.

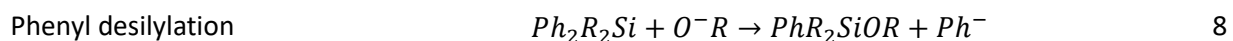
To ensure experimental observations and the historically proposed mechanism align, kinetic equation derivation was conducted using Eq 1 and Eq 2 to explain the mechanistic aspects. However, derivation was done using two different approaches. In the first approach, Eq1 was assumed to be rate limiting and significantly slower than Eq 2. This aligns with historic studies using hydroxide catalysts and correlated to a pseudo-first-order reaction in terms of silane concentration [13, 25]. However, this study has demonstrated the sodium ion does not always lead to this result, indicating a different rate limiting step. The second derivation was done by assuming Eq2 was rate limiting and Eq1 was in equilibrium.

Several considerations apply to both kinetic models. First, cyclic and linear oligosiloxanes being formed in the presence of a strong base opens reaction conditions to side reactions seen in polysiloxane systems. These general reactions are expressed in Eq 4-7 below; diphenyl designation is assumed for each silicon atom and is only removed to improve clarity to the reader.



The * in Eq 4 is shorthand for the active catalyst site, with $*_{OH}$ equivalent to a hydroxide anion and $*_{SiO}$ equivalent to a silanolate anion. This nomenclature is convenient for evaluating kinetic expressions later in this study.

Next, work by Zlatnic *et al.* showed evidence for siloxane branching at diphenyl centers by removal of a single phenyl group, thus introducing the possibility of forming T-branched structures in polysiloxanes and another side reaction that may impact kinetic models[52].



This process was monitored by the phenyl peak of the siloxane species at 1428 cm^{-1} , but no significant changes were seen in this peak leading to the conclusion that this reaction is negligible in the existing systems studied.

Finally, there are a variety of species present in the system at any given time. The once-oxidized silane (diphenyl silanol, $HO - Ph_2SiH$) and hydride terminated oligosiloxanes ($H - (Ph_2SiO)_nH$) can provide hydrogen sources that are differentiable from Ph_2SiH_2 . Hydroxyl sources come from water, diphenylsilanol, diphenylsilanediol, and hydroxyl terminated oligomers. Demonstrated prior, steric effects

play a strong role based on the hydroxyl group as well as the silane. However, the Si-O bond length is longer than the C-O bond length reviewed with alcohols. In addition, electronic effects may also play a role. Table 1.4 summarized all the species that, at first glance, may affect system kinetics and modeling.

Table 1.4: Expected reactive species in a water-silane system.

Hydrogen Source	Hydroxyl Source
Ph_2SiH_2	H_2O
$HO - Ph_2SiH$	$HO - Ph_2SiH$
$H - (Ph_2SiO)_nH$	$HO - Ph_2SiOH$
	$HO - (Ph_2SiO)_nH$

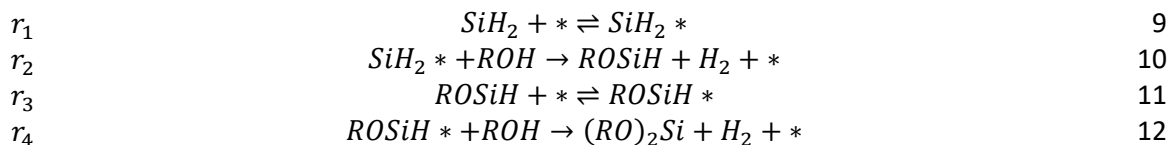
As mentioned, there was no measurable accumulation sources outside of Ph_2SiH_2 , indicating other hydrogen sources act as quasi-steady state assumption (QSSA) species. The QSSA indicates that the concentration of $HO - Ph_2SiH$ and $H - (Ph_2SiO)_nH$ were constant. Clean first and second-order responses were frequently seen in the collected data even as cyclic siloxane structures were produced. This may suggest that hydroxyl source variation had minimal effect on kinetic rates for this system. Because of this, hydroxyl sources will be assumed indistinguishable from each other and instead be described as a net sum dedicated by ROH . This assumption also significantly simplifies accountability for the condensation and hydrolysis reaction.

Given the above points, two assumptions are applied to evaluate the system kinetics based on the observed data.

- I. The catalytic activity in the system is essentially constant so that Equation 4 has no effects on observed rate
- II. All necessary reaction steps are elementary and first-order with respect to participating species

Under Assumption I, the active catalysts species as a silanolate ($*_{SiO}$) or as a hydroxide ($*_{OH}$) are either indistinguishable or exist only in one form which can be written as $*$ instead. Now the rate limiting

step in Eq 1 can be rewritten. In the following derivation, diphenyl substituents on the silicon center are implied but removed for readability. There are four main reactions that will be used to describe the system, a simplification made by condensing the species in Table 1.4. The hydrogen evolving reactions are written as irreversible by assuming H_2 is readily vented from the system and retained in negligible amounts.



Derivation of the first condition is now applied. The rate limiting step is the formation of the pentacoordinated silicon species and is much slower than the Si-O bond formation step. The ensuing kinetics put focus on the rate of consumption of Ph_2SiH_2 only, since once-oxidized species were below detection limit.

$$\frac{d[SiH_2]}{dt} = -k_1[SiH_2][*] + k_{-1}[SiH_2 *] \quad 13$$

k_1 and k_{-1} are the rate constants for the forward and reverse reaction, respectively. Since $SiH_2 *$ can react with any hydroxyl-containing species in Table 1.4, the reaction rate is the sum of reactions with all hydroxyl species with an n_i reaction order. Again, these hydroxyl species are assumed indistinguishable in the determination of reaction rate and are combined for simplicity.

$$\frac{d[SiH_2 *]}{dt} = k_1[SiH_2][*] - k_{-1}[SiH_2 *] - k_2[SiH_2 *][ROH] \quad 14$$

By assuming that the species $[SiH_2 *]$ is rapidly consumed in the second reaction step, the QSSA may be applied, its accumulation can be considered negligible, and its derivative is zero. The species concentration can be solved to get Eq 15.

$$[SiH_2 *] = \frac{k_1[SiH_2][*]}{k_{-1} + k_2[ROH]} \quad 15$$

The amount of free catalyst can be solved for using a site balance of all bound and unbound species.

$$[*]_{tot} = [*] + [SiH_2 *] + [ROSiH *] \quad 16$$

$[ROSiH *]$ is evaluated in the same manner as Ph_2SiH_2 in Eq 13-15. The QSSA is applied so the net accumulation 0 and species concentration is solved. This evaluation will be considered in terms of moles of reactive groups rather than moles of actual hydride containing siloxanes, which avoids complications in accounting for condensation and hydrolysis reactions that form oligomers, which are not within the measurable range of the instrument in use.

$$\frac{d[ROSiH *]}{dt} = k_3[ROSiH][*] - k_{-3}[ROSiH *] - k_4[ROSiH *][ROH] \quad 17$$

$$[ROSiH *] = \frac{k_3[ROSiH][*]}{k_{-3} + k_4[ROH]} \quad 18$$

Substitution of Eq 15 and 18 into the site balance of Eq 16 yields Eq 19. The total number of sites is simply the amount of catalyst initially added to the system; solving for free catalyst $[*]$ is now possible. Substituting in the definitions for $[*]$, $[SiH_2 *]$ into Eq 13 with minor simplification leads to a final equation that can be used for monitoring the consumption rate of Ph_2SiH_2 .

$$[*]_{tot} = [*] + \frac{k_1[SiH_2][*]}{k_{-1} + k_2[ROH]} + \frac{k_3[ROSiH][*]}{k_{-3} + k_4[ROH]} \quad 19$$

$$[*] = \frac{[*]_{tot}}{1 + \frac{k_1[SiH_2]}{k_{-1} + k_2[ROH]} + \frac{k_3[ROSiH]}{k_{-3} + k_4[ROH]}} \quad 20$$

$$\frac{d[SiH_2]}{dt} = -k_1[SiH_2] \left(\frac{[*]_{tot}}{1 + \frac{k_1[SiH_2]}{k_{-1} + k_2[ROH]} + \frac{k_3[ROSiH]}{k_{-3} + k_4[ROH]}} \right) \left(1 - \frac{1}{1 + \frac{k_2}{k_{-1}}[ROH]} \right) \quad 21$$

With the QSSA assumption and assuming the values $k_1[SiH_2] \ll k_{-1} + k_2[ROH]$ and $k_3[SiH_2] \ll k_{-3} + k_4[ROH]$ for sufficiently large concentrations of hydroxyl groups, this will push $\frac{k_1[SiH_2]}{k_{-1} + k_2[ROH]}$ and $\frac{k_3[ROSiH]}{k_{-3} + k_4[ROH]}$ close to zero and give rise to Eq 22.

$$r_{obs} = \frac{d[SiH_2]}{dt} = -k_1[*]_{tot}[SiH_2] \left(1 - \frac{1}{1 + \frac{k_2}{k_{-1}}[ROH]} \right) \quad 22$$

As $\lim[ROH] \rightarrow 0$, then the last term approaches zero, ultimately reducing the net rate to zero as expected. In instances where the concentration of free hydroxyls is sufficiently high or $k_2/k_{-1} \gg 1$, Eq 22 reduces to an approximately first-order expression in terms of $[SiH_2]$, which is easily integrated to a concentration curve. This first-order response agrees with the observed rate order in this study and predominantly agrees with previous works on the subject.

$$\frac{d[SiH_2]}{dt} = -k_{eff}[SiH_2] \quad 23$$

$$k_{eff} \approx k_1[*]_{tot} \quad 24$$

$$[SiH_2] = [SiH_2]_0 \exp(-k_{eff}t) \quad 25$$

Now derivation of the observed rate is based around r_2 being the rate limiting step. As described, an observed rate order of 2 was observed with stoichiometrically equivalent amounts of water and silane with NaOH as the acting catalyst.

$$r_{obs} = k_{obs}[SiH_2][ROH] \quad 26$$

The assumption made to evaluate this condition is that Eq 1 will be assumed to be in equilibrium. With rearrangement, the pentacoordinated species can be solved for and the determined value can be substituted into the rate limiting equation r_2 .

$$\frac{r_1}{k_{-1}} \approx 0 = \frac{k_1}{k_{-1}} [SiH_2][*] - [SiH_2 *] \quad 27$$

$$[SiH *] = \frac{k_1}{k_{-1}} [SiH_2][*] \quad 28$$

$$r_2 = k_2 [SiH *][ROH] = \frac{k_2 k_1}{k_{-1}} [SiH_2][*][ROH] \quad 29$$

Given the site balance of Eq 16, a definitive expression for $[ROSiH *]$ is needed, which comes from evaluating r_3 and r_4 in a similar manner to r_1 and r_2 . The site balance for the catalyst species is then easily evaluated.

$$\frac{r_3}{k_{-3}} \approx 0 = \frac{k_3}{k_{-3}} [ROSiH][*] - [ROSiH *] \quad 30$$

$$[ROSiH *] = \frac{k_3}{k_{-3}} [ROSiH][*] \quad 31$$

$$[*_{tot}] = [*] \left(1 + \frac{k_1}{k_{-1}} [SiH_2] + \frac{k_3}{k_{-3}} [ROSiH] \right) \quad 32$$

$$[*] = \frac{[*_{tot}]}{1 + \frac{k_1}{k_{-1}} [SiH_2] + \frac{k_3}{k_{-3}} [ROSiH]} \quad 33$$

Substitution of the catalyst species into Eq 26 gives the final rate equation.

$$r_2 = \frac{k_2 k_1 [*_{tot}]}{k_{-1} \left(1 + \frac{k_1}{k_{-1}} [SiH_2] + \frac{k_3}{k_{-3}} [ROSiH] \right)} [SiH_2][ROH] \quad 34$$

If the ratios k_1/k_{-1} and k_3/k_{-3} are sufficiently small or the system operated with low concentration of silane, then an observable rate order of 2 will be seen. This is a similar simplification done with Eq 22.

$$r_2 = k_{obs} [SiH_2][ROH] \quad 35$$

$$k_{obs} = \frac{k_2 k_1 [*_{tot}]}{k_{-1}} \quad 36$$

These derivations confirm that first and second-order responses may be seen by applying the same mechanism to Ph_2SiH_2 but altering the rate limiting step. With this, discrepancy in rate order seen that is instigated by the sodium cation compared to the potassium and tetramethylammonium cations is readily explained.

For direct validation that the NaOH system is described by Eq 22 at higher temperatures, experimental data were collected with silane in excess to water at temperatures of 50°C. This removed uncertainty in hydroxide or water concentrations because these values can be back calculated by the Si-H bond signal. That is, the reaction reaches a plateau in the Si-H IR signal indicating full water consumption. A differential equation solver was used to find optimal rate constants for Eq 22 and Eq 35, with a parity plot of the two models versus the measured silane concentration shown below. Eq 35 describes the data set incredibly well while Eq 22 is lacking.

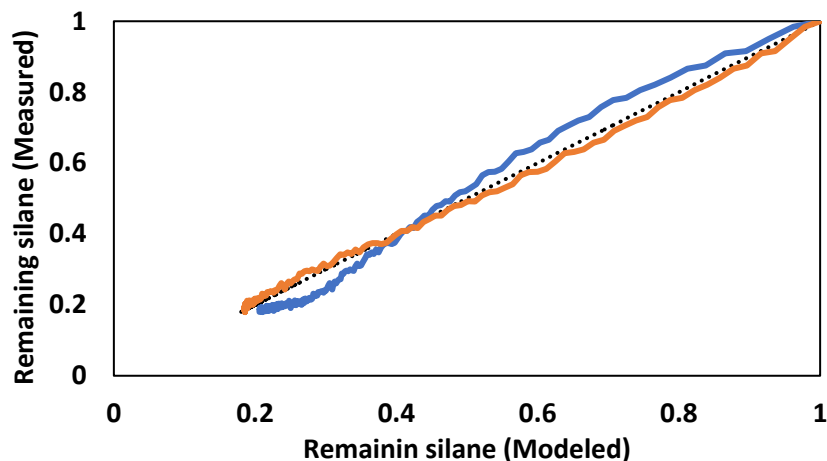


Figure 1.9: Parity plot of remaining extent of reaction for Ph_2SiH_2 consumption at $50^\circ C$ with excess silane for (black, dotted) 1:1 plot of experimental data (orange) best fit model using Eq 35 (blue) best fit model using Eq 22. Data is scaled to a maximum of 1.

The change between the best descriptive kinetic model is a strong indicator that the hydrogen release reaction is rate limiting at low temperatures and low concentrations of reactive hydroxyl groups, but silane activation by the base catalyst becomes rate limiting at higher temperatures and hydroxyl concentrations.

1.4.3 Catalytic activity of amines

Hydroxide-based catalysts showed high activity for the formation of Ph_8D_4 with little to no measurable accumulation of once-oxidized silane. This category of catalysts may be difficult to implement, however, due to low solubility of these salts in organic solvents without silane, difficult removal of solid product (such as in Ph_8D_4 synthesis), and hygroscopicity of the solid powder. Amines have also been used to promote the dehydrogenation reaction with good success, offer good solubility, can be more readily removed from solid product, and are commercially available. Previous reports have noted distinctly lower catalytic ability in primary and secondary amines [28], but general surveys of catalytic activity have not, to our knowledge, been made available.

Except for ammonium, which has significantly decreased basicity compared to alkyl substituted amines, each of the amine catalysts was able to catalyze the dehydrogenation reaction, with peak growth in the 1100 cm^{-1} region indicating new Si-O bond formation. In stark contrast to the hydroxide catalysts, all amine catalysts showed moderate accumulation of the second peak near 824 cm^{-1} corresponding to $RO - Ph_2SiH$. Peak deconvolution was used to separate the signals of Ph_2SiH_2 and $HO - Ph_2SiH$ for analysis with Ph_2SiH_2 showing multiple reaction patterns that may possibly be indicators of more complex reaction mechanisms than previously reported. Particularly, amine 6 showed a long induction period of low reactivity followed by increased reaction rate, a pattern that repeatedly evolved when the experiment was completed in triplicate. This amine was also by far the slowest, taking over 6 hours to reach 50% conversion and over 15 hours to reach completion.

Amine 2 was the only catalyst to demonstrate 2nd order behavior, an interesting observation given that water was present in excess. Amines 3, 4, and 5 all demonstrated first-order behavior in silane for the majority of the reaction but plateaued to non-zero asymptotic values (Figure S6). While some crystalline Ph_3D_4 product could be recovered, some residual material after solvent and catalyst removal was non-crystalline and likely included siloxane oligomers and residual amine.

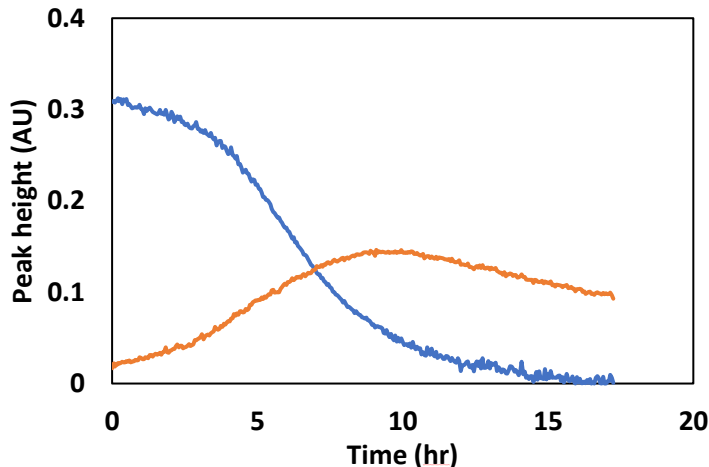


Figure 1.10: Ph_2SiH_2 (blue) and OR – Ph_2SiH (orange) time-series absorbances for Ph_2SiH_2 dehydrogenation with water catalyzed by amine 6. Peak height absorbances are not directly comparable due to differences in molar absorptivity.

Rate constants for the first and second dehydrogenation reaction were calculated to compare reactivity of amine catalysts (Table 1.5). Estimates for k_1 using amines 3, 4, and 5 were calculated using data between 0-75% consumption of Ph_2SiH_2 for each amine to avoid non-zero asymptote values given by the deconvolution.

Table 1.5: Observed first-order rate constants for Ph_2SiH_2 dehydrogenation with water to form OR – Ph_2SiH . Constants were calculated using extent of reaction from 0-75% in each case. (a) modeled with 2nd order observed model, units s^{-1}/M (b) modeled with 1st observed order, units s^{-1} .

Amine ID	$k_1, * 10^4$	r_1^2	$k_2 * 10^4$	r_2^2	k_2/k_1
2 ^a	7.61	0.993	6.60	0.972	0.86
3 ^b	8.05	0.997	11.30	0.992	1.40
4 ^b	4.94	0.999	1.56	0.994	0.32
5 ^b	2.59	0.999	0.87	0.991	0.34

Amines 3 and 4 showed the highest reactivity likely because they are diamines and have effectively twice the molar concentration of basic component. The effect of substituting the methyl groups to ethyl groups from amines 4 to 5 seemed to have little impact on site selectivity as rate constants k_1 and k_2 were essentially halved between the diamine and the amine. Amine 2 reacted significantly slower than the rest, likely resulting from the non-first order reaction profile observed.

Comparing 2 to amine 4 may suggest that increased alkyl substitution may improve reactivity, although side reactions such as silazane formation, should be reviewed in more detail. The addition of increasingly large alkyl groups also likely led to some steric inhibition in the steady state concentration of the active catalyst, which would explain the induction period present in amine 6.

To determine if the selectivity of towards one hydrogen site compared to hydroxide salts is primarily a steric effect, dehydrogenation with Et_3N was repeated in a more polar environment. The original THF solvent was replaced with a 4:1 mixture of THF and DMSO. Observed rate of the Ph_2SiH_2 peak remained essentially constant: $2.7 \times 10^{-4} s^{-1}$ vs $2.54 \times 10^{-4} s^{-1}$ for THF/DMSO and DMSO respectively. However, the secondary hydrogen peak was dramatically affected by the solvent change.

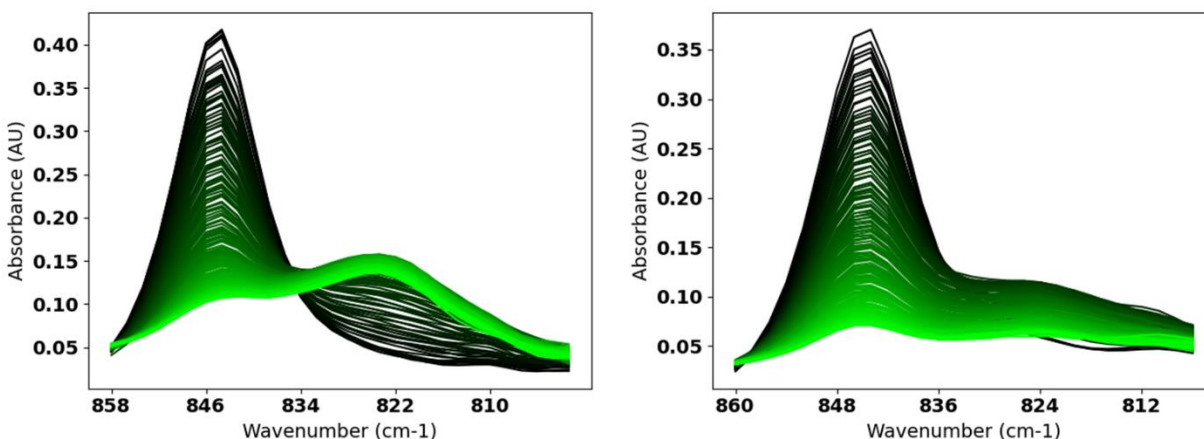


Figure 1.11: FTIR spectra corresponding to Si-H peaks of Ph_2SiH_2 and $RO - Ph_2SiH_2$ catalyzed by Et_3N in (left) THF and (right) 4:1 ratio THF/DMSO. Darker and lighter lines represent spectra collected early and late in the experiment respectively.

This near-full removal of the second hydrogen peak made the reactivity pattern of the amine more aligned with the reactivity pattern of the hydroxide catalysts. This newly described capability of selectively altering one dehydrogenation step by the solvent polarity may provide new opportunities for selectivity between the two hydrogen sites or a means for tuning selective alcohol protection schemes.

1.4.4 Monoalkoxylated diphenylsilane synthesis by CuIPr-NHC

The catalytic effects of Chloro[1,3-bis(2,6-diisopropylphenyl)imidazol-2-ylidene]copper(I) N-heterocyclic carbene (CuIPr-NHC) with a basic co-catalyst were reviewed as a means of Si-O bond formation. Prior work by Albright and Gawley claimed the CuIPr-NHC-base complex rapidly reacted with Ph_2SiH_2 in the presence of O_2 however, their original workup had several concerning factors including stoichiometrically excess amounts of $NaOtBu$ as the activator as well as access to open air and humidity. Currently, it is clear that dehydrogenation between Ph_2SiH_2 and water is readily catalyzed by strong bases alone, making these two points of great concern. Thus, studies were conducted to understand whether CuIPr-NHC exhibits catalytic activity towards Si-O bond formation and whether the reaction is facilitated using O_2 as an oxygen source.

Dehydrogenation of Ph_2SiH_2 catalyzed by CuIPr-NHC showed surprising result when the base activator was present in limiting amounts. With a base activator of KOH and hydroxyl source of water, the decay of the Si-H peak at 844 cm^{-1} (Ph_2SiH_2) was met with high accumulation of the peak at 824 cm^{-1} ($RO - Ph_2SiH$). The accumulation of the once-oxidized silane strongly exceeded any selectivity towards Ph_2SiH_2 observed with other catalysts in this study. While the 824 cm^{-1} peak did decay, it took excess water and excessive time compared to its rate of formation. Peak deconvolution was completed through the time domain of the $800\text{-}900\text{ cm}^{-1}$ region with two Voigt peaks used to analyze the two Si-H peaks. Deconvolved peak heights were plotted against each other in Figure 1.12 and presented along with a 3D FTIR surface plot. Peak heights remain in absorbance units because no calibration curve is available to convert the peak at 824 cm^{-1} to molar concentration.

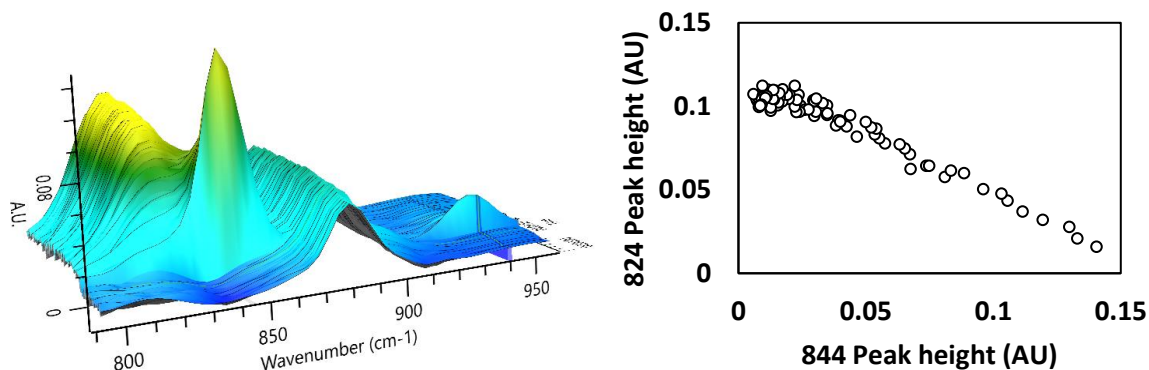


Figure 1.12: (Left) 3D time series IR spectra showing the decay of the Si-H peak at 844cm^{-1} of Ph_2SiH_2 and the formation of RO – Ph_2SiH_2 peak at 824cm^{-1} in the presence of CuIPr-NHC and KOH catalyst (Right) Deconvolved peak height for the two Si-H bond signals relative to each other showing strong linear correlation.

The excellent linearity between Ph_2SiH_2 and RO – Ph_2SiH_2 absorbances highlights the extent of the selectivity towards the original silane. This is also supported by high linearity ($r^2 = 0.988$) between 844 cm^{-1} peak decay and peak growth in the $1100\text{ -}1150\text{ cm}^{-1}$ region which represents Si-O bond formation. In addition, systems with only a hydroxide catalyst, the peak at 2140 cm^{-1} decays proportionally to the peak at 844 cm^{-1} , however in the CuIPr-NHC catalyzed systems the 2140 cm^{-1} peak decayed much more slowly than the 844 cm^{-1} . Full peak decay of the original silane was also remarkably fast at room temperature, with 90% Ph_2SiH_2 peak consumption occurring in about 10 minutes at 22°C . In a second workup, Ph_2SiH_2 was added at 2x stoichiometric amounts to water. In this case, the peak corresponding to the once-oxidized silane did not show any decrease over for the 5 hours that the system was monitored. The Ph_2SiH_2 peak underwent near-full consumption indicating the likely formation of 1,1,3,3-tetraphenyldisiloxane. At the present, it is not clear if diphenylsilanol is an active hydroxy species for the dehydrogenation reaction, or if water was being reformed by silanol condensation only to be subsequently consumed.

This unique selectivity for a single hydrogen site, along with high catalytic activity, may be of interest for custom functionalization to produce mono-alkoxylated diphenylsilanes using a variety of

alcohols. To investigate, a stock solution of KOtBu (10 mM) and CuIPR-NHC (15 mM) was prepared in THF. KOtBu was chosen to replace KOH as the base species from the previous section to reduce potential for water contamination that may lead to unwanted silanol production. Reaction flasks were flame dried and purged with dry nitrogen, then loaded with dry THF and catalyst solution (1.4 mM by KOtBu concentration) and heated to 40°C. Ph_2SiH_2 was added. Si-H bond peak at 844 cm^{-1} was monitored for stability prior to addition of 2x molar amounts of alcohol. Alcohols used were EtOH, IPA, and tBuOH as representative primary, secondary, and tertiary alcohols.

Ph_2SiH_2 was non-reactive towards tBuOH, likely indicative of strong steric inhibition, but was very reactive towards EtOH and IPA. The characteristic growth of a new peak at $\sim 818\text{ cm}^{-1}$ in each case was indicative of monoalkoxy diphenylsilane formation as the Ph_2SiH_2 peak decayed. Review of deconvolved spectra showed what appeared to be peak drift and broadening of the Ph_2SiH_2 peak at 844 cm^{-1} . This was indicative of a third hidden peak between the Si-H bonds of the original and once-oxidized silane. Deconvolution of the Si-H bond region using this new three peak model showed full decay of the original silane signal in less than one hour in each instance. Shown in Figure 1.13, Ph_2SiH_2 and the alkoxyated silane displayed an excellent linear relationship until full consumption of the former, indicative of near-full selectivity towards Ph_2SiH_2 over $RO - PH_2SiH_2$. After an additional reaction time of 30 minutes from their maximum absorbance values, the ethoxy diphenylsilane and isopropoxy diphenylsilane peaks decayed by 15% and 7% respectively. This suggested the new silanes were still reactive in the system but only slightly.

The reaction between the alcohols and Ph_2SiH_2 was modestly slower than the reaction with

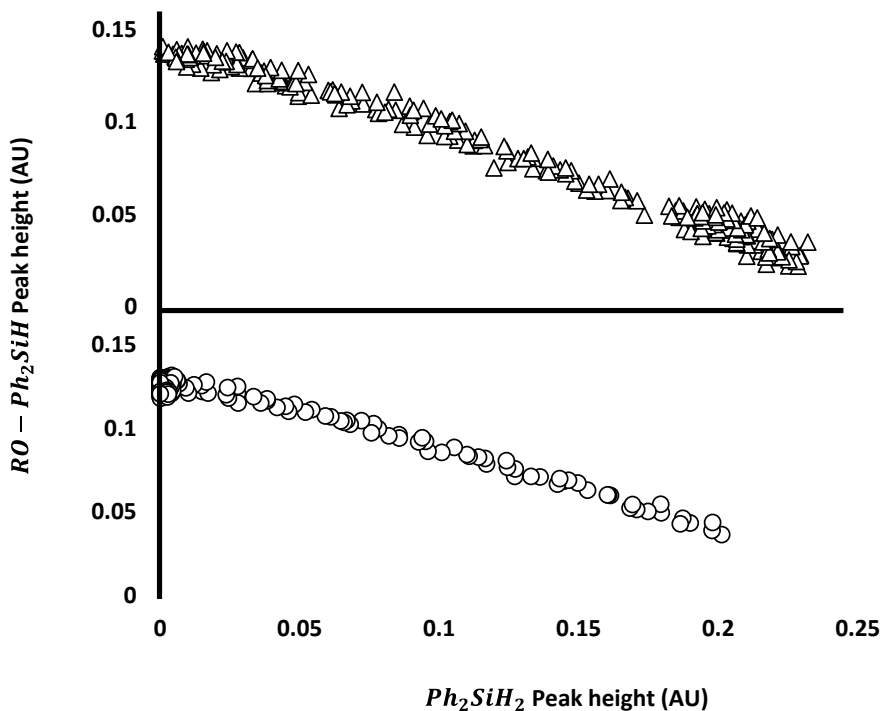


Figure 1.13: Deconvolved peak heights for Ph_2SiH_2 versus (top) ethoxydiphenylsilane and (bottom) isopropoxydiphenylsilane determined by in situ FTIR monitoring.

water, even at a higher temperature, and demonstrated a nearly constant consumption rate over a wide range of the silane concentration. The consumption rate, shown in Figure 1.14, was similar for both EtOH and IPA. This may point to the lowered reaction rate caused by the replacement of the hydroxide anion by the tertbutoxide anion as the base activator.

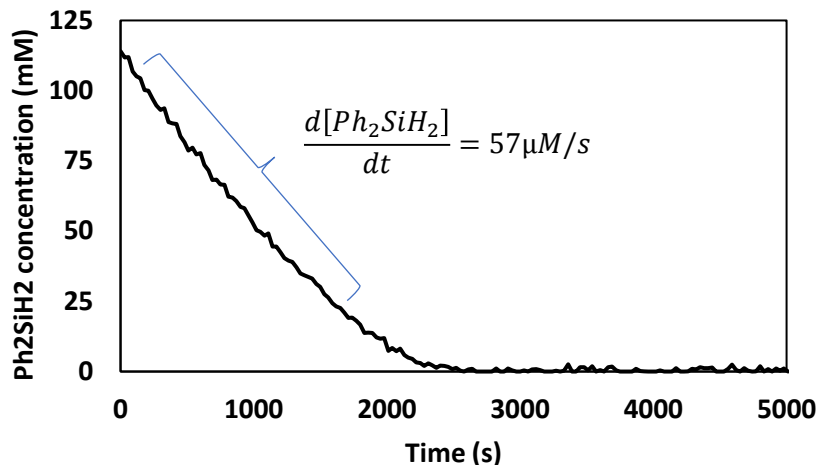


Figure 1.14: Ph_2SiH_2 consumption profile for CuIPr-NHC/KOtBu catalyzed dehydrogenation with IPA at 40°C.

To isolate product for structural analysis, workups with IPA and EtOH were repeated in minimal solvent systems with THF only added in μL quantities as a catalyst carrier. Catalyst in THF, silane, or alcohol was added into flame dried scintillation vials and allowed to react with stirring at room temperature for several hours. The mass ratio of CuIPr-NHC to Ph_2SiH_2 was targeted to be less than 2%. Excess THF and alcohol were removed by a Rotovap system and the collected silanes were analyzed by ^1H NMR for product confirmation. These spectra are available in the Supplementary information and confirm that these monoalkylated silanes can be recovered in high yields.

Mechanistic details of the alkoxylation of Ph_2SiH_2 require further investigation and fall outside of the scope of this study. However, two observations are noteworthy that give clues about the catalyst activity: (I) CuIPr-NHC was not active without a base catalyst (II) a notable color change of solution on addition of silane was observed even in the absence of available hydroxyl groups. The scheme shown below provides a possible route to key activation steps of the catalyst, which is based on previous works clarified by the observations in this study [22].

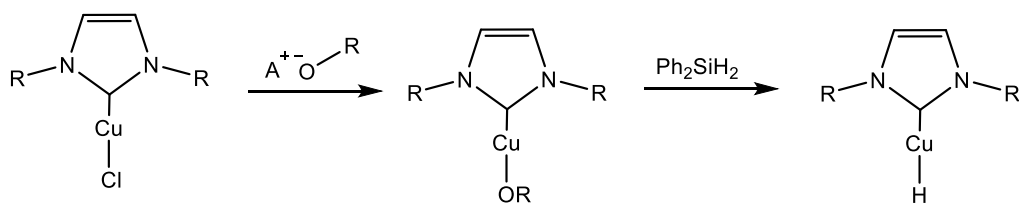


Figure 1.15: Proposed activation steps for CuIPr-NHC with a base activator and silane.

The mechanistic cycle did not appear to be active towards tertiary alcohols, likely due to steric congestion around the hydroxyl site. Poor reactivity towards a once-oxidized silane likely cannot be explained solely by steric effects alone since reactions with water, primary, and secondary alcohols all showed similar reaction patterns. The near-full selectivity of CuIPr-NHC towards removal of only a single hydrogen site allowing for a novel approach to production of customizable monoalkoxy silanes with possible use as reducing agents or alcohol protectors, however future work is necessary to determine if this effect extends to other silanes beyond Ph_2SiH_2 .

1.5 Conclusions

Mild operating conditions and highly active common catalysts make Si-O bond formation between silanes and hydroxyl groups an attractive alternative to procedures dominated by chlorosilanes. In this study, a review of base catalyzed dehydrogenation of diphenylsilane has been presented using *in situ* IR reaction monitoring with a focus on kinetics and selectivity to Ph_2SiH_2 and its once-oxidized form that has not been previously produced in literature. Steric restrictions involving a large 3° alkoxide catalyst was found to limit silane coupling to 3° alcohols (tertbutanol) to only one hydrogen, resulting in accumulation of a monoalkoxylated diphenylsilane. Under the same conditions, Ph_2SiH_2 was fully reactive towards 1° and 2° alcohols at both hydrogens.

The cation identity of hydroxide salts significantly impacted the observed rate order of reaction when Ph_2SiH_2 was reacted with water to form octaphenylcyclotetrasiloxane (Ph_8D_4).

Tetramethylammonium hydroxide (TMAH) and potassium hydroxide both exhibited first-order rate laws

in silane and zeroth order in water, while sodium hydroxide only showed first-order response at higher temperature or with significant excess water available. Arrhenius modeling among the three hydroxides showed similar temperature responses, supporting a two-step mechanism for dehydrogenation. Cation identity did play a significant role in rate constant, with sodium and potassium cations reacting at similar rates but TMAH reacting 17 times faster in THF as a solvent.

A survey of amines as catalysts was also completed for the reaction between Ph_2SiH_2 and water. Six amines reviewed had varying degrees and sizes of alkyl substitution which, unlike hydroxides, moderate accumulation of once-oxidized silane for each amine. However, this effect appears to have electronic dependence, as running the reaction in a more polar environment removed the accumulation. Amine selection led to unpredictable observed rate orders. Both first- and second-rate orders were observed, even with excess water present. Very large amines also showed a reaction profile with an extended induction period. The array of reaction profiles generated by amines is a topic that questions mechanism and requires further investigation.

Finally, a catalyst with near-full selectivity towards a single hydrogen site on Ph_2SiH_2 has been uncovered. Chloro[1,3-bis(2,6-diisopropylphenyl)imidazol-2-ylidene]copper(I) N-heterocyclic carbene (CuIPr-NHC) with a base activator was found to react almost exclusively with Ph_2SiH_2 over $RO-PhSiH_2$ under a variety of conditions. Using water as a hydroxyl source and a KOH activator, 1,1,3,3-tetraphenyldisiloxane is likely produced either by direct dehydrogenation or through condensation of silanols. Using potassium tertbutoxide as a base activator, isopropoxy- and ethoxy-diphenylsilanes were produced in high yield, indicating addition of 1° and 2° to Ph_2SiH_2 can be readily achieved. However, the catalyst system was not reactive towards 3° alcohols, possibly due to steric effects. This system may open the door for wider and simpler custom silane syntheses for use as reducing agents and hydride donors, or as a means of selective Si-O bond formation in more complex molecules with multiple alcohol moieties.

In general, base-catalyzed Si-O bond formation between silanes and hydroxyl groups can be activated by many low-cost catalysts. *In situ* FTIR monitoring of dehydrogenation reactions have shown hydroxide salts are particularly easy handle, have high activity, and conform well to proposed mechanisms. Amines and niche catalysts like CuIPr-NHC allow for accumulation of oxidized intermediates that may be beneficial in selective alcohol protection or synthesis of custom silanes. Broader applications of this work may realize the benefits of silane-hydroxyl coupling producing only H_2 as a byproduct as opposed to chlorosilane equivalents, which produce high levels of hydrochloric acid.

Supplementary Information

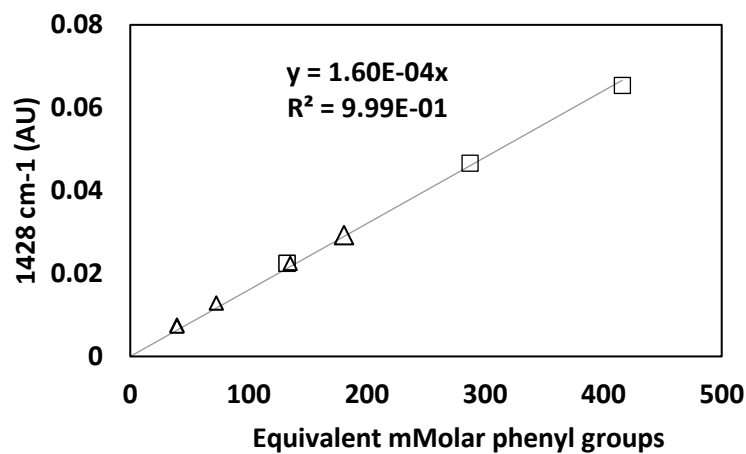


Figure S1: Calibration curve for phenyl group concentration for (\square) Ph_2SiH_2 and (Δ) Ph_8D_4 . Absorbance at 1428 cm^{-1} calculated from 2pt baseline method at 1420 and 1440 cm^{-1} . Peak absorbance is independent of structure and is used to monitor Ph_2SiH_2 additions and changes in system volume.

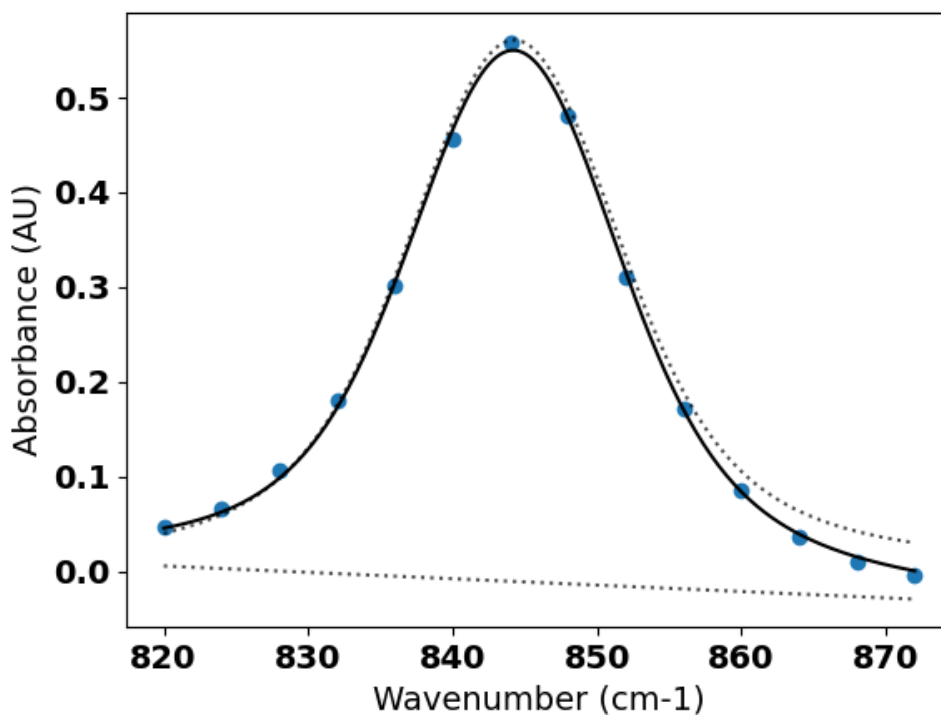


Figure S2: Voigt peak fit of the Si-H absorbance peak at 844 cm^{-1} for Ph_2SiH_2 .

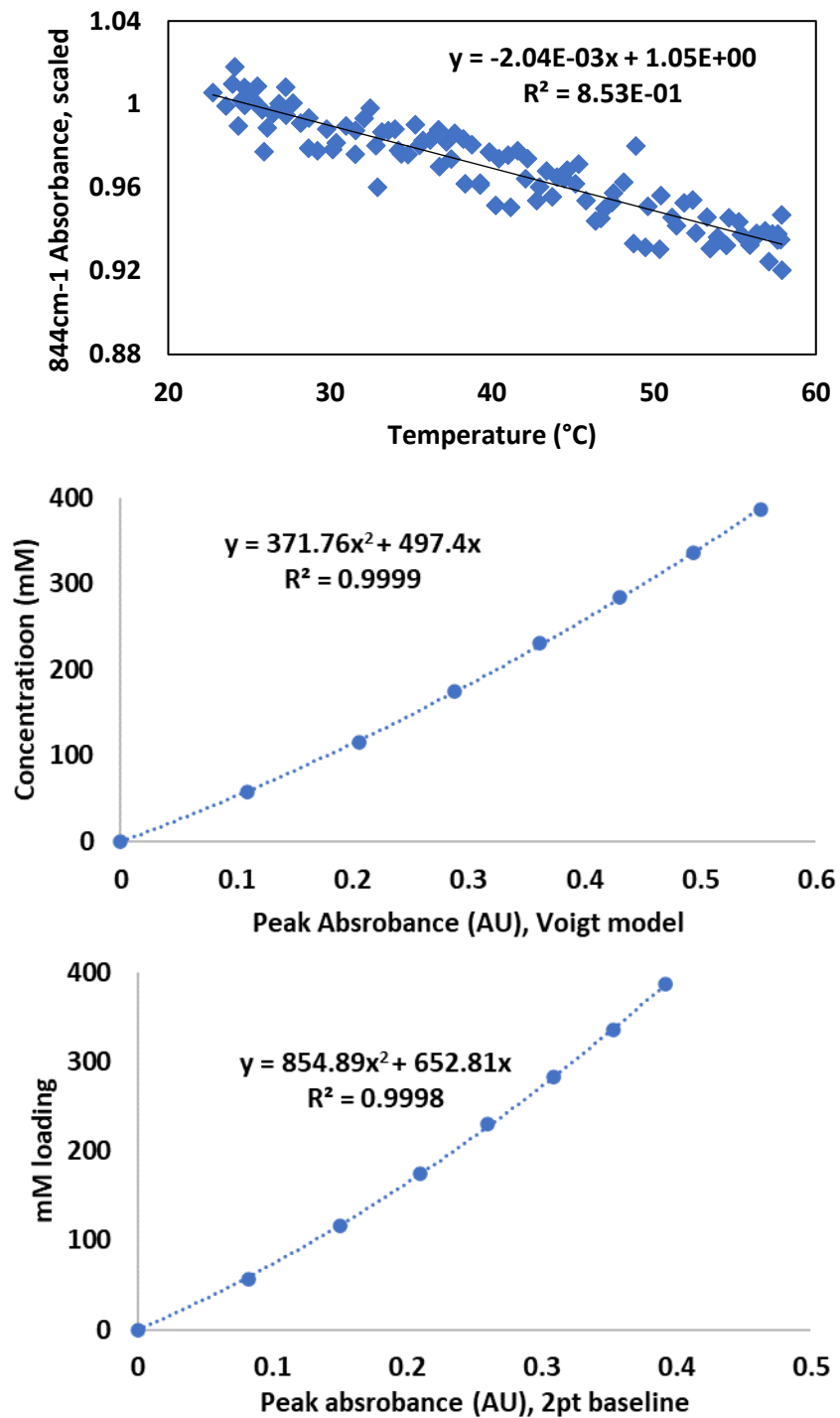


Figure S3: Si-H absorbance peak at 844 cm⁻¹ for Ph₂SiH₂ using (top) least squares fitting of Voigt peak (bottom) 2 point baseline method using absorbances at 836 and 856cm⁻¹.

Ph_2SiH_2 was heated from 22°C to 58°C and back to 22°C over a period of 1 hour, in accordance with the temperature ranges used in the experiments. At the 60°C, the absorbance at constant concentration is 92% of the value at 25°C.

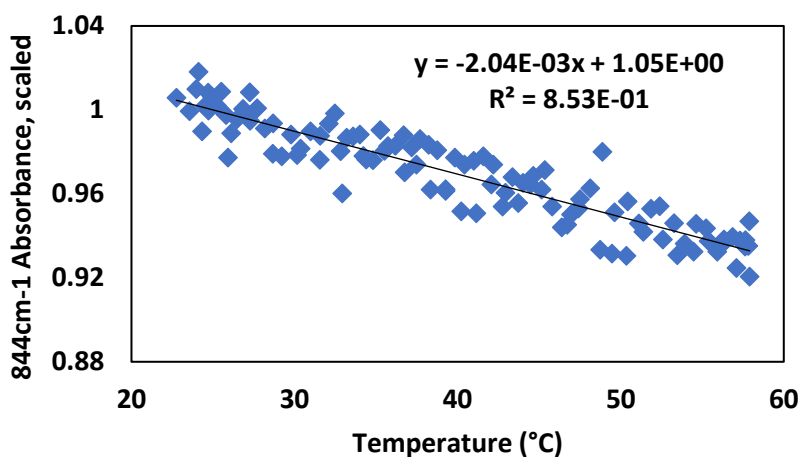


Figure S4: Si-H bond at 844cm^{-1} absorbance response to temperature. Data is scaled by the regression value at 25°C, ie at 25°C the temperature correction is 1.

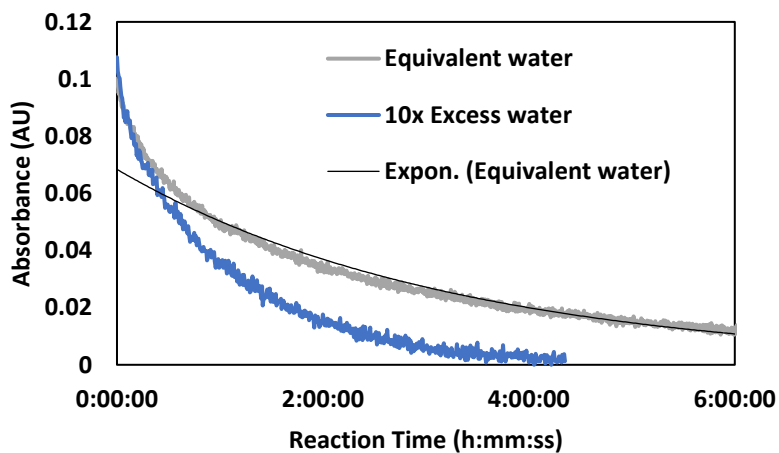


Figure S5: NaOH catalyzed dehydrogenation, showing 1st order response in silane with excess water available but 2nd order response with equimolar water available. An exponential fit to the equivalent water case is shown to

highlight deviation from first-order. Reaction temperature 20.6°C. 2-point baseline method used for absorbance values.

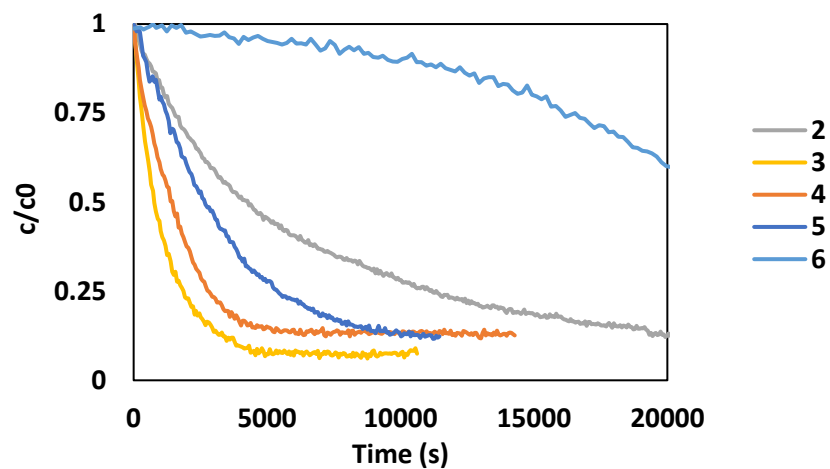


Figure S6: Relative deconvolved Si-H bond concentration of Ph_2SiH_2 at 844 cm^{-1} for each amine catalyzed dehydrogenation. See Table 1.3 for corresponding amine ID. Reaction temperature 43°C for each case.

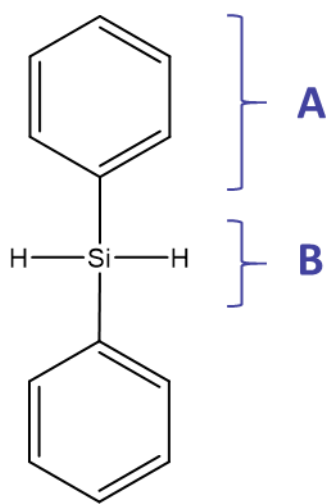
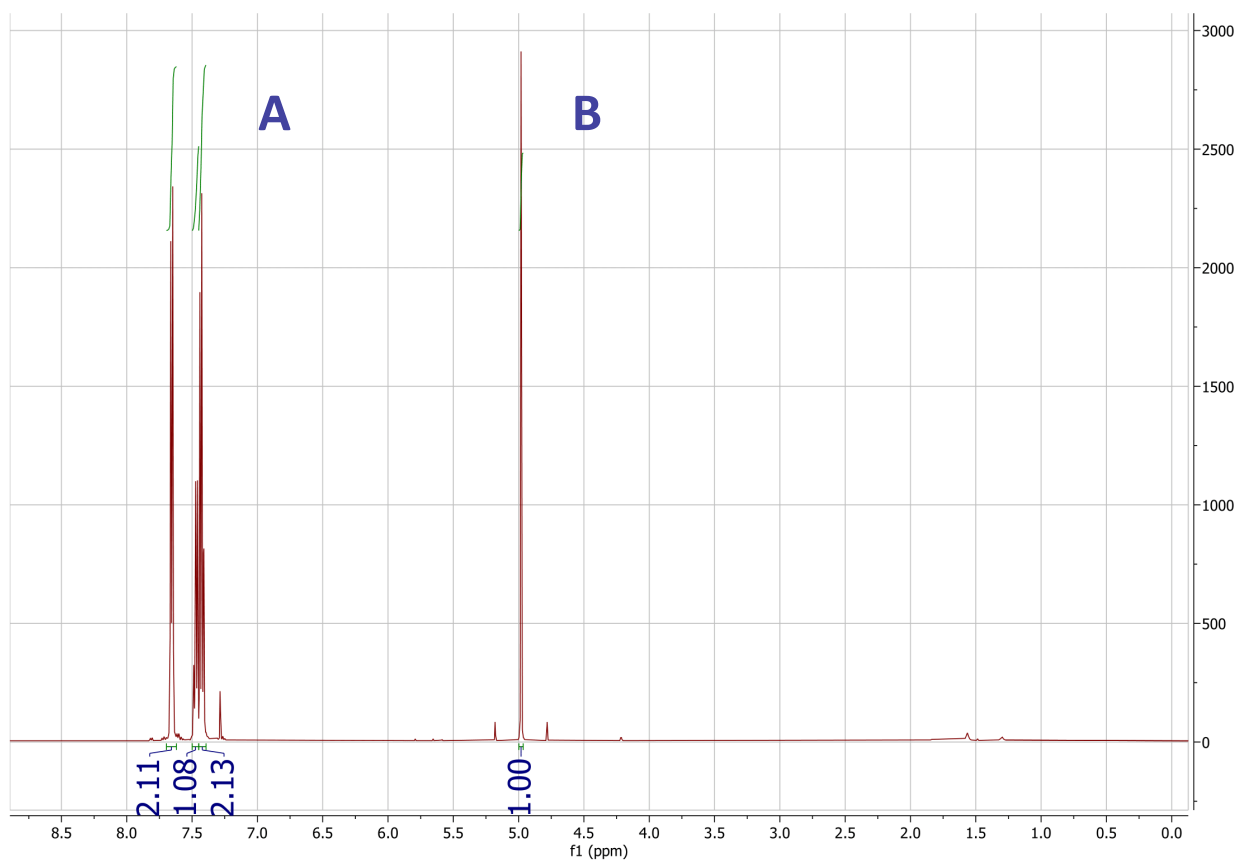


Figure S7: Ph_2SiH_2 reference ^1H NMR spectra

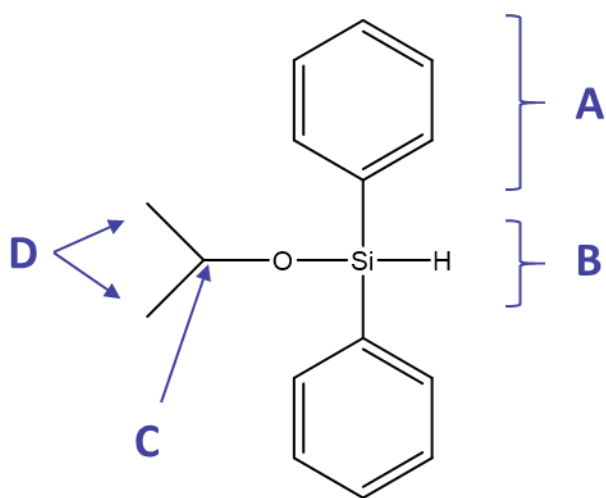
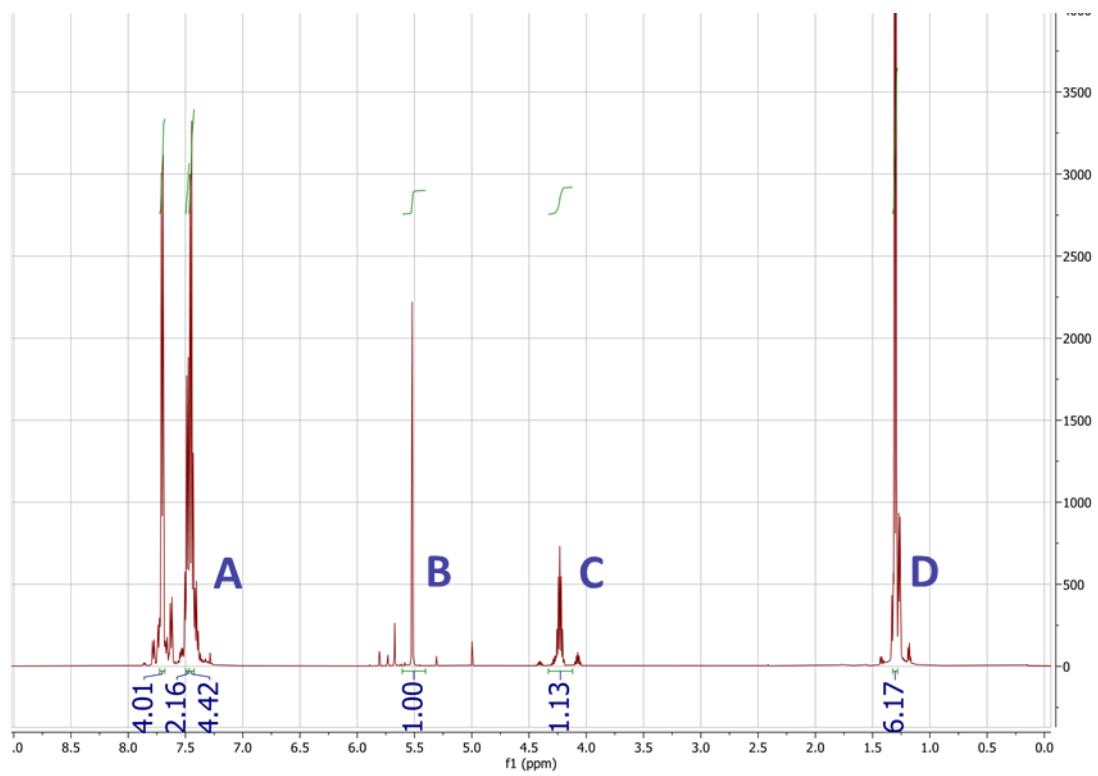


Figure S8: ¹H NMR spectra and structure of isopropoxydiphenylsilane produced by CuIPR-NHC catalyzed dehydrogenation

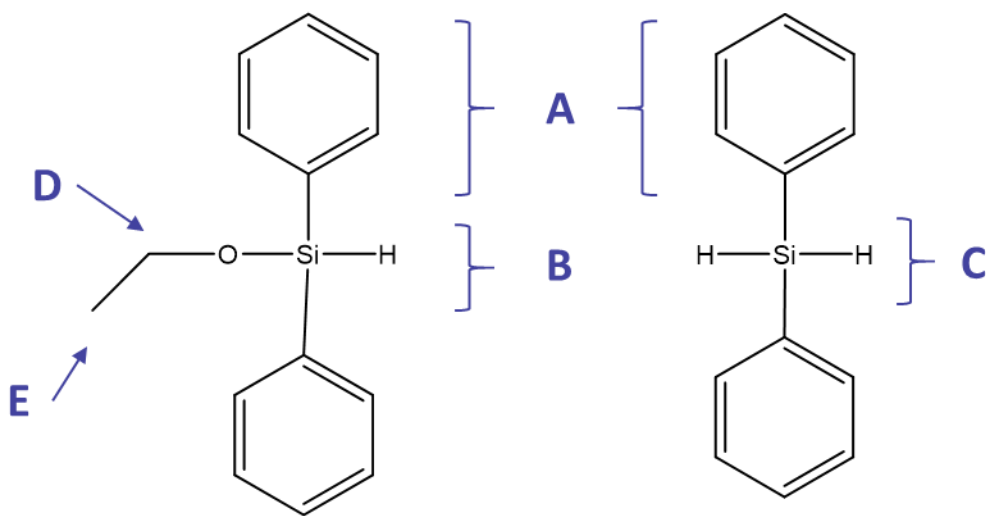
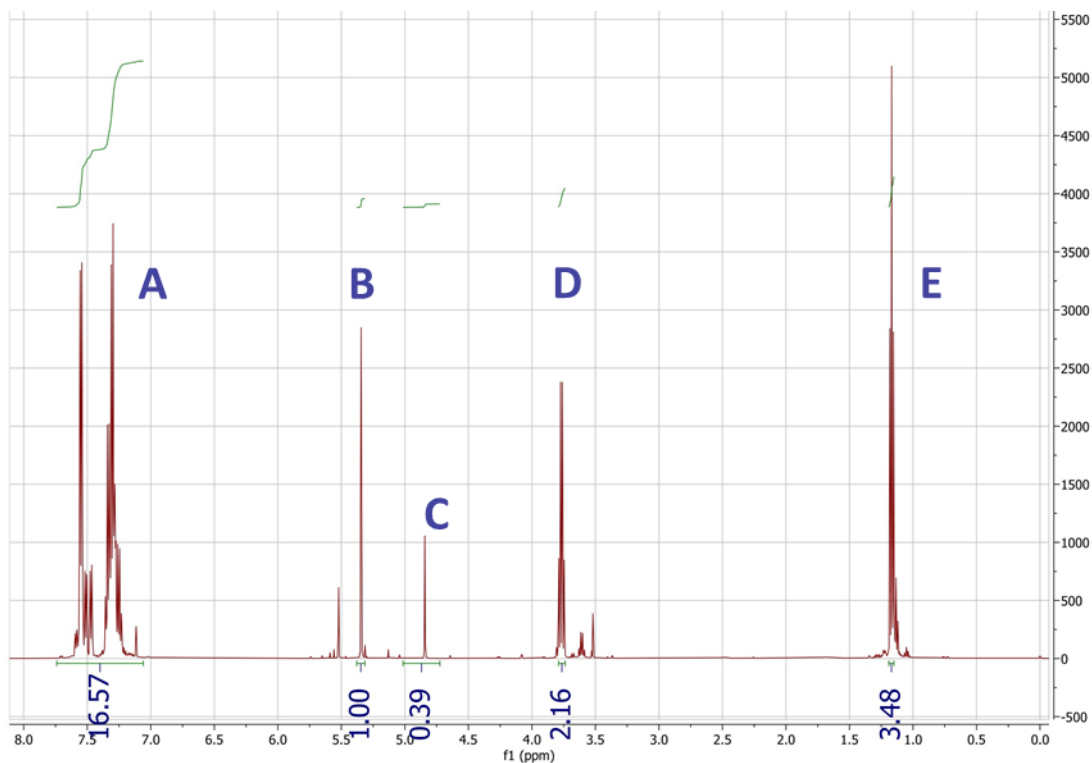


Figure S9: ^1H NMR spectra of ethoxydiphenyl silane produced from CuIPR-NHC catalyzed dehydrogenation. Unreacted diphenylsilane appears in the sample as indicated by the peak at 4.9 ppm and the excess phenyl hydrogens relative to peaks B, D, and E. Peak at 5.5 ppm is believed to be hydride terminated dimers or oligomers, possibly due to water contamination during synthesis

References

1. Corey, E.J. and A. Venkateswarlu, *Protection of hydroxyl groups as tert-butyldimethylsilyl derivatives*. Journal of the American Chemical Society, 1972. **94**(17): p. 6190-6191.
2. Crouch, R.D., *Recent Advances in Silyl Protection of Alcohols*. Synthetic communications, 2013. **43**(17): p. 2265-2279.
3. Tripp, C.P. and M.L. Hair, *Chemical attachment of chlorosilanes to silica: a two-step amine-promoted reaction*. Journal of physical chemistry, 1993. **97**(21): p. 5693-5698.
4. Hair, M.L. and W. Hertl, *Reactions of chlorosilanes with silica surfaces*. Journal of physical chemistry, 1969. **73**(7): p. 2372-2378.
5. Marchioni, F., et al., *Protection of Lithium Metal Surfaces Using Chlorosilanes*. Langmuir, 2007. **23**(23): p. 11597-11602.
6. Pujari, S.P., et al., *ChemInform Abstract: Covalent Surface Modification of Oxide Surfaces*. ChemInform, 2014. **45**(36).
7. Yamamoto, E., et al., *Mesoporous Silica Nanoparticles with Dispersibility in Organic Solvents and Their Versatile Surface Modification*. Langmuir, 2020. **36**(20): p. 5571-5578.
8. Huttenloch, P., K.E. Roehl, and K. Czurda, *Sorption of Nonpolar Aromatic Contaminants by Chlorosilane Surface Modified Natural Minerals*. Environmental Science & Technology, 2001. **35**(21): p. 4260-4264.
9. Kimble, E., B. Arkles, and R. Cameron, *Symmetric siloxane macromers*. Polymer Preprints, 2009. **50**(2): p. 859-860.
10. Goff, J., E. Kimble, and B. Arkles, *Living polymerization routes to siloxane macromers and higher order silicone structures*, in *Progress in Silicones and Silicone-Modified Materials*. 2013, American Chemical Society: S. Clarson. p. 59-78.
11. Fuchise, K., et al., *Organocatalytic controlled/living ring-opening polymerization of cyclotrisiloxanes initiated by water with strong organic base catalysts*. Chemical Science, 2018. **9**(11): p. 2879-2891.
12. Ward, W.J., et al., *Catalysis of the Rochow Direct Process*. Journal of catalysis, 1986. **100**(1): p. 240-249.
13. Price, F., *Mechanism of the Alkaline cleavage of Silicon-Hydrogen Bonds: Temperature Coefficients of the Rate of Cleavage of Several Trialkylsilanes*. Journal of the American Chemical Society, 1947. **69**(11): p. 2600-2604.
14. Oestreich, M. and A. Grajewska, *Base Catalyzed Dehydrogenative Si-O Coupling of Dihydrosilanes: Silylene Protection of Diols*. Synlett, 2010. **2010**(16): p. 2482-2484.
15. Weickgenannt, A. and M. Oestreich, *Potassium tert-Butoxide-Catalyzed Dehydrogenative SiO Coupling: Reactivity Pattern and Mechanism of an Underappreciated Alcohol Protection*. Chemistry- An Asian Journal, 2009. **4**(3): p. 406-410.
16. Raffa, P., et al., *First examples of gold nanoparticles catalyzed silane alcoholysis and silylative pinacol coupling of carbonyl compounds*. Tetrahedron Letters, 2008. **49**(20): p. 3221-3224.

17. Sridhar, M., et al., *An Efficient Synthesis of Silyl Ethers of Primary Alcohols, Secondary Alcohols, Phenols and Oximes with a Hydrosilane Using InBr₃ as a Catalyst*. ChemInform, 2012. **43**(8).
18. Kim, S., M.S. Kwon, and J. Park, *Silylation of primary alcohols with recyclable ruthenium catalyst and hydrosilanes*. Tetrahedron Letters, 2010. **51**(34): p. 4573-4575.
19. Ventura - Espinosa, D., et al., *Catalytic Dehydrogenative Coupling of Hydrosilanes with Alcohols for the Production of Hydrogen On - demand: Application of a Silane/Alcohol Pair as a Liquid Organic Hydrogen Carrier*. Chemistry – A European Journal, 2017. **23**(45): p. 10815-10821.
20. Ventura-Espinosa, D., et al., *High Production of Hydrogen on Demand from Silanes Catalyzed by Iridium Complexes as a Versatile Hydrogen Storage System*. ACS catalysis, 2018. **8**(3): p. 2558-2566.
21. Albright, A. and R. Gawley, *NHC-catalyzed dehydrogenative self-coupling of diphenylsilane: a facile synthesis of octaphenylcyclotetra(siloxane)*. Tetrahedron Letters, 2011. **52**(46): p. 6130-6132.
22. Hubbard, A., et al., *The design, synthesis and application of a novel class of N-heterocyclic carbene catalysts*. ProQuest Dissertations and Theses, 2012.
23. Santoro, O., et al., *N-heterocyclic carbene copper(I) catalysed N -methylation of amines using CO₂*. Dalton Transactions, 2015. **44**(41): p. 18138-18144.
24. Welle, A., et al., *A Three-Component Tandem Reductive Aldol Reaction Catalyzed by N-Heterocyclic Carbene–Copper Complexes*. Organic Letters, 2006. **8**(26): p. 6059-6062.
25. Kaplan, L. and K.E. Wilzbach, *Hydrogen Isotope Effects in the Alkaline Cleavage of Triorganosilanes*. Journal of the American Chemical Society, 1955. **77**(5): p. 1297-1302.
26. Anslyn, E. and D. Dougherty, *Modern Physical Organic Chemistry*. 2006: University Science Books.
27. Toutov, A.A., et al., *Sodium Hydroxide Catalyzed Dehydrocoupling of Alcohols with Hydrosilanes*. Organic Letters, 2016. **18**(12): p. 5776-5779.
28. Deka, K., R.J. Sarma, and J.B. Baruah, *Amine catalysed silicon-oxygen bond formation*. Inorganic Chemistry Communications, 2005. **8**(12): p. 1082-1084.
29. Voronova, E.D., et al., *Dichotomous Si–H Bond Activation by Alkoxide and Alcohol in Base-Catalyzed Dehydrocoupling of Silanes*. Inorganic Chemistry, 2020. **59**(17): p. 12240-12251.
30. Crouch, D., *Selective deprotection of silyl ethers*. Tetrahedron, 2013. **69**(11): p. 2383-2417.
31. Jarowicki, K. and P. Kocienski, *Protecting groups*. Contemporary Organic Synthesis, 1995. **2**(5): p. 315-336.
32. Nelson, T. and D. Crouch, *Selective deprotection of silyl ethers*. Synthesis, 1996. **1996**(09): p. 1031-1069.
33. Wuts, P.G.M., *Greene's Protective Groups in Organic Synthesis, 5th ed.* 2014, Hoboken: John Wiley & Sons, Inc.
34. Kantor, S.W., *The hydrolysis of methoxysilanes. Dimethylsilanediol*. Journal of the American Chemical Society, 1953. **75**(11): p. 2712-2714.

35. Smith, K.A., *A study of the hydrolysis of methoxysilanes in a two-phase system*. Journal of Organic Chemistry, 1986. **51**(20): p. 3827-3830.
36. Arkles, B., et al., *Factors contributing to the stability of alkoxysilanes in aqueous solution*. Silanes and Other Coupling Agents, 1992: p. 91-104.
37. Issa, A.A., M. El-Azazy, and A.S. Luyt, *Kinetics of alkoxysilanes hydrolysis: An empirical approach*. Scientific Reports, 2019. **9**(1): p. 1-15.
38. Altmann, S. and J. Pfeiffer, *The hydrolysis/condensation behavior of methacryloyloxyalkylfunction alkoxysilanes: structure-reactivity relations*. Monatshefte für Chemie / Chemical Monthly, 2003. **134**(8): p. 108-1092.
39. Jiang, H., et al., *Effects of Temperature and Solvent on the Hydrolysis of Alkoxysilane under Alkaline Conditions*. Industrial & engineering chemistry research, 2006. **45**(25): p. 8617-8622.
40. Revunova, K. and G.I. Nikonov, *Base - Catalyzed Hydrosilylation of Ketones and Esters and Insight into the Mechanism*. Chemistry - A European Journal, 2014. **20**(3): p. 839-845.
41. Fedorov, A., et al., *Lewis-base silane activation: from reductive cleavage of aryl ethers to selective ortho -silylation*. Chemical Science, 2013. **4**(4): p. 1640-1645.
42. Bellini, C., et al., *Alkaline - Earth - Catalysed Cross - Dehydrocoupling of Amines and Hydrosilanes: Reactivity Trends, Scope and Mechanism*. Chemistry- A European Journal, 2016. **22**(13): p. 4564-4583.
43. Liu, H.Q. and J.F. Harrod, *Dehydrocoupling of ammonia and silanes catalyzed by dimethyltitanocene*. Organometallics, 1992. **11**(2): p. 822-827.
44. Liu, H.Q. and J.F. Harrod, *Copper(I)-catalyzed cross-dehydrocoupling reactions of silanes and amines*. Canadian Journal of Chemistry, 1992. **70**(1): p. 107-110.
45. Gatineau, D., et al., *N -Heterocyclic carbene-initiated hydrosilylation of styryl alcohols with dihydrosilanes: a mechanistic investigation*. Dalton Transactions, 2013. **42**(20): p. 7458-7462.
46. Iosub, A.V., et al., *Nickel-Catalyzed Selective Reduction of Carboxylic Acids to Aldehydes*. Organic letters, 2019. **21**(19): p. 7804-7808.
47. Nam, T.K. and D.O. Jang, *Radical "On Water" Addition to the C • N Bond of Hydrazones: A Synthesis of Isoindolinone Derivatives*. Journal of Organic Chemistry, 2018. **83**(14): p. 7373-7379.
48. Shanghai Chuqing New Materials Technology Co, L., *Methods for preparing phenyl silane and diphenyl silane*. 2016: People's Republic of China.
49. Greve, K., E. Nielsen, and O. Ladefoged, *Siloxanes (D3, D4, D5, D6, HMDS) Evaluation of health hazards and proposal of a health-based quality criterion for ambient air*. 2014, The Danish Environmental Protection Agency: Copenhagen.
50. A. Zlatanovic, D.R., X. Wan, J. Messman, D. Bowen, P. Dvornic, *Dimethyl - methylphenyl copolysiloxanes by dimethylsilanolate - initiated ring opening polymerization. Evidence for linearity of the resulting polymer structures*. Journal of Polymer Science Part A: Polymer Chemistry, 2019. **57**(10): p. 1122-1129.

51. A. Zlatanovic, D.R., X. Wan, J. Messman, P. Dvornic, *Monitoring of the Course of the Silanolate-Initiated Polymerization of Cyclic Siloxanes. A Mechanism for the Copolymerization of Dimethyl and Diphenyl Monomers*. *Macromolecules*, 2018. **51**(3): p. 895-905.
52. A. Zlatanovic, D.R., X. Wan, J. Messman, P. Dvornic, *Suppression of Crystallization in Polydimethylsiloxanes and Chain Branching in Their Phenyl-Containing Copolymers*. *Macromolecules*, 2017: p. 3532-3543.
53. Riley, M.O., J.R. Kolb, and E.S. Jessop, *The commercial synthesis of M97KVB gum, a precursor to cellular silicone cushions, Part I*. 1982, Lawrence Livermore Laboratory: Livermore.
54. Hensen, K., et al., *Two Cyclotetrasiloxanes at 143K*. *Acta Crystallographica Section C Crystal Structure Communications*, 1997. **53**(12): p. 1867-1869.

Chapter 2: Tunable PDMS microspheres by continuous flow premix emulsification

2.1 Introduction

PDMS polymers consist of repeating units of silicone and oxygen bonds. Polydimethylsiloxane is the most widely used silicone polymer and can form 3D networks by a cross linking reaction between reactive groups throughout the polymer backbone or on the polymer terminals. PDMS exhibits high biocompatibility, thermal stability, high elasticity, durability, gas permeability, optical transparency, and hydrophobicity that make it attractive for applications in including sensor development, drug delivery, manufacturing, additive manufacturing, and biomedical applications. The use of PDMS microspheres has seen significant growth in the past decade, with new advances in sensing applications, analytical methods, and microfluidics.

Fabrication routes of PDMS and other polymeric microspheres typically revolve around low throughput microfluidics or high shear-high throughput methods. The former can produce monodisperse microspheres with complex architectures one microsphere at a time while the later uses methods that can be applied at industrial scale but produce wide particle size distributions. In this chapter, continuous flow premix membrane emulsification is demonstrated as a bridge between these two methods for high throughput microsphere production with tunable diameters. A custom design is presented for a single-pass emulsification column that is robust to fouling, easily disassembled and cleaned, and accepts commercially-available membranes with no major modifications. The continuous flow system was characterized by feed rates, feed ratios, membrane type, and membrane quantity with transmembrane pressures and microsphere size being the primary response variables.

2.2 Literature review

2.2.1 Linear polysiloxane chemistry

Polysiloxanes consist of alternating silicon-oxygen bonds in a linear or network structure. The silicon atom in linear polymers is substituted with two additional functional groups which provide tunability of mechanical and chemical characteristics with polydimethylsiloxane (PDMS) being by far the most common linear polysiloxane. One of the key characteristics of siloxanes is the increased bond length compared to carbon analogs in organic polymer chains. Bond lengths for Si-O and Si-H have been measured at 1.64 Å and 1.492 Å while C-C measures 1.53 Å and C-H measures 1.09 Å [1]. Another key feature in siloxanes is the extended bond angle of the Si-O-Si bond. A bond angle of disiloxane has been determined at 144.1°, a wide increase from its carbon analogue, dimethyl ether, at 111.5° [1]. The extended bond length and bond angle allow the polymer backbone to exhibit incredible flexibility, which gives PDMS unique properties compared to carbon-based polymers. This includes very low glass transition temperatures (-125°C in PDMS, although deficiencies can result in a T_g of -40 to -50°C), low bulk viscosities, temperature coefficients, chemical resistance, hydrophobicity, and gas permeability.

The manufacturing of siloxanes originates from the Rochow process. High purity elemental silicon, produced by reduction of SiO_2 with carbon, will react directly with alkyl and aryl halides at high temperatures which produces the precursors for polysiloxanes [1]. To produce methyl siloxanes for PDMS, the silicon and CH_3Cl are combined in a fluidized bed at 300°C in the presence of a catalyst to produce a mixture of methyl chlorosilanes. The makeup of this mixture depends on system purity and processing conditions but primarily consists of Me_2SiCl_2 (30-80%) and $MeSiCl_3$ (10-40%) as the most abundant species [1]. Chlorosilanes readily react with water to produce hydrochloric acid and silanols which undergo polycondensation to convert them into more useful linear and cyclic oligo and polysiloxanes. Condensation of silanols is equilibrium limited and requires elevated temperatures or vacuum to promote water removal to manufacture higher molecular weight chains [2]. The condensation/hydrolysis reaction

is strongly pH dependent, and if left unchecked can lead to system decay by loss of low molecular weight volatiles or water which leads to shifts from equilibrium. In general, hydrolysis has been shown to be significantly faster under basic conditions than under acidic conditions for PDMS [3], but strict pH control can allow for stable storage of silanol terminated siloxanes.

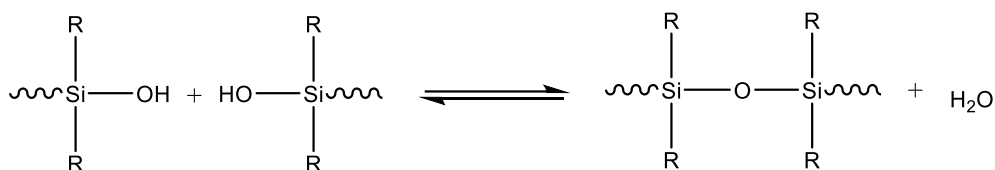


Figure 2.1: Condensation/hydrolysis between silanol groups in a polysiloxane system.

Cyclic oligomers produced by the Rochow method most commonly form with 4, 5, or 6 repeating $-R_2SiO-$ groups. When R is a methyl group, rings with repeating groups of 4 units (octamethylcyclotetrasiloxane), 5 units (decamethylcyclopentasiloxane), and 6 units (dodecamethylcyclohexasiloxane) are referred to in shorthand as D_4 , D_5 , and D_6 . Cyclic polymers undergo ring opening polymerization catalyzed by a wide variety of acids and bases. Base catalysts for anionic ring opening polymerization (AROP) are commonly used as they are inexpensive, effective, and prevent damage to acid sensitive groups like vinyl functionality. Common base catalysts include hydroxides, alkoxies, and silanulates [1-5]. Instead of these single site catalysts, dual site catalysts of α,ω -bissilanulates can be used which are siloxane oligomers with active silanolate ions at each terminal. The use of bissilanulates allows for chain growth in both directions and as well as better control of functionalization at both polymer terminals. AROP proceeds with a fairly simple nucleophilic attack on a silicone atom, relocating the active site to the opposite end of the chain as a silanolate anion, as shown in Figure 2.2 [2].

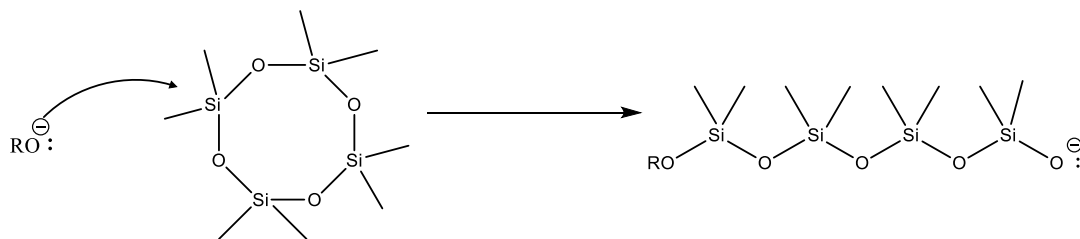
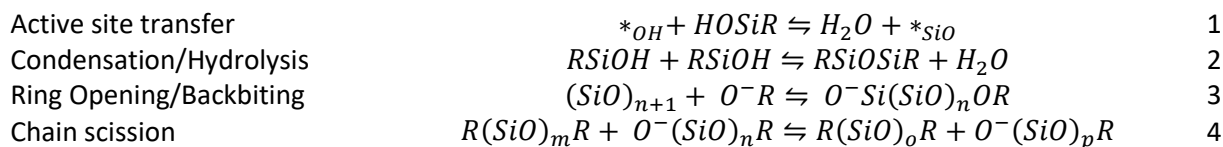


Figure 2.2: Anionic ring opening polymerization process of D4

In an instance of an unstrained cyclic monomer (>3 Si-O units), AROP is primarily driven by entropy resulting in an equilibrium mixture of long chains of polysiloxanes and cyclic oligomers. The equilibrium constant depends on the chain substituents, temperature, solvent, and dilution where there is a point of “critical dilution” and only cyclic species are present [2, 6]. For dimethylsiloxane, cyclics are entirely produced when diluted below 35%, while polymerization yields about 85% linear formation when carried out in bulk [1], but the critical dilution heavily depends on the substituent groups present.

In AROP, active sites are not specific to targeting ring structures, thus an active chain end can attack itself to revert back to a cyclic form (backbiting) or attack the middle of a separate chain (chain scission). A summary of common reactions in polysiloxane systems are expressed in Eq 1-4 below. The shorthand R represents some functionality along the direction of the linear chain, and the two substituent groups on each silicon atom are removed for readability. The $*$ in Eq 1 represents the form the catalyst is in, essentially being the location of the negative charge with $*_{OH} = HO^-$ and $*_{SiO} = RSiO^-$ for hydroxide catalysts.



Chain scission allows for the randomization of functional groups throughout the polymer chain when cyclic siloxanes with different functionalities are used [5]. Common functionality for crosslinking

sites include vinyl, hydride, silanol, amines, and epoxy groups [7]. Ethyl and phenyl groups act as crystalline disruptors capable of reducing glass transition temperatures below -80°C , making PDMS useful in ultra-low temperature applications [5]. Fluorinated organic groups are used to improving chemical and solvent resistance of the PDMS. For example, Li *et al.* used PDMS copolymers with a high substitution of fluorinated side chains (trifluoropropyl) to stabilize polysiloxane membranes for vegetable oil separation in cyclohexane, which is a strong solvent for polydimethylsiloxane.

Molecular weight of the resulting polymer is controlled by the ratio of catalyst to bulk materials and by the addition of short chain polysiloxane oligomers into the reaction mixture known as “end blockers”[1]. End blockers also function to add functionality to polymer chains, and typically come in the form of disiloxanes like 1,3-divinyltetramethyldisiloxane. When added in excess to the catalyst, the chain scission reaction split the disiloxane end blocker which fixes vinyl activity to the main polymer chain.

2.2.2 Applications of PDMS and PDMS microspheres

While the applications of PDMS are far too numerous to review here, a few key applications are highlighted to demonstrate the utility of these polymers. PDMS liquids (silicone oils) are commonplace in heating elements in laboratories. Chemical resistance, biological compatibility, and hydrophobicity make PDMS useful in biological applications and it is commonly used for rapid development of microfluidic devices [8]. Hydrophobicity also makes siloxanes ideal for surface treatments, such as commercially available glass treatments, although the tunability of PDMS’s reactivity allows for treatment of a variety of materials [9]. Easy handling of low viscosity uncured polymers has allowed for novel production techniques of wearable sensors with tunable mechanical properties for a variety of biomechanics applications [10, 11]. Optical transparency of PDMS is also a major benefit and has been used for development of thin films for improved Raman spectroscopy [12].

The scope of applications for microsphere-based PDMS structures is much more focused but has opened up a wide variety of utility outside of traditional bulk PDMS. Roy *et al.* demonstrated PDMS microspheres coated with epoxy as additives for modifying the mechanical properties of bulk epoxy resins [13]. Microsphere-based systems for novel drug delivery [14] and cell entrapment in acoustofluidics cells [15, 16] have also been investigated because of the biocompatibility of PDMS. PDMS microsphere based sensors have seen wide growth, with sensing capability for mechanical [17, 18], thermal [19], and UV signals [20]. Use of microspheres has also opened the ability to additively manufacture structures with no support. Roh *et al.* demonstrated direct 3D printing of porous silicone structures by incorporating pre-cured PDMS microspheres into liquid polymer precursor to form a paste of suitable consistency for printing [21].

So far, direct 3D printing of polysiloxanes remains somewhat elusive. While some commercial siloxane compounds are suitable for direct printing, they lack wide tunability of mechanical properties and stiffness. The low surface tension and flowability of PDMS means liquid PDMS must be impregnated with stiffening agents like silica particles which alter the post-cured mechanical properties of the silicone. The direct additive manufacturing of PDMS microsphere inks is a particularly exciting prospect because it opens opportunities to fields where porous PDMS structures are already employed. Open-cell PDMS foams have been used for the production of hydrophobic gas exchange membranes in microfluidics systems, sensing materials, photocatalysts, and in separations [22]. The opportunity of direct 3D printing of porous silicone structures may allow for more complex and efficient structures to be used.

Currently, literary works rely on multistep processes to make porous PDMS structures for their applications. A basic approach is the use of a sacrificial negative template with tight pore spaces, such as a sugar cube. The structure is exposed to the liquid PDMS, which infiltrates the structure pores via capillary action. After curing, the negative template is dissolved in water or alcohol leaving behind only the porous PDMS structure [10, 22, 23]. Simple sacrificial templates may be made of common materials like salts and

sugars and more complex templates with well-defined structures can be made by 3D printing the template from PVA. The complexity of the 3D printed template is still limited, as capillary action is still needed to draw the PDMS through the entirety of the structure. Hinton *et al.* was able to print complex structures directly with PDMS by printing in a Bingham fluid support bath [24]. The support bath in this method liquifies under the shear forces caused by the printing nozzle then solidifies around the printed liquid polymer after extrusion. The support bath was liquified by addition of a salt leaving behind only the PDMS structure. This method benefits from being able to use any liquid PDMS as the ink but fails in that it needs a specialized setup and specialty chemicals for the bath, which increases setup complexity and cost.

2.2.2 Emulsion stabilization

Emulsion techniques dominate synthesis routes for microsphere production composed of PDMS or other polymers. Emulsions, which consist of one fluid (dispersed phase) dispersed as droplets into another immiscible fluid (continuous phase), find wide use in many commercial and scientific applications. Food, cosmetics, pharmaceuticals, and materials science have extensively employed the use of emulsions. The dissipation of the dispersed phase leads to a very high surface area between the two immiscible fluids, resulting in a high positive free energy. The interfacial tension at the droplet interface creates a positive pressure difference between the fluid inside the droplet and the bulk continuous phase called the Laplace pressure given by Eq 5 where σ is the interfacial tension and R is the radius of curvature of the droplet. This pressure thermodynamically favors fluid to move from small droplets to larger droplets requiring higher energy to reduce droplet diameter [25]

$$\Delta P_{Laplace} = \frac{2\sigma}{R} \quad 5$$

This pressure differential makes emulsions unstable and promotes droplet coalescence until the phases separate entirely. Surface active agents (surfactant or emulsifier) are amphiphilic molecules that adsorb to the phase interface, reducing surface tension and providing stability to the emulsion.

Consider the mixing of oil and water in equal amounts, along with a surfactant, to form an emulsion. As a general rule, a surfactant that is more soluble in the oil will result in oil being the continuous phase and water being the dispersed phase [26]. This is known as a water-in-oil emulsion, or W/O emulsion. If the surfactant is more soluble in the water phase, then an oil-in-water (O/W) emulsion will be formed. Higher complexity emulsions have also been possible where the first emulsion mixture is itself emulsified into another phase. For example, a W/O emulsion may be mixed into a second water phase containing a new water-soluble surfactant to form a W/O/W double emulsion. Double emulsions are attractive due to the ability to encapsulate high priority materials like drugs or because of high porosity. The inner phase may contain a drug for controlled release inside the body, encapsulate active materials, modify material properties, or may simply act to reduce material usage without sacrificing volume.

Emulsions typically are stabilized by amphiphilic molecules or particles that aggregate at the interface between the continuous and dispersed phases [27]. Proteins and low molecular weight polymers both act as surfactants and can be either neutral or charged. The hydrophilic-lipophilic balance (HLB value) is a rating that describes the affinity a surfactant has for either the water or oil phases [26]. Surfactants with a low HLB value (<6) are more lipophilic and predicted to form stable W/O emulsions. High HLB values (>10) denote high water affinity and are more suitable for O/W emulsions. The HLB value described by Davies is given by Eq 6, where HLB contributions are provided for various molecular groups (e.g. cetyl alcohol) [28].

$$HLB = \sum(\text{hydrophilic group numbers}) - n * (\text{group number per } CH_2 \text{ group}) + 7 \quad 6$$

Concentration of surfactant added to a system monotonically (decreasing) affects the stable size distribution of droplets. After enough surfactant is added, the emulsion size no longer depends on additional surfactant and is instead characterized by the process used to make the emulsion. The point where additional surfactant no longer affects the emulsion size is the critical micelle concentration (CMC) [29]. Aside from the concentration, several general rules that govern the stability of an emulsions is that higher viscosity continuous phase will decrease the collision frequency of dispersed droplets, leading to longer term stability, and that the surface elasticity and the surface viscosity at the phase interface play major roles as well [26, 30].

2.2.3 Methods of emulsification and microsphere synthesis

The simplest conventional emulsion systems (e.g. rotor-stator systems) break apart the dispersed phase by applying high shear on the fluid. In its most basic embodiment, these systems may be a vessel with a stir arm, which leads to droplet breakup of the dispersed phase as mixing progresses—an approach that can only produce rough emulsions with wide size distributions. Smaller emulsions and colloidal suspensions can be made with a different type of rotor-stator system such a colloidal mill. High pressure homogenizers force rough emulsions through a homogenizing valve or narrow orifice to produce ultra-fine systems, an approach used for industry and in food production [31], and ultrasonic emulsification can also be employed for producing very fine emulsions without relying on high shear of the continuous phase [32]. While these approaches are straightforward, high shear methods are energy inefficient due to viscous heat dissipation and generally too destructive to the produce more complex architecture like double emulsions.

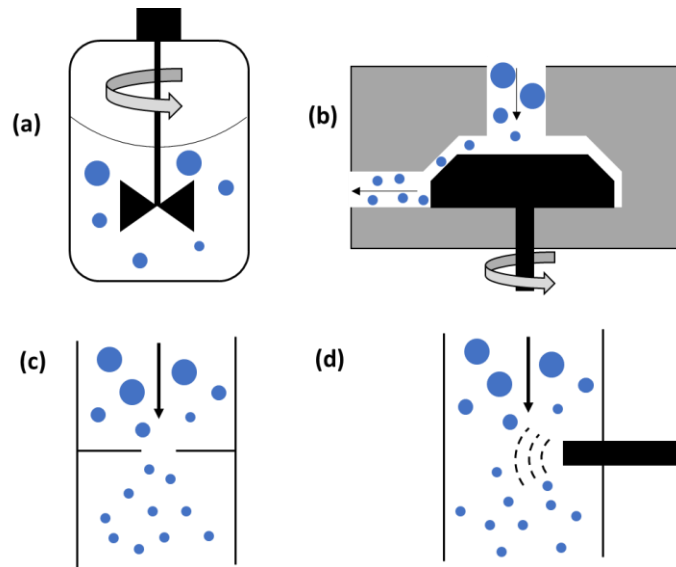


Figure 2.3: Common large-scale approach to emulsion homogenization. (a) Stirred vessel which produces coarse emulsions (b) colloidal mill where droplet breakup occurs in the gap of a rotor-stator system (c) high pressure homogenizing valve where coarse emulsions are forced through an orifice at high velocity (d) ultrasonic breakup shown with an in-line ultrasonic head.

Microfluidics approaches are an alternate method for droplet production that provides users unparalleled control over droplet size and architecture at a fraction of the energy required in high volume systems. The field of droplet production has been extensively researched with a variety of geometries and flow designs suitable for different droplet regimes [33-38]. Several of the most common methods are shown in Figure 2.4 below.

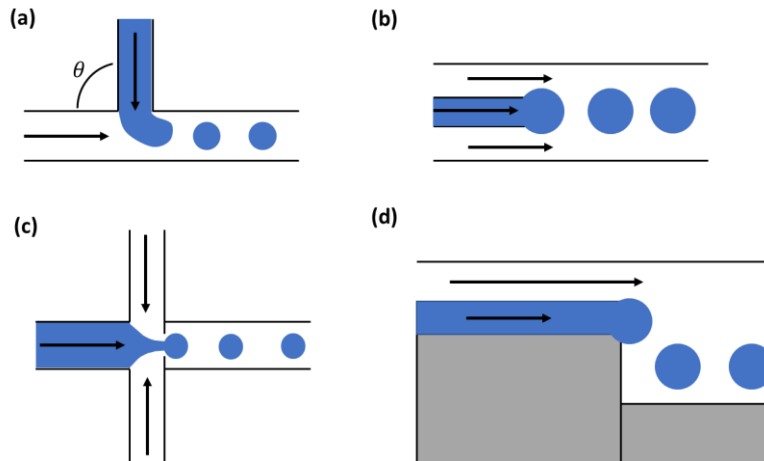


Figure 2.4: Common microfluidic methods for uniform droplet generation. (a) T-junction with dispersed and continuous phase meeting at cone angle θ (b) co-flow with dispersed and continuous phase flowing in parallel (c) flow focusing where droplets are forced through a narrow capillary (d) step flow where droplets fall into a wider channel of continuous phase fluid.

Unlike large scale methods, microfluidics are well suited for making double emulsions and other complex architectures including gas entrapment in double emulsions to produce G/O/W [39]. Double emulsions typically follow a flow focusing route, where one or more droplets of immiscible fluid are sheared off into an outer encapsulating fluid for continuous production, a process iteratively repeated until the desired multilayer emulsion is reached. While monodisperse droplets are frequently desired, there are several downsides to the microfluidics approach. As the name suggests, microfluidics operates with very low working volumes and production rates, which typically operate on the order of $\mu\text{L/hr}$ for single channel systems [20, 38-41]. Second, from our experience, working with microfluidics devices with thermoset polymers, as is done in this study, creates systems that are prone to clogging. Because of the geometry of most microfluidics devices, once polymer is cured within a channel it is almost impossible to recover the reactor, however simple designs using a co-flow approach have been noted to be easy to clean [20]. However, these systems still require direct monitoring to clear clogs to prevent PDMS curing in flow channels.

Membrane emulsification provides a middle ground between the complexity and low shear environment of microfluidics with the scalability and robustness of traditional techniques. Membrane emulsification processes are defined as cross-flow emulsification or as premix emulsification [42-44]. In cross flow emulsification, pure dispersed phase is forced through a porous membrane into the bulk emulsion solution. Shear is applied by the continuous phase across the face of the membrane to aid in droplet removal, which may be applied using a continuous flow system or through a stirred cell batch system. Droplets may also naturally lift off the membrane surface by buoyancy forces and interfacial pressure differences. In premix emulsification, a prepared course emulsion is passed through a membrane to break apart larger droplets to reduce polydispersity.

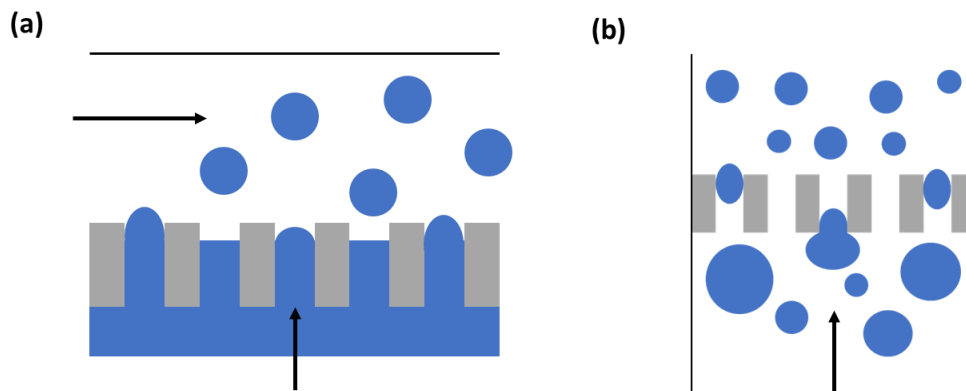


Figure 2.5: (a) Cross flow membrane emulsification where pure dispersed phase is released into continuous phase (b) premix emulsification where a course emulsion is homogenized.

Generally cross-flow emulsification requires more specialized equipment, results in narrower size distribution, and has is more limited in the maximum dispersed phase concentration. Alternatively, premix emulsification allows for higher throughput which makes scalability a realistic option but leads to wider polydispersity. Droplet size in cross-flow systems have also been shown to be robust against changes in continuous flow rate [45]. In the cross-flow process, emulsion droplets are formed at the membrane

surface, and thus depend less on internal membrane structure than premix systems. This means that in cross-flow emulsification, droplet geometries are determined at the surface of the membrane whereas in premix emulsification, droplet size is determined by breakup mechanism inside membrane pores. In each setup, it is crucial that the membrane be wetted by the continuous phase to prevent surface coverage by the dispersed phase which will not lead to good emulsification [44]. One prominent drawback of premix emulsification is that membranes may foul, yet use of a packed beds of particles, rather than membranes, has also been shown as a simple approach to minimize this concern [46, 47]. Both types of membrane emulsification have been shown gentle enough to retain double emulsion architecture, which is a strong contrast to other large scale systems [48, 49]. Chen *et al.* even demonstrated that Janus membranes can be used to produce porous PDMS microspheres (G/O/W double emulsions) in a single step process using N_2 flow through liquid PDMS which is subsequently cured [50].

A variety of other novel microsphere production methods have been reported in literature, ranging from very simple modifications of traditional methods for lab use, to methods designed for scalability and complex production. Rankin *et al.* used ultrasonic spray pyrolysis (USP) to make very fine PDMS microspheres on the order of a few microns in diameter[51]. USP creates a fine mist from a solution of PDMS and hexanes, which is swept by an inert gas through a heated column where the PDMS cures and the solvent is removed. The cured microspheres were then collected in bubblers of ethanol for analysis. This method was used to make microspheres with fluorescent tags and solid particle loadings of magnetic fillers.

Choi *et al.* used a double syringe method, which is essentially a modified homogenizing valve suitable for small scale lab operations. Two luer lock syringes were filled with PDMS and an aqueous phase repeatedly forced through a connecting needle of various gauges [52]. The resulting emulsion was collected and cured. Choi *et al.* report very small microspheres, 700-1300 nm. Choi's publication notes that large microspheres were deliberately removed after curing and not analyzed for size distribution,

making it impossible to gauge control over the true size distribution and product yield using this method. Lopez *et al.* modified the double syringe method by adding a stainless steel frit between the two syringes, making it more similar to premix emulsification than a homogenizing valve [53]. PDMS microspheres were produced without a frit and with frits of pore sizes 20 μm and 10 μm . Introduction of a frit significantly tightened the distribution of particle sizes and gave moderate control over mean diameter, shown in Figure 2.6.

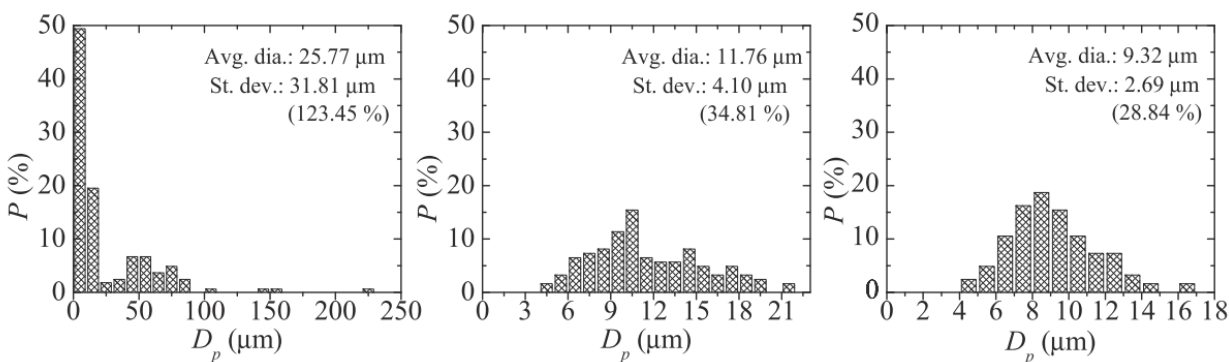


Figure 2.6: Particle size distributions of PDMS particles using a double-syringe premix emulsification method using stainless steel frits of different pore sizes. (Left) No frit (Middle) 20 μm frit (Right) 10 μm frit. Reproduced with permission from [53].

The double syringe method provides fast and easy production of PDMS microspheres and microparticles in lab but cannot be readily scaled. Manual involvement in the emulsification process (i.e. flow rate between the syringes) is not automated in the methods presented by Choi and Lopez, which makes fabrication prone to user variation.

2.3 Materials and Methods

Vinyl terminated PDMS (DMS-V21, 100 cSt) and methylhydro siloxane (HMS-301, 25-35 cSt) were purchased from Gelest for microsphere production. DMS-V21 and HMS-301 were mixed in an 8:1 ratio, according to manufacturer's recommendations. Trimethyl(methylcyclopentadienyl) platinum(IV) (Sigma) complex was used as a UV active catalyst to facilitate the crosslinking reaction. Catalyst was

dissolved in cyclohexane and used at a concentration of 0.01 wt% to the overall weight of polysiloxane. The water phase solution in the emulsification process was 2 wt% Tween 80 and 1 wt% poly(vinyl alcohol) (PVA, 88% hydrolyzed, 145-186 kDa). This mixture of surfactants was found to work well for stability while maintaining low viscosity. Sylgard 184 elastomer kit was used in the making of PDMS reactor structures at a 10:1 ratio.

Membranes used for premix emulsification included track etched membranes and cellulose filters. Hydrophilic polycarbonate track etched membranes were purchased from Sterlitech with 10 μm and 20 μm pore sizes. Whatman filter papers Grade 1 (11 μm average retention) and Grade 3 (6 μm average retention). Grade 3 filters are significantly thicker than the Grade 1 counterpart, at 390 μm and 180 μm nominal thicknesses respectively. Track etched membranes consist of highly regular straight through pores, compared to traditional polymer filters which have arrays of overlapping filaments and inconsistent pore sizes. Microspheres were sized by laser diffraction using a Malvern Mastersizer 3000.

2.4 Design of continuous flow system

Continuous flow processes generally allow for higher throughput and better control over product quality than manual-involved batch processes. A miniaturized reactor system was developed to demonstrate premix emulsification for microsphere synthesis, shown in the diagram below. Vinyl and methylhydro siloxanes were mixed into one solution (4:1 wt ratio) and the Pt catalyst was mixed into vinyl siloxanes. Flow of the two siloxane mixtures was controlled by a Syrris Asia syringe pump at equal flow rates and mixed in-line using a static mixer. While the Pt catalyst has low activity at room temperature, post-pump mixing was chosen to prevent curing of residual siloxanes in the syringe pump valve mechanisms post-experiment. Premixing of all siloxanes and catalyst may be done if a simple syringe pump is used as long as the syringe is UV opaque. The outer water phase flow rate was controlled using a Vapourtec SF-10 peristaltic pump. Both the Vapourtec and Syrris pumps are equipped with built-in pressure sensors to monitor head loss over the full system. Water and silicone phases were mixed using

a simple T-junction before input into the emulsification column. Post emulsification, the emulsion was collected semi-batch style in a stirred vessel with excess surfactant solution and UV exposure from a 365 nm UV floodlight.

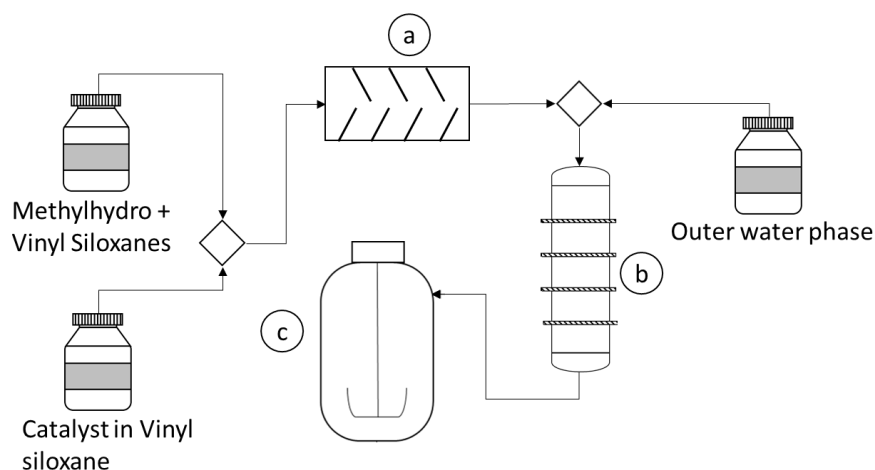


Figure 2.7: Continuous flow system for microsphere production (a) In-line static mixing element (b) Emulsification column (c) Stirred collection and curing beaker with UV light exposure.

The emulsification column was comprised of a 10 mm diameter Omnifit glass chromatography column with PDMS plugs to act as gaskets and membrane sealers. Plugs were molded to the diameter of the column using Sylgard 184. Sylgard 184 is an optically transparent silicone resin so that the process could be visually monitored, and leakage or membrane breakthrough could be easily identified. A 3 mm diameter flow channel was punched in the center of each plug using a standard biopsy punch, giving a cross sectional membrane area of $7.1 \times 10^{-6} \text{ m}^2$. Membranes were cut to size using a 10 mm biopsy punch as needed and held in place between two silicone plugs. The system was held in place by the column endcaps with sufficient pressure that no leakage was observed around the membranes during operation. This column design allows the use of a wide variety of commercially available membranes and filters, can be modified for wider or narrower membrane areas, and is simple to disassemble and clean.

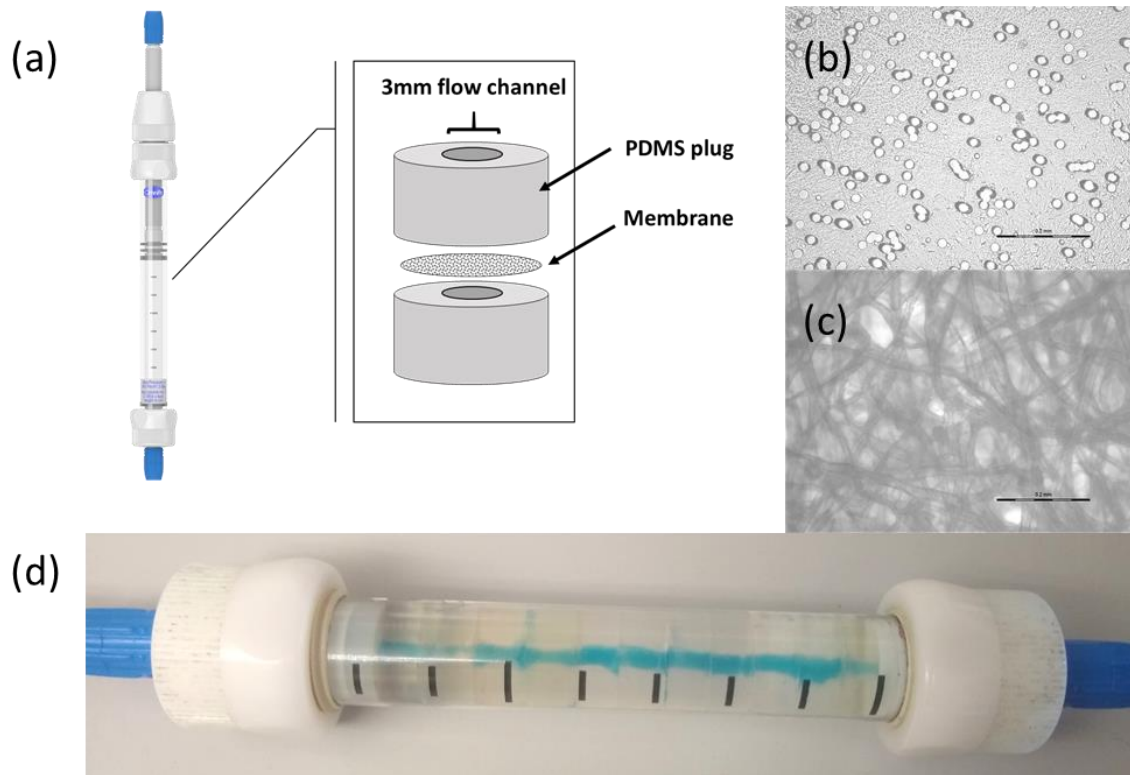


Figure 2.8: (a) Emulsification column using an Omnifit chromatography column as the enclosing sheath and PDMS plugs as gaskets for securing membranes (b) Brightfield image, track etched polycarbonate membrane used with 20 μm pore size- scale bar 200 μm (c) Brightfield image, Grade 1 Whatman cellulose membrane- scale bar 200 μm (d) Emulsification column with dye to show flow channel.

2.5 Results and discussion

The emulsion column design was able to produce PDMS microspheres with good consistency and repeatability and at steady state operating conditions without supervision for long periods of time (>1 hr). Pressure curves were developed using the Grade 3 membranes, which gave much higher pressure loss than the other membranes as it was the thickest and had the most tortuous internal flow path. Pressure profiles were developed using an 8:1 ratio of DMS-V21 and HMS-301 with no catalytic agent to ensure material curing within the membranes did not affect pressure profiles.

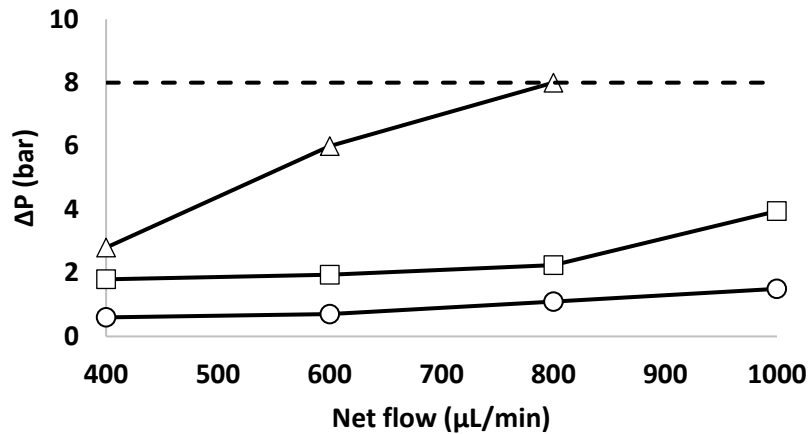


Figure 2.9: Pressure loss across a single Whatman Grade 3 cellulose membrane with 8:1 DMS-V21:HM301 silicone phase. Water to silicone phase flow rates were (Δ) 5:1 (□) 10:1 and (○) 20:1. Dashed line indicates system overpressure limit.

The silicone to water phase flow rate was found to be the most significant contributor to pressure loss for cellulose membranes. This appears to be due to the increased viscosity of the emulsion within the emulsion columns and within membrane pores, rather than because of increased energy flux required for droplet breakup. When multiple cellulose membranes were used in parallel at water:silicone flow ratios of 5:1 or less, accumulation of PDMS between cellulose membranes was also a significant contributor to system overpressure at low flow rates. This process was slow, occurring after several mL is well over 10x the residence volume of the system. Reduction of the PDMS and water flow rates to a 1:10 ratio was able to fully mitigate the issue even at higher flow rates and multiple membrane in series. For example, pressure losses across Grade 3 membranes with silicone phase and water phase flow rates of 100 μL/min and 1000 μL/min respectively experienced steady state pressure loss of 6 bar with 4 membranes in series.

Track etched membranes did not experience high increase in pressure loss or accumulation between membranes at silicone phase fractions as high as 20%. However, difficulty with droplet breakup across individual membranes was observed. As well documented in literature, premix emulsification works best when the course emulsion is passed multiple times over the desired membrane. This is particularly true in the current system, which bypasses forming course emulsions in favor of feeding the PDMS/water mixture as larger droplets from a T mixing joint. Because the emulsion column was transparent, large emulsion droplets on the order of hundreds of microns were visibly seen passing across single track etched membranes, and much less pronounced as subsequent filters were added. This effect was also seen with the cellulose membranes but to a much lesser extent, as internal flow channels are much more tortuous. Visible change in emulsion appearance was essentially nil after three or more track etched membranes were used in series. To confirm this observation, three 20 μm track etched membranes were put in series in the column and a recycle stream was added to allow material to have increased net average passes across membranes. Net flow through the column was maintained at 1 ml/min with a 1:4 PDMS:water phase ratio for all samples collected to maintain the same shearing conditions in each.

Recycle-to-feed ratios (RFR) of 0, 1/3, 1, and 3 with 15 minutes between sample collection to give time for the system to approach steady state. Pressure drop

across the column operated at approximately 1.5 bar in steady state with variation up to 0.5 bar.

Collection of the sample with a RFR of 1 experienced higher pressure drops (~3 bar) and it was found the

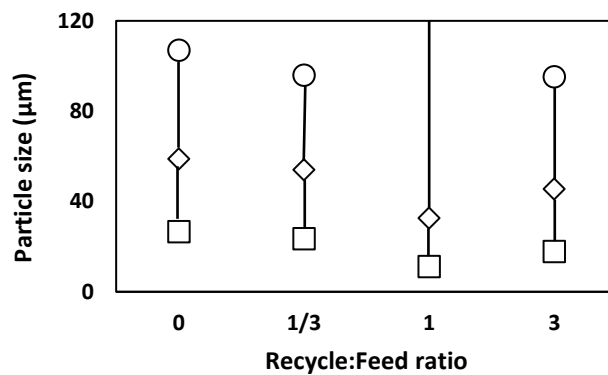


Figure 2.10: D10 (\square), D50 (\diamond) and D90 (\circ) of PDMS microspheres generated by an emulsification column with $3 \times 20 \mu\text{m}$ track etched membranes and varying recycle-to-feed ratios. PDMS:water ratios and net flow through the column were maintained at 1:4 and 1ml/min. D90 of Recycle:Feed ratio of 1(not shown) is 1520 μm .

first membrane in the column was partially fouled and was subsequently replaced collection of an RFR of 3 sample. This fouling, which occurred after nearly an hour of continuous operation, is a likely explanation for a bimodal distribution and high D90 (1520 μm) seen in this sample compared to the other three samples. In general, D10 and D50 values for each sample slightly decreased with increasing recycle ratio, as anticipated, but only gradually.

The tunability of microsphere diameter was demonstrated by selecting an appropriate membrane. Microspheres were generated using each of the four membranes, with 3 membranes used in series at a 4:1 water:silicone flow ratio and net flow rate of 1000 $\mu\text{L}/\text{min}$ to give direct comparison to the results in Figure 2.10 with the 20 μm membranes. Samples produced by the 10 μm track etched membranes showed flocculation prior to testing, resulting in a bimodal distribution and some particles $>500 \mu\text{m}$. Because this effect was not seen with the other 3 membranes (except for RFR 1, Figure 10), the volume of large particles was removed in Figure 11 to focus on the main peak.

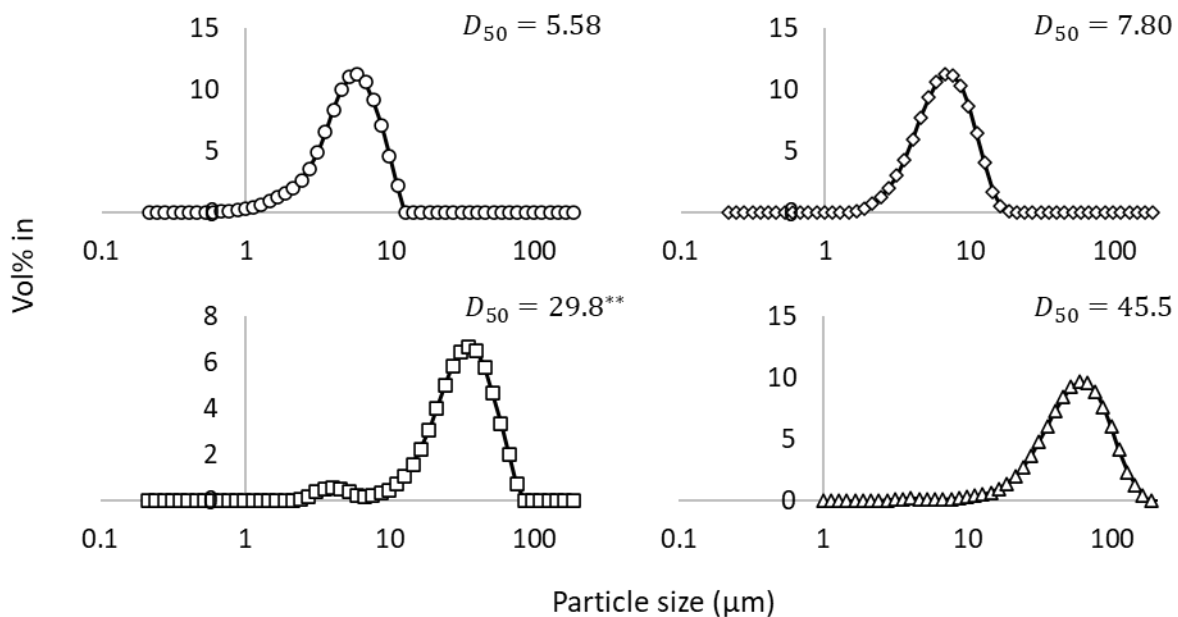


Figure 2.11: Particle size results using premix emulsification column using 3x (top right) Whatman Grade 1 (top left) Whatman Grade 3 (bottom left) 10 μm track etched (bottom right) 20 μm track etched membranes. ** Samples showed visible flocculation with particles above 500 μm , D_{50} value calculated from main peak shown in the figure above.

Tightened distributions in particle size using the premix membrane emulsification method is a strong improvement compared to high shear emulsification. As a comparison between the two, PDMS microspheres were produced using the double syringe method similar to the method described by Choi [52]. Two luer lock syringes were connected with a 1 mm orifice between them. 1 ml of PDMS and 2 ml surfactant solution was loaded into the syringes and emulsified. The mixture was passed through the orifice 30 times, then diluted with more surfactant solution and cured with UV exposure. These microspheres showed a broad, trimodal distribution with peaks at 2.13 μm , 40.1 μm , and 1430 μm , although the later may be due to agglomeration/flocculation seen in other samples.

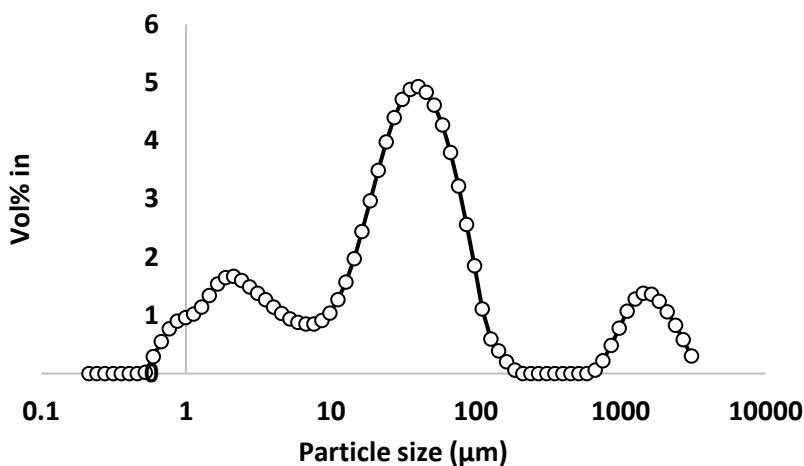


Figure 2.12: PDMS microsphere distribution using the double syringe method with 1 mm orifice.

Customization of microsphere diameter has been demonstrated and several important processing considerations should be mentioned. First, a UV active catalyst was chosen in this experiment. Initially, a thermal platinum catalyst, SIP6832.2 (Gelest), was used. The thermal catalyst worked well but comes with the trade off with increasing activity at room temperature. A highly active

catalyst is more likely to lead to membrane fouling but catalysts with lower activity take more time to cure in a collection beaker, leading to high chances of droplet coalescence. High curing temperatures may also affect emulsion stability during curing, something that was noted when only PVA was used as a surfactant. A second important note on using thermally active catalysts is the formation of cured rubber at the surfaces of tubing. Since most plastic tubing is hydrophobic, PDMS tended to form thin films on the inner surface of the tubing where it eventually cured. These skins formed over multiple hours of use and would eventually break free from flow shear, be flushed downstream, and accumulate on membrane surfaces. This issue was not seen after switching to the UV active catalyst, since its room temperature activity is low in the absence of a UV source.

Because the feed into the emulsion column was in the form of small slugs dispersed in water, pressure swings were observed when the slugs made first contact with the first membrane. To confirm this, the first membrane was removed from the emulsification column and put into a custom filter holder to produce a rough emulsion prior to the column. A pressure meter between the filter holder and the emulsion column showed no pressure swings, while a pressure meter monitoring overall system pressure did. Usually these swings were in the range of ± 0.5 bar and is something to keep in mind if the pumped used have limited pressure ranges, if pumps used are not operating with constant volumetric flow, or if membranes used are subject to breakage over small pressure ranges. It is recommended that a coarse emulsion be made using a robust membrane, such as a frit. Hydrophobic frits were successfully tested but only worked well at high flow rates. When a polyethylene frit (25 μm pore size) was used to produce the first coarse emulsion in the column, PDMS accumulated inside the porous structure and was released in large globs onto the second membrane. Again, this led to mild pressure swings. Increasing the net flow rate through the frit mitigated this even while the ratio of PDMS:water remained constant. Another option is to use membranes in series that subsequently decrease in pore size to

reduce the transmembrane energy needed for droplet breakup because the change in droplet diameter across each membrane is reduced.

2.6 Conclusions

In this section, the use of premix emulsification has been shown as a viable method for producing PDMS microspheres of tunable size. Membrane choice is the predominant factor in control of microsphere distribution, with track etched membranes performing well with low transmembrane pressure but with higher dependency on the number of membranes needed. Volume fraction of the silicone phase strongly impacted transmembrane pressure drop with 10 vol% silicone phase or lower recommended to prevent membrane fouling. An emulsification column design is presented that takes advantage of cheap and commercially available membranes for the fabrication process and can easily be disassembled for cleaning and repair. This contrasts other methods that may rely on specialty equipment such as microfluidics chips or homogenization equipment. Finally, the described method is shown to have high throughput at PDMS generation rates exceeding $2 \text{ m}^3/(\text{hr m}^2)$ while being scalable with membrane area.

References

1. Zeigler, J. and F.W.G. Fearon, *Silicon-Based Polymer Science A Comprehensive Resource*. 1990, Washington D.C.: American Chemical Society.
2. *Silicone chemistry Overview*. 1997, Dow Corning Corporation: Midland.
3. Ducom, G., et al., *Hydrolysis of polydimethylsiloxane fluids in controlled aqueous solutions*. Water Science and Technology, 2013. **68**(4): p. 813-820.
4. Barrere, M., et al., *Anionic polymerization of octamethylcyclotetrasiloxane in miniemulsion II. Molar mass analyses and mechanism scheme*. Polymers, 2001. **42**: p. 7239-7246.
5. Zlatanovic, A., et al., *Suppression of Crystallization in Polydimethylsiloxanes and Chain Branching in Their Phenyl-Containing Copolymers*. Macromolecules, 2017: p. 3532-3543.
6. Cypriak, M., *Polymerization of Cyclic Siloxanes, Silanes, and Related Monomers*, in *Polymer Science: A Comprehensive Reference, Volume 4*. 2012, Elsevier Science. p. 451-476.
7. *Reactive Silicones: Forging new polymer links*. 2016, Gelest Inc: Morrisville.
8. Johnston, I.D., et al., *Mechanical characterization of bulk Sylgard 184 for microfluidics and microengineering*. Journal of Micromechanics and Microengineering, 2014. **24**: p. 035017.
9. Xie, Y., et al., *Surface Hydrophobic Modification of Microcrystalline Cellulose by Poly(methylhydro)siloxane Using Response Surface Methodology*. Polymers, 2018. **10**(12): p. 1335.
10. Jung, Y., et al., *A Highly Sensitive and Flexible Capacitive Pressure Sensor Based on a Porous Three-Dimensional PDMS/Microsphere Composite*. Polymers, 2020. **12**: p. 1412.
11. Pruvost, M., et al., *Polymeric foams for flexible and highly sensitive low-pressure capacitive sensors*. NPJ Flexible Electronics, 2019. **3**(1): p. 1-6.
12. Xing, C., et al., *Flexible Microsphere-Embedded Film for Microsphere-Enhanced Raman Spectroscopy*. ACS Appl Mater Interfaces, 2017. **9**(38): p. 32896-32906.
13. Roy, P., et al., *Polysiloxane-based core-shell microspheres for toughening of epoxy resins*. Journal of Polymer Research, 2014. **21**(1): p. 1-9.
14. Tang, Q., et al., *Poly (dimethyl siloxane)/poly (2-hydroxyethyl methacrylate) interpenetrating polymer network beads as potential capsules for biomedical use*. Current Applied Physics, 2011. **11**(3): p. 945-950.
15. Shields, C.W., et al., *Elastomeric Negative Acoustic Contrast Particles for Capture, Acoustophoretic Transport, and Confinement of Cells in Microfluidic Systems*. Langmuir, 2014. **30**(14): p. 3926-3927.
16. Yin, D., et al., *Effective cell trapping using PDMS microspheres in an acoustofluidic chip*. Colloids and surfaces. B. Biointerfaces, 2017. **157**: p. 347-354.
17. Li, T., et al., *A flexible strain sensor based on CNTs/PDMS microspheres for human motion detection*. Sensors and Actuators. A. Physical, 2020. **306**.

18. Otungen, T.I.U.K.A.M.V., *High-resolution force sensor based on morphology dependent optical resonances of polymeric spheres*. Journal of Applied Physics, 2009. **105**(1).
19. Dong, C.-H., et al., *Fabrication of high- Q polydimethylsiloxane optical microspheres for thermal sensing*. Applied Physics Letters, 2009. **94**(23).
20. Amjadi, A., et al., *Durable Perovskite UV Sensor Based on Engineered Size-Tunable Polydimethylsiloxane Microparticles Using a Facile Capillary Microfluidic Device from a High-Viscosity Precursor*. ACS Omega, 2020. **5**(2): p. 1052-1061.
21. Roh, S., et al., *3D Printing by Multiphase Silicone/Water Capillary Inks*. Advanced Materials, 2017. **29**(30).
22. Zhu, D., S. Handschuh-Wang, and X. Zhou, *Recent progress in fabrication and application of polydimethylsiloxane sponges*. Journal of Materials Chemistry A, 2017. **5**(32): p. 16467-16497.
23. Yu, C., et al., *Facile Preparation of the Porous PDMS Oil - Absorbent for Oil/Water Separation*. Advanced Materials Interfaces, 2017. **4**(3).
24. Hinton, T.J., et al., *3D Printing PDMS Elastomer in a Hydrophilic Support Bath via Freeform Reversible Embedding*. ACS biomaterials science & engineering, 2016. **2**(10): p. 1781-1786.
25. Jiao, J. and D. Burgess, *Multiple Emulsion Stability: Pressure Balance and Interfacial Film Strength*, in *Multiple Emulsions: Technology and Applications*. 2008, John Wiley & Sons, Inc.: Hoboken. p. 1-27.
26. Claesson, P., E. Blomberg, and E. Poproshev, *Surface Forces and Emulsion Stability*, in *Food Emulsions, 4th ed.* 2004, Marcel Dekker: New York.
27. Zembyla, M., B.S. Murray, and A. Sarkar, *Water-in-oil emulsions stabilized by surfactants, biopolymers and/or particles: a review*. Trends in Food Science & Technology, 2020. **104**: p. 49-59.
28. Davies, J.T. *A Quantitative Kinetic Theory of Emulsion Type I. Physical Chemistry of the Emulsifying Agent*. in *Gas/Liquid and Liquid/Liquid Interfaces. Proceedings of 2nd International Congress Surface Activity*. 1957. London.
29. Ruckenstein, E. and R. Nagarajan, *Critical micelle concentration. Transition point for micellar size distribution*. Journal of Physical Chemistry, 1975. **79**(24): p. 2622-2626.
30. Boyd, J., C. Parkinson, and P. Sherman, *Factors Affecting Emulsion Stability, and the HLB Concept* Journal of Colloid and Interface Science, 1972. **41**(2): p. 359-370.
31. *High pressure homogenizer*. Bertoli Homogenizers.
32. Kaci, M., et al., *Emulsification by high frequency ultrasound using piezoelectric transducer: Formation and stability of emulsifier free emulsion*. Ultrasonics sonochemistry, 2014. **21**(3): p. 1010-1017.
33. Chong, D., et al., *Advances in fabricating double-emulsion droplets and their biomedical applications*. Microfluidics and Nanofluidics, 2015. **19**(5): p. 1071-190.
34. Gao, W. and Y. Chen, *Microencapsulation of solid cores to prepare double emulsion droplets by microfluidics*. International journal of heat and mass transfer, 2019. **135**: p. 158-163.

35. Nabavi, S.A., G.T. Vladislavljević, and V. Manović, *Mechanisms and control of single-step microfluidic generation of multi-core double emulsion droplets*. Chemical engineering journal, 2017. **322**: p. 140-148.
36. Zhao-Miao, L., D. Yu, and P. Yan, *Generation of Water-In-Oil-In-Water (W/O/W) Double Emulsions by Microfluidics*. Chinese Journal of Analytical Chemistry, 2018. **46**(3): p. 324-330.
37. Li, W., et al., *Microfluidic fabrication of microparticles for biomedical applications*. Chemical Society Reviews, 2018. **47**(15): p. 5645-5683.
38. Zhu, P. and L. Wang, *Passive and active droplet generation with microfluidics: a review*. Lab on a Chip, 2017. **17**: p. 34-75.
39. Wang, W.-T., et al., *One-step microfluidic production of gas-in-water-in-oil multi-cores double emulsions*. Chemical engineering journal, 2015. **263**: p. 412-418.
40. Wang, J., et al., *Microfluidic Rapid Fabrication of Tunable Polyvinyl Alcohol Microspheres for Adsorption Applications*. Materials, 2019. **12**(22): p. 3712.
41. Ji, Q., et al., *A Modular Microfluidic Device via Multimaterial 3D Printing for Emulsion Generation*. Sci Rep, 2018. **8**(1): p. 4791.
42. Giorno, L., *The Principle of Membrane Emulsifier*. Encyclopedia of Membranes, 2015.
43. Gijsbertsen-Abrahamse, A., *Membrane emulsificationL process principles*. 2003, Wageningen University: Wageningen.
44. Nazir, A., *Premix Eulsification Systems*. 2013, Wageningen University: Wageningen.
45. Yasuno, M., et al., *Visualization and characterization of SPG membrane emulsification*. Journal of membrane science, 2002. **210**(1): p. 29-37.
46. Van Der Zwan, E.A., C.G.P.H. Schroën, and R.M. Boom, *Premix membrane emulsification by using a packed layer of glass beads*. AIChE Journal, 2008. **54**(8): p. 2190-2197.
47. Nazir, A., R.M. Boom, and K. Schroën, *Droplet break-up mechanism in premix emulsification using packed beds*. Chemical engineering sciences, 2013. **92**: p. 190-197.
48. Shima, M., et al., *Preparation of fine W/O/W emulsion through membrane filtration of coarse W/O/W emulsion and disappearance of the inclusion of outer phase solution*. Food hydrocolloids, 2004. **18**(1): p. 61-70.
49. van Der Graaf, S., C.G.P.H. Schroën, and R.M. Boom, *Preparation of double emulsions by membrane emulsification—a review*. Journal of membrane science, 2005. **251**(1): p. 7-15.
50. Chen, Y.L., Zhenzhen ; Liu, Qingxia, *Janus membrane emulsification for facile preparation of hollow microspheres*. Journal of membrane science, 2019. **592**.
51. Rankin, J.M., et al., *Magnetic, Fluorescent, and Copolymeric Silicone Microspheres*. Advanced Science, 2015. **2**(6).
52. Choi, Y.H., et al., *Production of PDMS microparticles by emulsification of two phases and their potential biological application*. International journal of polymeric materials, 2018. **67**(11): p. 686-692.

53. López, M., et al., *A simple emulsification technique for the production of micro-sized flexible powder of polydimethylsiloxane (PDMS)*. Powder Technology, 2020. **366**: p. 610-616.

Chapter 3: Double emulsion PDMS microspheres by interfacial reactive stabilization

3.1 Introduction

In Chapter 2, methods of fabrication and usages for PDMS microspheres was discussed in detail. From sensor applications to additive manufacturing, PDMS microspheres and porous PDMS structures are a growing field with unique applications. Mechanical and physical properties of PDMS microspheres can be further tuned by producing more complex architectures than just simple solid spheres. Double emulsions and complex emulsion architecture would allow for encapsulating multiple phases into droplets within the microspheres. If the encapsulated phase is replaced by a gas, such as by evaporating out entrapped water, a porous microsphere would be retained that has low density, weight, and stiffness. As noted earlier, large scale methods of emulsion production typically involve high shear environments, making them incompatible for double emulsions. That is, too high of shear and the double emulsion will break down, leaving behind a simple emulsion and a solid PDMS microsphere.

In this study, the sensitivity of the silicon-hydrogen bond to hydroxyl groups is investigated as means of stabilizing the interface of the inner and middle phases in W/O/W double emulsions as well as produce a blowing gas for entrapment as way to make highly porous PDMS microspheres at high throughputs. The dehydrogenation of methylhydro siloxanes with hydrophilic phase components is investigated to make high molecular weight molecules and crosslinked networks that can stabilize the interface even in high shear environments. Batch preparations of double emulsions are produced, screening through a variety of different polymers, surfactants, and additives to determine the best formulation. In culmination, a formulation and method presented that may be adaptable to produce porous PDMS microspheres in a scalable manner.

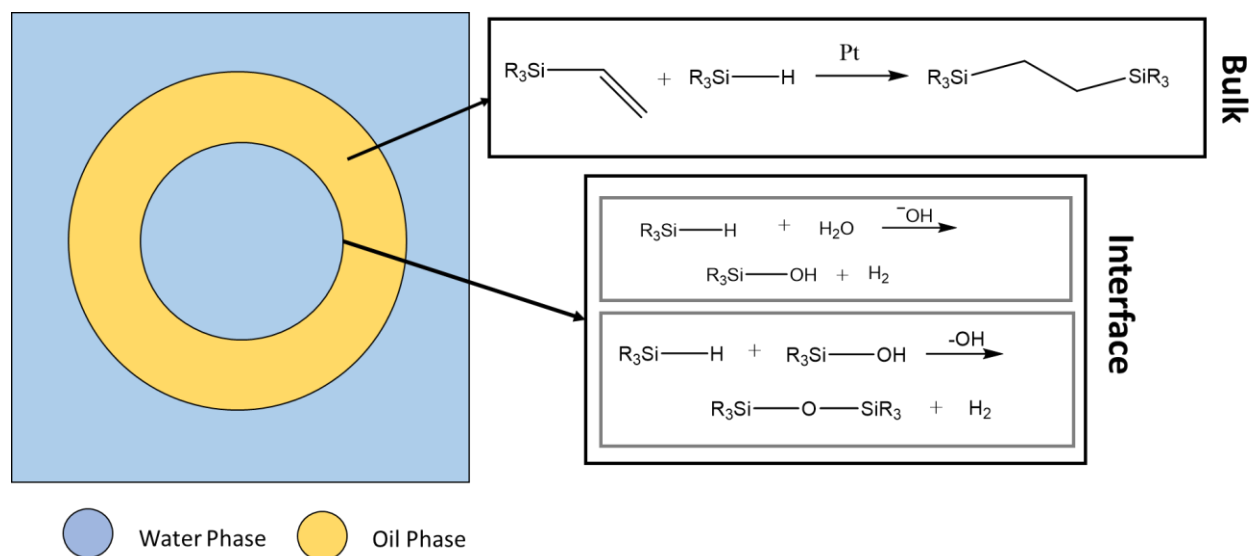


Figure 3.1: Schematic summary of interfacial polymerization for stabilizing PDMS double emulsions.

3.2 Literature Review

So far in this work, significant aspects on polysiloxane chemistry and microsphere fabrication routes have already been highlighted. In general, low shear and microfluidics methods mentioned dominate the literature as means of producing highly uniform double emulsions. Interfacial polymerization is an alternative approach for the encapsulation and stabilization of an emulsion. Widely used, this approach polymerizes two materials at the phase interface, one in the oil phase and one in the water phase, which creates a thin stabilizing layer of high molecular weight material rather than relying on stabilization by an emulsifier layer [1-4]. Similar approaches have been used that rely on complexation and electrostatic interactions rather than conventional polymerization [5]. Interfacial polymerization has been previously proven to make high infill PEG-in-PDMS structures as demonstrated by Giustiniani [6]. In this process, a PDMS curing catalyst was dissolved in PEG which was dropwise added to a liquid PDMS. As the catalyst diffused to the PEG-PDMS interface, PDMS polymerization stabilized the interface. Emulsion stabilization and core encapsulation is also possible by solvent removal of the outer emulsion phase, which

solidifies the outer emulsion phase [7, 8]. A modification of the solvent evaporation method has also been used to produce porous microspheres of PLGA [9].

The chemistry of the dehydrogenation reaction is covered in detail in Chapter 1 and will not be covered here. However, a note on catalyst selection for the dehydrogenation reaction is made. Silanol dehydrogenation with hydride containing polysiloxanes is an industrially-applied technology with a variety of commercial catalysts designed for this purpose—these are typically metal salts. Common examples include bis(2-ethylhexanoate) tin(II), dibutyldilauryltin, zinc octoate, and iron octoate and are designed to have lipophilic moieties to improve dispersion in PDMS [10]. Here, it is most beneficial to have a catalyst with strong affinity for the inner aqueous phase so that the catalyst does not migrate away from the inner W/O interface. Depending on the selection, these catalysts may be incompatible with Pt catalysts used in vinyl addition PDMS cure. For example, tin(II) is incompatible with commercial vinyl addition Pt catalysts, and deactivation of both catalysts occurs when the two catalysts are used in the same system.

3.3 Materials and Methods

PDMS microspheres were produced by vinyl addition reaction between vinyl terminated PDMS and methylhydro siloxanes. SIP6830.3 and SIP6832.2 (Gelest) thermally activated and trimethyl (methylcyclopentadienyl) platinum(IV) (Sigma) UV activated platinum catalysts were used to complete the crosslinking reaction. Potassium hydroxide pellets (>85% purity, 10-15 wt% water; Sigma) were to make aqueous catalyst solution to activate the dehydrogenation reaction. KOH was used over traditional metal salt catalysts because it is compatible with Pt catalysts, has high water affinity, and does not impact or activate vinyl addition cure. Table 3.1 lists the variety of polysiloxanes, surfactants, solvents, and non-surfactant materials used.

Table 3.6: Materials used for porous PDMS microsphere fabrication. Materials sourced from (a) Gelest (b) Dow chemical (c) Sigma-Aldrich (d) Fisher (e) Spectrum (f) Acros (g) Swan (h) Alfa Aesar (i) Fluka.

Polysiloxanes	Surfactants	Solvents	Non-surfactant additives
DMS-V21 ^a	Tween 80 ^d	Methanol ^c	PEG200 ^h
DMS-V31 ^a	Poloxamer F68 ^e	Ethanol ^d	PEG400 ^c
HMS-301 ^a	Poloxamer F123 ^c	Isopropanol ^g	PEG1500 ⁱ
Sylgard 184 ^b	Dowsil ES5600 ^b	DMSO ^c	PEG8000 ^d
Silanol terminate PDMS (65 cSt) ^c	Dowsil ES5300 ^b	Water	Glycerol ^c
	100% hydrolyzed PVA ^f		

The general procedure for screening tests were as follows. Liquid PDMS mixture was made of 8:1 volume ratio of DMS-V21 to HMS-301. Silicone emulsifiers (ES5300 and ES5600) were added in amounts from 0-8 wt% of the siloxane phase. PDMS and the hydrophilic phase were emulsified in a 3:1 volume ratio in a 1.5 mL centrifuge tube using a vortex mixer followed by a resting period of 10 minutes with intermittent mixing to allow the interfacial reaction to proceed. Following the resting period, diluted platinum catalyst SIP6830.3 in DMS-V21 was added at 1/3 the initial PDMS phase volume. The final hydrophilic phase constituted 20 vol% of the emulsion. Once the catalyst was added, the entire emulsion was immediately added to 5 mL of 2-2.5 wt% PVA (88% hydrolyzed, 145-186 kDa) aqueous solution as the outer phase and emulsified using a vortex mixer. Emulsions were viewed under a brightfield microscope to evaluate double emulsion retention and reactivity was qualitatively assessed by monitoring hydrogen release rate from the original W/O emulsion. Fluorescein was used to tag hydrophilic phase for microscopy imaging.

3.4 Results and discussion

Solvent selection requires optimization between cost, reactivity, safety, and efficiency. Water, of course, is the ideal choice but high hydrogen bonding levels between water and the hydroxide catalyst limits the mobility of the hydroxide across the interface, which was necessary to promote dehydrogenation. This leads to longer reaction periods needed to form a stable interface or higher hydroxide concentration. Small alcohols are a good alternative as their ion affinity is lower while polar

aprotic solvent would be expected to promote the reaction the most. The hydrogen bond donor and acceptor abilities of the solvents tested in this experiment are shown below. In particular, lower donor ability would be expected yield loose binding with the hydroxide anion and make the system more reactive. This is seen in DMSO-based hydrophilic phases, which had to have KOH concentrations reduced to a fraction of a weight percent to control hydrogen release.

Table 3.7: Hydrogen bonding abilities of the solvents used [11].

Solvent	Donor Ability (α)	Acceptor Ability (β)
Water	1.17	0.47
Methanol	0.93	0.66
Ethanol	0.83	0.75
Isopropanol	0.76	0.84
DMSO	0.00	0.76

Despite higher reactivity, DMSO, ethanol, and isopropanol could not form stable emulsions—a typical result in traditional, nonreactive emulsion systems. Methanol was able to form emulsions stable on the order of tens of minutes when mixed in high concentrations of PEG400 with KOH loadings of 1-5 wt%, but emulsion stability was significantly less than the stability seen when water is used as the primary solvent. Using water/alcohol mixtures of up to 10% alcohol formed stable emulsions and kept viscosity and surface tension low enough to ensure easy water droplet breakup. However, the improvements with water/alcohol mixtures were not significantly above a simple water inner phase and thus were ruled out on the grounds of increased cost and complexity. In addition to emulsion stability issues, rejection of KOH

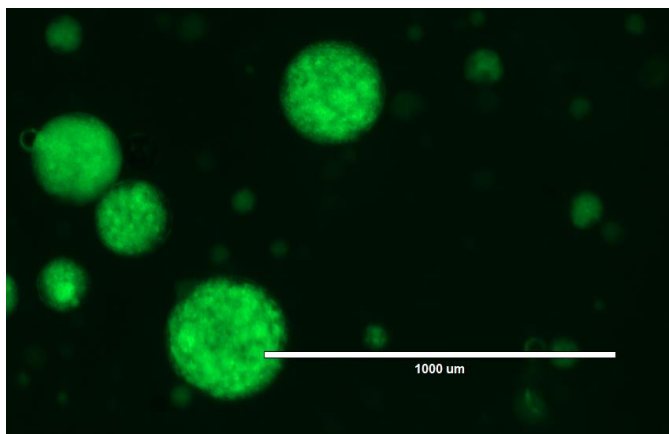


Figure 3.2: Fluorescein tagged double emulsion PDMS microspheres. Inner hydrophilic phase of 1 wt% KOH, 29 wt% PEG400, 70 wt% MeOH with fluorescein. Silicone phase of 8:1 DMS-V21:HMS-301 with 5 wt% ES5600.

by lower polarity solvents may result in permanent catalyst migration to the PDMS phase resulting in hard-to-remove silanolates. Studies of microemulsion polymerization of PDMS in water have shown that KOH catalysts preferentially stay at the interface or in the aqueous phase and transport of silanolates into the PDMS bulk is minimal [12, 13].

Several options for hydrophilic phase polymers, additives, and surfactants were investigated. Ideally, a water phase surfactant adsorbs to the water-oil interface, as well as carries multiple hydroxyl sites. In theory, these attributes would allow the additives to take part in network formation with hydroxysilanes in the silicone phase. However, low concentrations of the water-soluble polymers tested did not have a significant impact on the stability of the double emulsion architecture. One challenge to complexing the surfactant into a siloxane-based co-polymer is control of the successive cleavage of the formed silyl ether into a silanol and the original surfactant molecule. As mentioned in Chapter 2, hydrolysis rates greatly depend on steric effects, so it is difficult to predict if any additives into the aqueous solution were beneficial. In addition, free hydroxyl groups of water simply outnumber available surfactant alcohol, which may yield silanol groups rather than silyl ethers with the surfactant molecules. Water phase surfactants may also be detrimental to the system by lowering the maximum concentration of the inner water phase before phase inversion. In general, it was found that water soluble surfactants did not significantly improve the formation of double emulsions.

Non-surfactant additives should share similar properties to water phase surfactants such as multiple hydroxyl sites for network formation and reasonable partitioning between the two phases. PEG was found to be the best additive to the hydrophilic phase and promoted significantly higher hydrogen release rates. This is most likely explained by PEG's ability to complex with KOH for improved phase transfer ability as has previously been reported [14, 15]. Higher molecular weight PEG performed significantly better than short chain PEG which may be due to the decreased hydrophilicity of the ester backbone compared to the hydroxyl terminals and promoting better phase partitioning. Glycerol

generally did not improve interface networking for W/O/W emulsions when added as an aqueous solution but did promote another type of double emulsion. A 50/25/25 vol% mixture of PEG400/glycerol/DMSO resulted in a high population of double emulsions shown in Figure 3.3. These double emulsions have a thick opaque outer shell that is clearly different from similar sized solid-PDMS microspheres that also appeared in the image. Fluorescent imaging showed high concentrations of fluorescein trapped in this shell whereas no fluorescein appears in the standard PDMS microspheres. It is as though the shell consisted of a PEG-glycerol-PDMS copolymer that underwent inversion during the second emulsification step with a cured PDMS core.

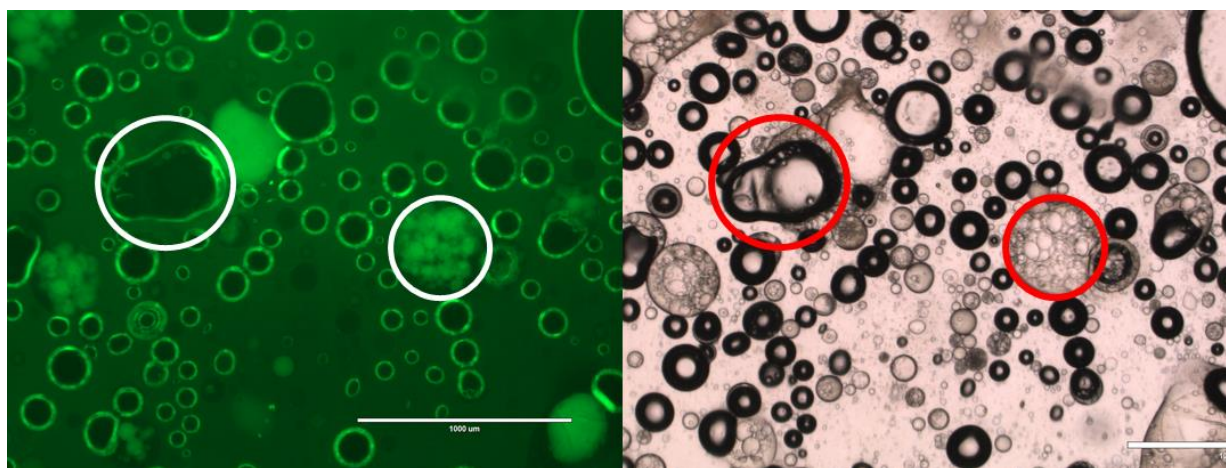


Figure 3.3: Inverted double emulsions produced by a hydrophilic phase of 50/25/25 vol% PEG400/glycerol/DMSO (~1 wt KOH catalyst) was dosed with fluorescein. PDMS is encapsulated by what is suspected to be a PEG/glycerol/PDMS copolymer shell. Fluorescein is insoluble in the PDMS phase and is expected to accumulate where the hydrophilic phase exists. Circles are used to aid in orientation only.

While the inverted double emulsion above is not desirable for this project, it may provide a novel method for encapsulating lipophilic payloads. As mentioned, siloxane-alkoxide bonds are sensitive to hydrolysis meaning the copolymer outer shell formed may readily decompose back into biologically compatible species (PEG, glycerol, and PDMS). With the encapsulation occurring at the outer interface,

no hydrogen entrapment is seen in the inverted double emulsion, and the affinity for the hydrophilic phase may limit the amount of basic catalyst present in the double emulsions.

Dowsil ES5600 and ES5300 are silicone-based surfactants specifically designed for producing stable water-in-silicone emulsions. Both surfactants worked very well in producing double emulsions even when KOH was excluded. Mixtures with both KOH and the silicone emulsifiers had a noticeable decrease in hydrogen release rate compared to systems without the emulsifiers. Likely, the polymers create an obstructive layer at the interface that inhibited contact between hydride groups in the silicone phase and the hydroxyl groups of the water phase.

After initial screening tests, final formulations were used to make double emulsions in a higher shear environment. The double syringe method described in Chapter 2 was used due to its simplicity, with a 1 mm orifice used for droplet breakup. With this method, higher viscosity PDMS could be used, which promoted better retention of the double emulsions by reducing the frequency of droplet accumulation. Typical double emulsion microspheres ranged from 50-300 μm in diameter and were imaged using brightfield microscopy. Images of these microspheres showed many small water and gas domains trapped within, giving foggy and unfocused images. This contrasts with solid PDMS microspheres, which were clear. The hydrophilic phase was chosen to be an aqueous solution only of PEG8000 and KOH at concentrations of 5.5 wt% and 1 wt% respectively with resting period time increased to 15 minutes. The silicone phase was changed to a 10:1 weight ratio of DMS-V31 and HMS-301 with SIP6832.2 as the thermally activated catalyst. Water phase concentration was set to 25% of the total emulsion volume. As long as intermittent mixing was done during the resting period, it was found that silicone emulsifying agents ES5300 and ES5600 could be entirely excluded from the system. This is because produced silanols and PEG-siloxane copolymers have similar emulsifying capabilities and were fully capable of stabilizing the W/O interface. Figure 3.4 below shows a collection of porous microspheres collected from this final

formulation. Every large microsphere shows clear encapsulation of many small water and gas domains, as indicated by their foggy appearance, an encouraging result for this screening study.

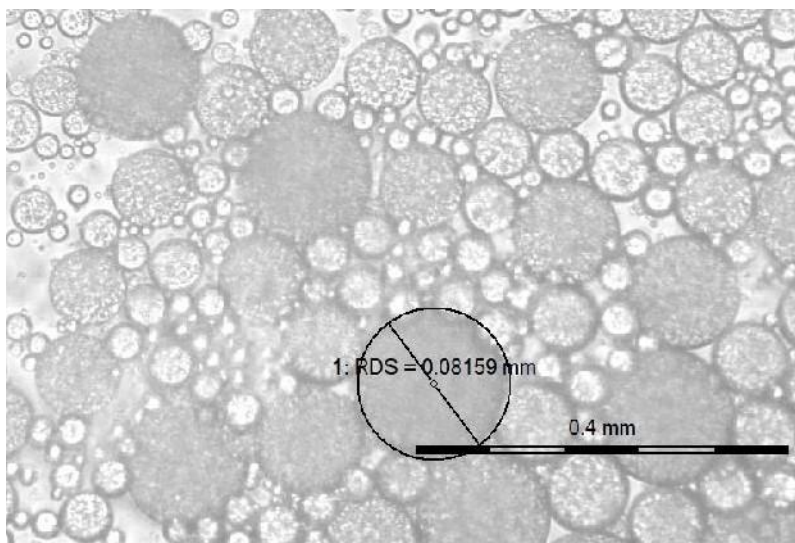
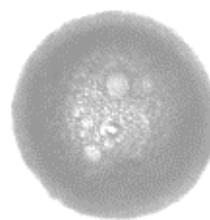


Figure 3.4: Double emulsion microspheres produced by double syringe method.

Further increasing viscosity of the of the silicone phase, double emulsions were made using Sylgard 184 (10:1 base:curing agent ratio). Sylgard 184 has a viscosity roughly 5 times greater than DMS-V31 and contains silica filler as a mechanical property modifier. Microspheres were made according the double syringe method in two cases. In the first case, Sylgard microspheres were thermally cured using the Pt catalyst already incorporated as part of the elastomer base formulation. Curing time and temperature was approximately 60°C for 3 hours. In the second case, (methylcyclopentadienyl) platinum(IV) was added (0.01 wt%) to cure the rubber at room temperature with UV exposure. UV cured microspheres were heated post-curing to activate the hydrogen release reaction. This caused a noticeable increase in microsphere diameter, which was not seen when the thermally cured microspheres were reheated. This indicates that the supply of hydride groups available for H_2 production was mostly exhausted during the 3-hour heated cure. This post-cured heating of the UV cured microspheres allowed for the entrapped water domains to grow in size and led to higher gas phase entrapment, reducing overall density and increasing porosity. This is specifically indicated by settling of the microspheres in water. The

thermally cured batch had density greater than water and settled to the bottom, whereas many of the UV cured microspheres (post-heating) rose to the top. For reference, Sylgard 184 has a bulk specific gravity of 1.05, which indicated some partial volume of the UV cured microspheres contained gas domains. These two



0.4 mm



Figure 3.5: Isolated Sylgard 184 PDMS microsphere with porous structure caused by post-cured hydrogen capture.

production routes of Sylgard microspheres indicated cure times and temperatures are additional variables that can lead to high gas phase entrapment for low density, high porosity structures.

Finally, the proposed method was compared to the performance of traditional H_2 blown foam siloxane reactions between silanols and methylhydro siloxanes. The curing reaction is simply the same as a dehydrogenation reaction used in the proposed method, however now a Si-O-Si bond is formed between the silanol and methylhydro silicone with the liberation of hydrogen still occurring. Silanol-terminated PDMS (65cSt) and HMS-301 were mixed in 2:1 ratio with tin(II) 2-ethylhexanoate at 2 wt% as catalyst. The PDMS mixture was emulsified using a vortex in 2 wt% PVA and cured at 60°C for several hours. Shown in Figure 3.6 below, poor gas entrapment was seen with microspheres produced using this method. Only small volumes of gas bubbles remained entrapped which appeared to primarily center around the core of sphere and were significantly lacking in comparison to the porous structures shown in figures 3.4 and 3.5.

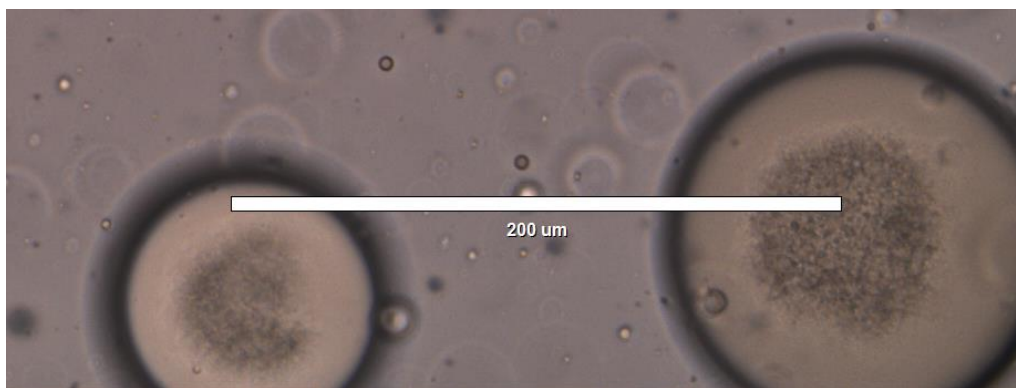


Figure 3.6: PDMS microspheres made using silanol dehydrogenation by metal salt cure.

3.5 Conclusions

Optimization of the hydrophilic phase for reactive interfacial stabilized water-in-silicone emulsions was done by screening multiple different solvents, surfactants, aqueous phase polymers, and other additives with potential to form a polymer network at the interface. Overall, interfacial networking was highly dependent on the affinity of the basic catalyst for the hydrophilic phase. Hydrophilic PEG was preferred as the aqueous phase polymer and seemed to promote the reaction due to its phase transfer capabilities of the water phase catalyst. This improved the reactivity at the interface to the point where water could be used as the sole solvent in the hydrophilic phase with KOH concentrations as low as 1 wt%. It was also found that addition of silicone phase surfactants inhibited the hydrogen blowing reaction likely due to the formation of a buffer region at the interface.

This study has demonstrated the basics for a novel approach to produce stable gas/oil/water and water/oil/water double emulsions in the form of porous PDMS microspheres. By decoupling the curing and gas blowing reactions, PDMS microspheres with high porosity were produced. The sensitivity of the silicon-hydrogen bond to hydroxyl groups in the presence of basic catalyst has been shown as a mechanism for forming a stable interface in silicone-water emulsions with no additional surfactant needed. While the dehydrogenation reaction was activated by a water phase catalyst, a separate

platinum catalyst in the PDMS phase activated vinyl addition cure and determined the level of gas entrapment.

3.6 Future directions

This study has only laid groundwork for a new method of porous microsphere production. Future studies should focus on catalyst selection and removal, microsphere size control, and mechanical property testing. KOH was used in this study because of its low health risks, ease of handling, high activity, and low cost. However, full removal of the hydroxide with post-processing would likely be challenging. Being a strong base, residual KOH may cause detrimental effects to the silicone rubber or to applications that use porous microspheres. Other catalysts such as amines or transient hydroxides have also been shown activate the hydrogen release reaction and can be tuned to have specific oil phase partitioning. Further catalyst studies may even reduce the need for PEG as a phase transfer agent, leading to minimal material requirements and high purity PDMS microspheres.

This study used only rough emulsification methods to make porous microspheres on the order of 100 μm in diameter. Studies with more sophisticated processing equipment are needed to focus on particle homogeneity and control, which extends to both the final PDMS microsphere and the entrapped water domains. Due to the size and architecture complexity of the microspheres, control over particle homogeneity is critical for determining actual porosities of these materials and the ability for gas entrapment under different conditions such as cure time and temperature.

Finally, these porous constructs are expected to have unique mechanical and physiological properties. The high porosity will lead to them being lightweight compared to solid PDMS while maintaining the same chemical properties. However, the mechanical toughness of these microfoam structures is difficult to predict, and the robustness of the microspheres to mechanical stimulus is critical to evaluating their applicability.

References

1. Wang, H.-C., et al., *pH-Triggered Release from Polyamide Microcapsules Prepared by Interfacial Polymerization of a Simple Diester Monomer*. ACS macro letters, 2017. **6**(3): p. 321-325.
2. Salaun, F., et al., *Microencapsulation of a cooling agent by interfacial polymerization: Influence of the parameters of encapsulation on poly(urethane-urea) microparticle characteristics*. Journal of Membrane Science, 2011. **370**: p. 23-33.
3. Aboubakar, M., et al., *Study of the mechanism of insulin encapsulation in poly(isobutylcyanoacrylate) nanocapsules obtained by interfacial polymerization*. Journal of biomedical materials research, 1999. **47**(4): p. 568-576.
4. Jia, Y., et al., *A combined interfacial and in-situ polymerization strategy to construct well-defined core-shell epoxy-containing SiO₂-based microcapsules with high encapsulation loading, super thermal stability and nonpolar solvent tolerance*. International Journal of Smart and Nano Materials, 2016. **7**(4): p. 221-235.
5. Zou, Y., et al., *Interfacial Complexation Induced Controllable Fabrication of Stable Polyelectrolyte Microcapsules Using All-Aqueous Droplet Microfluidics for Enzyme Release*. ACS Applied Materials & Interfaces, 2019. **11**(23): p. 21227-21238.
6. *Linking Adhesive Properties and Pore Organisation of Silicone Emulsions Obtained by Reactive Blending*. 2018, University of Paris-Saclay: Paris.
7. Iqbal, M., et al., *Double emulsion solvent evaporation techniques used for drug encapsulation*. International Journal of Pharmaceutics, 2015. **496**(2): p. 173-190.
8. Rosca, I.D., F. Watari, and M. Uo, *Microparticle formation and its mechanism in single and double emulsion solvent evaporation*. Journal of Controlled Release, 2004. **99**(2): p. 271-280.
9. Wang, S.-y., et al., *Preparation of PLGA Microspheres with Different Porous Morphologies*. Chinese Journal of Polymer Science, 2015. **33**(1): p. 128-136.
10. *Reactive Silicones: Forging new polymer links*. 2016, Gelest Inc: Morrisville.
11. Anslyn, E. and D. Dougherty, *Modern Physical Organic Chemistry*. 2006: University Science Books.
12. Jiang, S., T. Qiu, and X. Li, *Kinetic study on the ring-opening polymerization of octamethylcyclotetrasiloxane (D4) in miniemulsion*. Polymer (Guilford), 2010. **51**(18): p. 4087-4094.
13. Barrere, M., et al., *Anionic polymerization of octamethylcyclotetrasiloxane in miniemulsion II. Molar mass analyses and mechanism scheme*. Polymers, 2001. **42**: p. 7239-7246.
14. Cesteros, L.C., *A simple and green procedure to prepare poly(ethylene glycol) networks: Synthesis and properties*. Green Chemistry, 2011. **13**: p. 197-206.
15. Neumann, R. and Y. Sasson, *Mechanism of base-catalyzed reactions in phase-transfer systems with poly(ethylene glycols) as catalysts. The isomerization of allylanisole*. Journal of Organic Chemistry, 1984. **49**(19): p. 3448-3451.

Left Intentionally Blank